

UC San Diego

UC San Diego Electronic Theses and Dissertations

Title

Physiological Orchestration in Bacteria

Permalink

<https://escholarship.org/uc/item/0c03c3hw>

Author

Sauls, John Thomas

Publication Date

2019

Peer reviewed|Thesis/dissertation

UNIVERSITY OF CALIFORNIA SAN DIEGO

Physiological Orchestration in Bacteria

A dissertation submitted in partial satisfaction of the
requirements for the degree
Doctor of Philosophy

in

Bioinformatics and Systems Biology

by

John Thomas Sauls

Committee in charge:

Professor Suckjoon Jun, Chair
Professor Terence Hwa, Co-Chair
Professor Nathan E. Lewis
Professor Justin R. Meyer
Professor Milton H. Saier

2019

Copyright
John Thomas Sauls, 2019
All rights reserved.

The dissertation of John Thomas Sauls is approved, and it is acceptable in quality and form for publication on microfilm and electronically:

Co-Chair

Chair

University of California San Diego

2019

DEDICATION

To Mother and Father for having high expectations and no demands.

TABLE OF CONTENTS

Signature Page	iii
Dedication	iv
Table of Contents	v
List of Figures	viii
List of Tables	x
Acknowledgements	xi
Vita	xii
Abstract of the Dissertation	xiii
Chapter 1 Introduction to Bacterial Physiology	1
1.1 Introduction	1
1.2 Outline	3
1.3 Background on bacterial physiology	4
1.3.1 Principles of bacterial growth and measurement	5
1.3.2 Steady-state and description of bacterial growth	7
1.3.3 Background on size and cell cycle control	10
1.3.4 Background on size and cell cycle homeostasis	17
Chapter 2 Review of the Study of Replication and Division Coordination	21
2.1 Introduction	21
2.2 Does replication initiation regulate division?	22
2.3 The initiator threshold model	28
2.3.1 The replicon model	30
2.3.2 Beginnings of the initiator threshold model	31
2.3.3 Development of the initiator threshold model	32
2.3.4 The threshold model in application to division	35
2.3.5 The threshold model, balanced growth, and the adder principle	37
2.4 Molecular players and associated models	40
2.4.1 <i>dnaA</i> and replication initiation	40
2.4.2 <i>ftsZ</i> and division	41
2.4.3 Nucleoid occlusion	44
2.4.4 <i>ter</i> linkage	46
2.4.5 Regulators of FtsZ assembly with growth rate	47
2.5 Conclusion	49

Chapter 3	<i>B. subtilis</i> and <i>E. coli</i> Share Common Principles to Coordinate Growth and the Cell Cycle	50
3.1	Introduction	50
3.2	<i>B. subtilis</i> physiological control	53
3.2.1	Ensuring steady-state growth in <i>B. subtilis</i>	53
3.2.2	Growth law of cell size: <i>B. subtilis</i> size shows a positive but not exponential dependence on the nutrient-imposed growth rate	55
3.2.3	Single-cell determination of cell cycle parameters in <i>B. subtilis</i>	57
3.2.4	Complementary, ensemble determination of cell cycle parameters in <i>B. subtilis</i>	61
3.2.5	Invariance of initiation size: <i>B. subtilis</i> initiates at a fixed cell size per <i>ori</i>	62
3.2.6	Initiation size is invariant even during nutrient shifts at the single-cell level	64
3.2.7	<i>E. coli</i> and <i>B. subtilis</i> change cell shape differently under different growth conditions but maintain a constant initiation size	66
3.2.8	<i>B. subtilis</i> is both a division adder and an initiation adder	67
3.2.9	<i>B. subtilis</i> and <i>E. coli</i> share the same hierarchy of physiological parameters	68
3.3	Conclusion	70
Chapter 4	Replication and Division Coordination During Physiological Shifts	75
4.1	Introduction	75
4.2	Imaging replication and division coordination in <i>E. coli</i>	76
4.2.1	A constant initiation size is conserved during nutrient shift-up	76
4.2.2	A constant initiation size is conserved during nutrient shift-down	79
4.2.3	Division is controlled by FtsZ accumulation at the midcell	83
4.2.4	Nucleoid segregation occurs at a fixed size unrelated to ring formation	90
4.2.5	FtsZ accumulation and ClpX degradation control division at slow growth	93
4.3	Conclusion	96
Appendix A	Materials and methods	98
A.1	Strains	98
A.2	Growth media and experimental conditions	99
A.3	Microscopy configuration	99
A.4	Turbidostat cell preparation and sample collection	100
A.5	Turbidostat growth rate measurement	101
A.6	Turbidostat cell size measurement	101
A.7	Turbidostat C period measurement using qPCR	102
A.8	Mother machine cell preparation and image acquisition	102

	A.9 Mother machine image processing	103
	A.10 Single-cell cell cycle analysis	104
	A.11 Ensemble cell cycle analysis	104
	A.12 Tables	105
Appendix B	Mother machine image processing with mm3	110
	B.1 Introduction	110
	B.2 mm3 image processing workflow	112
	B.2.1 Crop and compile images	114
	B.2.2 Channel designation	118
	B.2.3 Background subtraction	121
	B.2.4 Segmentation routine 1: Otsu threshold and random walker .	122
	B.2.5 Segmentation routine 2: U-net convolutional network	126
	B.2.6 Region tracking and cell lineage creation	129
Bibliography	133

LIST OF FIGURES

Figure 1.1:	Growth of bacterial cultures	5
Figure 1.2:	Single-cell measurements	8
Figure 1.3:	Cell composition and size changes with growth rate	11
Figure 1.4:	The bacterial cell cycle (slow growth)	13
Figure 1.5:	The bacterial cell cycle (fast growth)	14
Figure 1.6:	Donachie’s critical mass	15
Figure 1.7:	Modern confirmation of the invariant initiation size	16
Figure 1.8:	Size homeostasis by the adder principle	18
Figure 2.1:	Eukaryotic and prokaryotic cell cycles	23
Figure 2.2:	Classification of replication and division coordination models	24
Figure 2.3:	Comparison of CVs of discrete cell cycle events	26
Figure 2.4:	Early experiments and models of DNA replication in bacteria	29
Figure 2.5:	Threshold model for initiation	34
Figure 2.6:	Division potential model by Teather and colleagues	36
Figure 2.7:	First image of FtsZ localization	42
Figure 2.8:	Nucleoid occlusion development	44
Figure 2.9:	Chromosome-membrane attachment models	46
Figure 3.1:	Population and single-cell methods to achieve steady-state growth	52
Figure 3.2:	Single-cell steady-state physiological parameters for all conditions	54
Figure 3.3:	Population cell size and C period measurements in <i>B. subtilis</i> and <i>E. coli</i>	55
Figure 3.4:	Length and width measurements in <i>B. subtilis</i> and <i>E. coli</i>	56
Figure 3.5:	Size and C period under translational inhibition in <i>B. subtilis</i> and <i>E. coli</i>	57
Figure 3.6:	Single-cell growth and cell cycle progression in <i>B. subtilis</i>	58
Figure 3.7:	Ensemble replisome count and localization for all conditions	60
Figure 3.8:	Initiation size is invariant in <i>B. subtilis</i> during steady-state growth	62
Figure 3.9:	<i>B. subtilis</i> cell cycle and initiation size behavior	63
Figure 3.10:	Initiation size is invariant in <i>B. subtilis</i> during shift-down	65
Figure 3.11:	Initiation size is invariant during shift-up and shift-down	66
Figure 3.12:	<i>B. subtilis</i> is an initiation and division adder	67
Figure 3.13:	<i>B. subtilis</i> and <i>E. coli</i> share the same hierarchy of physiological parameters	69
Figure 3.14:	Normalized physiological parameter distributions for all conditions	70
Figure 3.15:	<i>B. subtilis</i> and <i>E. coli</i> comparative summary	71
Figure 3.16:	Unnormalized physiological parameter distributions for all conditions	73
Figure 3.17:	Normalized cross-correlations	74
Figure 4.1:	Macromolecular accumulation and rate maintenance during nutrient shift-up	76
Figure 4.2:	Single-cell nutrient shift-up	77
Figure 4.3:	Single-cell parameters during shift-up	78
Figure 4.4:	Macromolecular accumulation and division during nutrient shift-down	80

Figure 4.5:	Single-cell nutrient shift-down	81
Figure 4.6:	Single-cell parameters during shift-down	82
Figure 4.7:	Measuring FtsZ ring formation in single cells	83
Figure 4.8:	FtsZ accumulation over the division cycle	85
Figure 4.9:	Division is triggered when the Z-ring contains a critical amount of FtsZ	86
Figure 4.10:	Division is determined by FtsZ accumulation in the Z-ring	88
Figure 4.11:	Tracking nucleoid segregation and replication	90
Figure 4.12:	Distribution of cell cycle event sizes	91
Figure 4.13:	Ring formation and nucleoid segregation are independent	92
Figure 4.14:	ClpX degrades FtsZ during starvation	94
Figure B.1:	mm3 workflow	113
Figure B.2:	Channel detection	115
Figure B.3:	Channel designation GUI	120
Figure B.4:	Standard segmentation algorithm	123
Figure B.5:	U-net segmentation workflow	127

LIST OF TABLES

Table A.1: Strain information.	105
Table A.2: Growth media.	106
Table A.3: Media components.	107
Table A.4: Amino acid supplement.	108
Table A.5: Turbidostat experimental conditions.	108
Table A.6: Mother machine experimental conditions.	109
Table A.7: qPCR primers.	109

ACKNOWLEDGEMENTS

Chapter 3, in full, has been prepared for submission for publication of the material. Sauls, John T; Cox, Sarah E; Do, Quynh; Castillo, Victoria; Ghulam-Jelani, Zulfar; Jun, Suckjoon. The dissertation author was the primary investigator and author of this material.

VITA

- 2013-2019 Ph.D. in Bioinformatics and Systems Biology, University of California, San Diego
- 2008-2011 M.S.E. and B.S.E. in Bioengineering, University of Pennsylvania

PUBLICATIONS

- Sauls, J. T., Cox, S. E., Castillo, V., Ghulam-Jelani, Z., & Jun, S. (2019). Gram-Positive and Gram-Negative Bacteria Share Common Principles to Coordinate Growth and the Cell Cycle at the Single-Cell Level. *bioRxiv*.
- Si, F., Le Treut, G., Sauls, J. T., Vadia, S., Levin, P. A., & Jun, S. (2019). Mechanistic Origin of Cell-Size Control and Homeostasis in Bacteria. *Current Biology*, 29(11), 1760-1770.
- Heirendt, L., Arreckx, S., Pfau, T., Mendoza, S. N., Richelle, A., Heinken, A., ... Sauls, J. T., ... Fleming, R. M. T. (2019). Creation and analysis of biochemical constraint-based models using the COBRA Toolbox v.3.0. *Nature Protocols*, 14(3), 639-702.
- Sekar, K., Rusconi, R., Sauls, J. T., Fuhrer, T., Noor, E., Nguyen, J., ... Sauer, U. (2018). Synthesis and degradation of FtsZ quantitatively predict the first cell division in starved bacteria. *Molecular Systems Biology*, 14(e8623).
- Si, F., Li, D., Cox, S. E., Sauls, J. T., Azizi, O., Sou, C., ... Jun, S. (2017). Invariance of Initiation Mass and Predictability of Cell Size in *Escherichia coli*. *Current Biology*, 27(9), 1278-1287.
- Cremer, J., Segota, I., Yang, C., Arnoldini, M., Sauls, J. T., Zhang, Z., ... Hwa, T. (2016). Effect of flow and peristaltic mixing on bacterial growth in a gut-like channel. *Proceedings of the National Academy of Sciences of the United States of America*, 113(41), 11414-11419.
- Sauls, J. T., Li, D., & Jun, S. (2016). Adder and a coarse-grained approach to cell size homeostasis in bacteria. *Current Opinion in Cell Biology*, 38, 38-44.
- Taheri-Araghi, S., Bradde, S., Sauls, J. T., Hill, N. S., Levin, P. A., Paulsson, J., Vergassola, M., & Jun, S. (2015). Cell-size control and homeostasis in bacteria. *Current Biology*, 25(3), 385-391.
- Taheri-Araghi, S., Brown, S. D., Sauls, J. T., McIntosh, D. B., & Jun, S. (2015). Single-Cell Physiology. *Annual Review of Biophysics*, 44, 123-142.
- Sauls, J. T., & Buescher, J. M. (2014). Assimilating genome-scale metabolic reconstructions with modelBorgifier. *Bioinformatics (Oxford, England)*, 30(7), 1036-1038.

ABSTRACT OF THE DISSERTATION

Physiological Orchestration in Bacteria

by

John Thomas Sauls

Doctor of Philosophy in Bioinformatics and Systems Biology

University of California San Diego, 2019

Professor Suckjoon Jun, Chair
Professor Terence Hwa, Co-Chair

Each cell must achieve the dual tasks of replicating the genetic material and dividing its components into its daughters. This thesis is concerned with how the cell coordinates those fundamental requirements. It approaches this question from the perspective of bacterial physiology, looking at the global relationship between these processes and growth at large. The thesis aims to uncover and test quantitative principles which govern this physiological orchestration. We first review the early quantitative principles, or growth laws, and their modern expansions. This includes cell size control, its connection with the cell cycle, and homeostatic control of each. We then explore these principles in the context of the model organisms *E. coli* and *B. subtilis*.

Despite their evolutionary distance, we find the two species to be fundamentally similar in their physiological control. Finally, we test the limits of replication and division coordination using single-cell measurements and nutrient-shift experiments. This leads us to reevaluate the canonical Helmstetter-Cooper cell cycle model. Instead of a strict dependency of division on replication initiation, we instead support the view that both processes are controlled by independent threshold mechanisms.

Chapter 1

Introduction to Bacterial Physiology

1.1 Introduction

The earliest cells are thought to have arisen in Earth's shallow seas less than a billion years into our planet's life¹. These cells were not as we would recognize them today. They likely did not yet contain DNA and perhaps were encapsulated by something other than a phospholipid membrane²⁻⁴. Nevertheless, the existence of these cells allowed for evolutionary force to first sway life. Cells are a prerequisite for evolution because they allow unique entities to be rewarded for their ability to grow and propagate^{5,6}. Before cells, prebiotic replicative molecules could not easily reap the benefits of their catalysis, as all resources were shared and all production dissipated through diffusion. A cell is born when those replicative molecules are encapsulated from their environment. If such a cell can grow and reproduce, it gifts to its daughters those same capabilities and in turn the chance to live, change, and flourish. To give this gift a cell must do exactly two things: replicate its information molecules and divide its growth into separate entities.

Replication and division amongst early life was a sloppy affair^{6,7}. It is doubtful that the two tasks were in any way coupled, so a genetic blebs or other sterile monstrosities were likely common. Four billion years later, evolution has shaped the descendants of those early forms

into extremely efficient species which thrive in aggressive environments and against ruthless competition. Modern bacteria are paragons of growth. *Escherichia coli* can double its size and divide in just under twenty minutes⁸. And it does so with impressive fidelity, with less than 1 in 100 divisions leading to death⁹. This is a testament to the species' ability to link replication with division.

This thesis addresses how bacteria coordinate replication and division with such fidelity. I use *E. coli* and *Bacillus subtilis* as my experimental organisms. I ask this question from the perspective of bacterial physiology and quantitative biology. The inspiration from bacterial physiology means that I consider replication and division in the context of the entire cell and its fundamental goal to grow and propagate. While molecular players are certainly discussed, the main work in this thesis did not intend to uncover the specific function of particular proteins. Instead it is to more broadly understand how molecular mechanisms lead to global coordination of the central biological processes.

Quantitative biology is the application of precise measurements, rigorous statistics, and mathematical modeling to biological questions. In the space of bacterial physiology, quantitative biology attempts to produce formal relations that can predict the growth and phenotype of prokaryotic life. Thus, this thesis work aimed to determine quantitative relationships among the cell, its environment, and its internal processes. This goal is an extension of the foundational works in the field from the middle of the 20th century, carried forward by recent discoveries made with the help of advances in microfluidics, microscopy, and computing¹⁰.

Indeed, the work described here was made possible by such advances. Though many of the original observations on which this thesis work is based were made at the population level, most of the experiments herein investigate large numbers of single cells. This approach affords many advantages, not least of which is that it allows the researcher to witness firsthand the harmony among growth, replication, and division.

1.2 Outline

This thesis is organized as follows.

In the rest of the introduction I describe the basic principles of bacterial physiology. This begins with the theory of measurements and description of bacterial populations. It ends with a summary of the major quantitative principles in the field, from the classic works to modern discoveries of which I was a part. These principles are then revisited through the thesis.

Chapter 2 addresses replication and division coordination in detail with a literature review. This covers the initial formulation of the phenomenon, early models and their development until today, and key molecular players. A major focus of Chapter 2 is history of the threshold model, which explains how cells can trigger events in relation to their own growth.

In Chapter 3 I explore the fundamental quantitative principles of bacterial physiology in the context of *B. subtilis* with comparison to *E. coli*. Most of the observations and theories in this field were developed using *E. coli* and *S. typhimurium*. Perhaps surprisingly, *B. subtilis* is extremely similar in its core physiological behavior. Chapter 3 is mostly a reproduction of Sauls et al.¹¹.

The unified physiological regulatory framework presented at the end of Chapter 3 is based on a threshold mechanism to control replication initiation and division^{12,13}. This mechanism is on display in single cells during nutrient shift-down, where initiation is delayed until cells regain growth. Shift-down also seemingly breaks the canonical connection between initiation and division.

Chapter 4 explores the shift paradigm in greater depth in order to push the limits of the cell's physiological coordination. Ultimately, we determine that the Helmstetter Cooper model, while useful to conceptualize the bacterial cell cycle, does not accurately describe replication and division coordination in individual cells. Instead, replication and division timing are primarily controlled by independent threshold mechanisms, themselves tied to global biosynthesis.

1.3 Background on bacterial physiology

Bacterial physiologists hope to understand how cells function given the environment in which they live¹⁴. Physiology is at its most basic level described by the culmination of an organism's biological program, the result of which is growth. For bacteria, growth is intimately connected to division (controlling size) and chromosome replication (controlling the cell cycle)^{12, 15}. I am thus centrally concerned with the control and coordination of growth, cell size, and the cell cycle.

In the following sections I give a brief overview of major principles in bacterial physiology on which my dissertation work is based. This begins with measurement concepts and a description of bacterial growth (Subsections 1.3.1 and 1.3.2). Bacterial physiology is particularly satisfying because even at its inception, its researchers were keen on finding quantitative relationships which described their subjects¹⁶⁻¹⁸. This approach necessitated careful experimental procedures and mathematical formalisms to describe cells and cell cultures.

From this I follow with the principles which govern cell size and cycle control and homeostasis (Subsections 1.3.3 and 1.3.4). By "control" I mean how a cell determines its absolute specifications (i.e. size or cell cycle duration) depending on its conditions. "Homeostasis" is how the cell maintains those specifications in light of variability or stochasticity. The control section covers the classic discoveries of the field and their modern expansion. The homeostasis section briefly covers the discovery of theadder principle and its application to both size and cell cycle homeostasis.

Note that I used cell size, cell mass, and cell volume interchangeably. The density of cells is more or less constant across conditions, so this is a reasonable equivalency¹⁹.

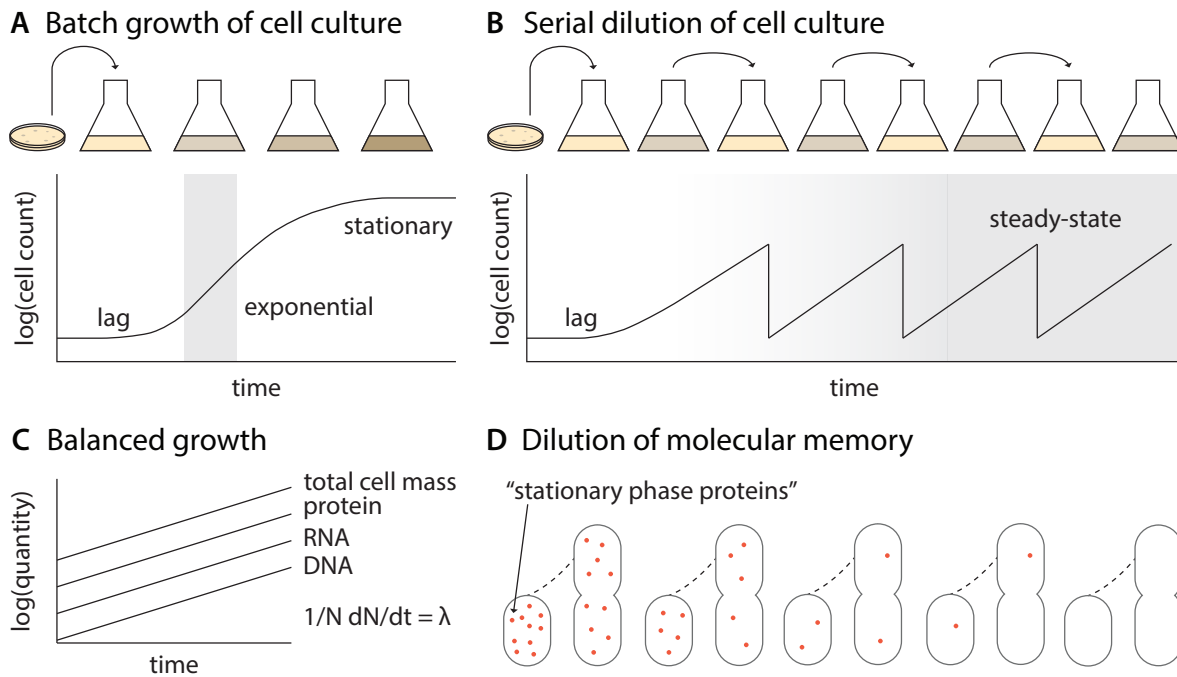


Figure 1.1: Growth of bacterial cultures. (A) During canonical bacterial growth, fresh medium is inoculated with a colony. Cells adjust to their new environment during the lag phase. They then increase in number and mass during the exponential phase as described in the text. As nutrients are consumed and become limiting, cells slow growth and enter stationary phase. The mass of the culture can be measured via the optical density (OD) using a spectrophotometer. (B) Steady-state populations are created by consecutively diluting an exponential culture into fresh media. (C) During balanced growth, all extrinsic properties of the culture increase in amount proportionally to one another. This is equivalent to the mass fraction of all macromolecules being time-invariant. (D) To achieve steady-state, cells must grow for long enough to dilute out molecules associated with a previous state. In this example, to be compared to panel B, proteins associated with the stationary phase become a smaller fraction of cell mass as cells grow without producing these proteins during exponential growth.

1.3.1 Principles of bacterial growth and measurement

Initial progress in bacterial physiology came after the critical insight that the attainment of general principles required the reproducible growth of cells²⁰. While this appears to be a truism, the task is non-obvious from the perspective of bacterial growth. The growth of a bacterial population involves both an increase in mass and number, and it is the balance of their increase that we will ultimately use to determine the physiological state of a culture.

Initially, the bacterial growth cycle was considered exclusively in the context of batch

growth until nutrient depletion²¹ (Figure 1.1). In this sequence, a seed colony of cells grown on an agar plate (or from a stationary culture) are inoculated into fresh medium with abundant nutrients. With proper temperature control and aeration, the cells of this colony will begin growth and are considered a liquid culture. After a lag phase in which the population slowly accumulates mass and number, they will begin exponential growth, intermittently and briefly sustaining a period of maximum increase. This is known as the exponential or log phase, and provides a toehold for attaining reproducible growth. As the culture grows, inevitably the concentration of a particular nutrient in the media drops below the consumption rate of the entire population. The growth (both in mass and number) of the culture slows. Finally, as more nutrients are exhausted, cells transition into stationary phase and cease to divide. Cell death eventually follows, but even today that phase remains poorly characterized.

While this sequence is reproducible, quantifiable aspects of the population's growth are not. This is because, even under the same environmental conditions such as temperature and media composition, the duration of the phases is a function of the physiological and environmental history of the seed culture²². But it is nearly impossible to produce identical bacterial colonies for seeding new cultures, as their physiology is in turn a function of their history. Phenomena in biology are extremely difficult to isolate from the subject's historical context, fundamentally undermining reproducibility. You cannot restart a biological system as easily as you could a circuit because all life is a continuous process that began billions of years ago.

Indeed, Neidhardt and Magasanic “realized, however, that the stationary phase does not represent a unique physiological state”²². The key is then to release the bacterial culture of its memory such that its physiology is only a function of its current environment. This can be achieved during the exponential phase of batch culture, when cells grow at a maximal rate determined by the growth conditions²³. During this time, cellular growth is limited only by their ability to transform the available nutrients into the molecules of which they are constituted. That is to say, they are only limited by how fast they can make themselves.

However, maximum exponential growth alone does not ensure reproducible measurements of the culture. This is because cells growing in this state will still retain molecules that are associated with a previous state Figure 1.1D. In bacteria, proteins account for around 50-80% of cell mass, and very few proteins are actively degraded^{19,24-26}. Thus, the only way to shed previous proteins is to dilute them out through growth. On average, cells double their mass and divide evenly every generation, and cellular components are homogeneously inherited by the two daughters. In this way, each cell before division is composed of one half “new” components, while the other half was inherited from its mother. The geometric series can be followed to see that of this inherited portion, half was made by the mother, half inherited from the grandmother, and so on. Then, to attain a bacterial culture that is only a function of its current environment, that culture must have growth through sufficient generations to dilute out the molecular memory of its past. A rule of thumb is that after 10 unimpeded generations have passed, cells are considered to be only a function of their current conditions^{14,27}.

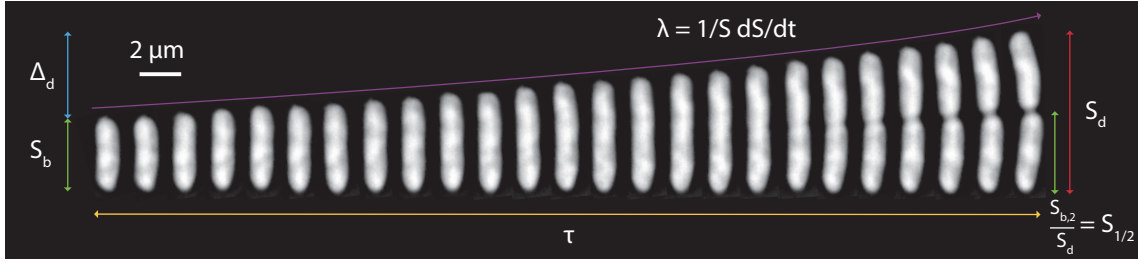
This is achieved practically by diluting an exponentially growing population into new media, allowing it to maintain its maximum growth rate over many generations Figure 1.1B¹⁸. In this way, a bacterial strain, defined by its genomic code, can be put reproducibly in the same physiological state that is based strictly on the chemical and physical environmental conditions. We know this as steady-state, and it forms the basis of all measurements in bacterial physiology.

1.3.2 Steady-state and description of bacterial growth

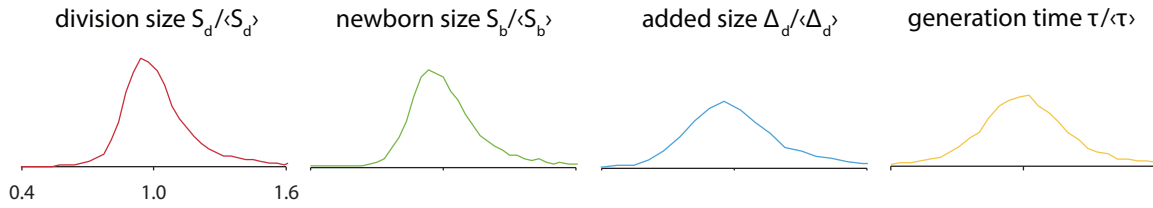
Steady-state growth implies both exponential growth and balanced growth^{14,28}. Exponential growth, described qualitatively above, is formally when the number of cells in the culture increases with time according to the following formula:

$$N(t) = N_0 \cdot e^{\lambda t}$$

A Single-cell growth of *E. coli*



B Distributions of physiological parameters



C Correlations of physiological parameters with newborn size

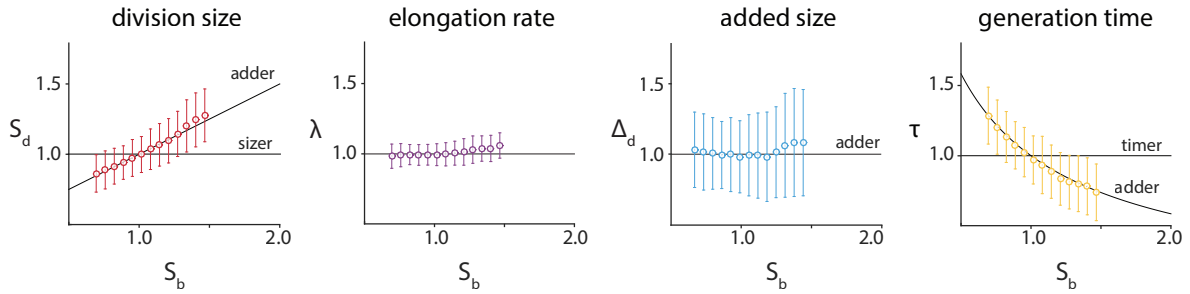


Figure 1.2: Single-cell measurements. (A) Example time-lapse images of a single *E. coli* growing in TSB medium taken every 45 seconds. Visual definitions of the major parameters measurable via bright field or phase contrast microscopy are shown. Septum position $S_{1/2}$ is the newborn size divided by the division size of the mother. (B) Single-cell distributions of some parameters, normalized by their respective means. The coefficient of variation (CV) of a parameter is associated with its regulation, but may be misleading when considering which parameters cells actively control. In either case, the CV of the major physiological parameters follows the order $S_{1/2} < \lambda < S_d < S_b < \tau < \Delta_d$. (C) Correlations among single-cell parameters allow for insight into physiological control. Here, correlation analysis favors the adder principle over sizer and timer.

Where λ is a constant (the growth rate), N_0 is the cell number at time zero, and t is the elapsed time. Note that the growth rate is related to the doubling time τ by $\lambda = \ln 2 / \tau$, as the

above equation can be written as:

$$N(t) = N_0 \cdot 2^{t/\tau}$$

Balanced growth means that every extensive property of the culture increases by the same rate (Figure 1.1C)^{10, 14, 29}. An extensive property is any measurable, additive aspect of the culture, such as the mass of RNA, DNA, or proteins, or the number of cells in the culture. For example, if an exponentially growing culture is in balanced growth, then the mass of ribosomes M_{rb} in the population will be:

$$M_{\text{rb}} = M_{\text{rb},0} \cdot e^{\lambda t}$$

Where $M_{\text{rb},0}$ is the mass of ribosomes at time zero.

While all extensive properties increase at the same rate during balanced growth, steady-state implies that all intensive properties are time-invariant. Intensive properties of the culture do not depend on the cultures size, but are instead derived from the physiological state of the cell. Intensive properties include the average cell size, the ratio of ribosomes to other proteins, and the duration of the cell cycle. In fact, steady-state demands that the distribution of these parameters are also time-invariant, though those distributions are not always readily measurable with population level measurements³⁰. It is intensive properties, when compared across growth conditions, that often lead to insight on the way bacteria orchestrate their lives.

So far we have considered steady-state measurements in the context of bacterial populations, but we also use the concept for single-cell growth experiments (Figure 1.2). Similarly, all intrinsic variables and their distributions are time-invariant. For single cells, we measure their growth by their elongation rate λ . This is because our principal model organisms, *E. coli* and *B. subtilis*, are rod-shaped bacteria and have constant width in a particular growth conditions³¹. Thus, an increase in length is proportional to an increase of mass. The single-cell elongation rate is equivalent to the population growth rate, as both are proportional to mass accumulation. Similarly, the single-cell interdivision time, or generation time, is equivalent to the population

level doubling time (and we use τ for both), as individual cells on average double their mass from birth to division.

The concept of balanced growth also applies to single cells, but with a large caveat. Processes like DNA replication and division are in reality discrete events, yet the number of cells in a liquid culture is so large that we consider the mass of DNA and cell number to increase continuously. This is not appropriate for single cells. As described below, the cell cycle is highly regulated in terms of when DNA replication is ongoing. This implies that cells of different ages do not accumulate DNA at the same rate³².

However, there is little or no cell cycle dependent regulation of proteins either in terms of production or degradation. Thus the production of all proteins in the cell is balanced: they all increase at the same rate within an individual cell. Their production can be considered constitutive. This can also be roughly applied to production of other macromolecules in the cell (besides DNA), such as RNA and lipids, with the additional caveat that there is a change in the rate of cell wall production during septation^{26,33}. In any case, the balanced production of proteins in single cells will prove extremely useful in understanding the triggering of discrete biological processes.

1.3.3 Background on size and cell cycle control

J. B. S. Haldane wrote in his 1926 essay *On Being the Right Size*:

For every type of animal there is a most convenient size, and a large change in size inevitably carries with it a change of form³⁴.

This sentiment certainly applies to bacterial domain, whose species' span several orders of magnitude³⁵. In fact, the size of *E. coli* itself spans one order of magnitude depending on its environmental conditions¹⁶.

Why does *E. coli*, as well as other species such as *B. subtilis*, vary its size based on conditions? Enabled by the steady-state techniques outlined above, it was this observation by Ole

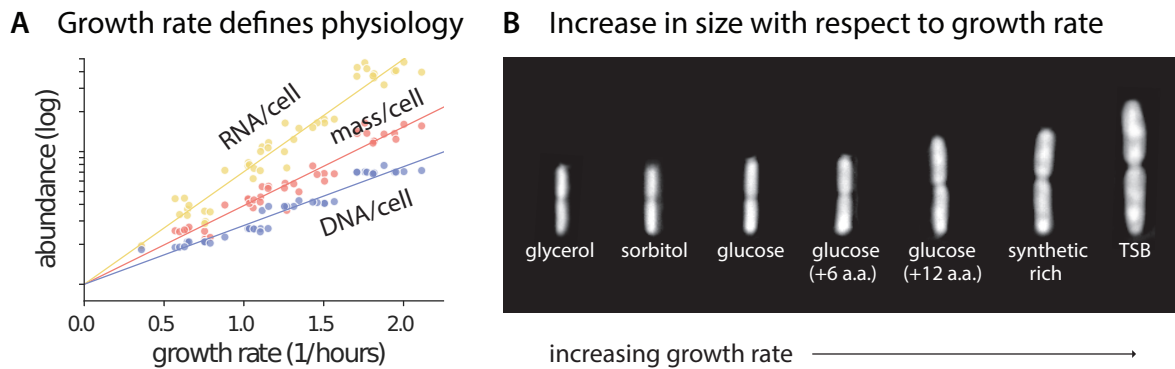


Figure 1.3: Cell composition and size changes with growth rate. (A) Cells largely determine their macromolecular composition based on their growth rate, regardless of the chemical details of the medium. Here, in a reproduction of the classic work by Schaechter and colleagues, using modern data from Si and colleagues, we see the relationship among RNA, cell size, and DNA as a function of the growth rate. Lines are linear regression fits and the data is plotted on a semi-log scale. Data has been normalized so all measurements have the same y-intercept. (B) Representative images of *E. coli* at division in various media which support different growth rates.

Maaløe's Copenhagen lab that became a keystone of bacterial physiology^{14,17}. Great strides were then made connecting cell size, the cell cycle, and growth in order to answer this question. It is on these works that modern quantitative and systems biology approaches to bacterial physiology are founded.

In 1958, Schaechter, Maaløe, and Kjeldgaard measured the extrinsic properties of total mass, DNA, and RNA in cultures of *Salmonella typhimurium* in balanced growth across twenty-two media compositions¹⁶. Using plate counts, they converted these measures to the intrinsic properties of average mass (size), DNA, and RNA content per cell. This allowed them to plot those quantities across the range of growth rates afforded by the different media, from about one to three doublings per hour Figure 1.3. This simple yet thorough approach revealed two important patterns.

The first is that it is the growth rate, not the chemical details of the of the media itself, which predicate the macromolecular composition of the cell. Thus if two bacterial cultures grown on two different media (for example, placenta broth and yeast extract with glucose used in the

paper) have the same growth rate, cells in those cultures will have the same size, DNA, and RNA. This is a boon to the quantitative power of the field, as it means we can use growth rate a state variable in order to build predictive relationships. It also indicates the cell has a global regulatory framework in which it connects growth to other processes. This is opposed to a molecularly specific regulatory framework epitomized by contemporaneous work with the *lac* operon¹⁶.

The second observation was that cell size, DNA, and RNA content all increase exponentially with growth rate, but not in the same proportion. RNA increase the fastest, followed by cell size and DNA. The increase in size is well described by $S \propto e^{\lambda} = 2^{\mu}$, which I refer to as the Schaechter line (note the relationship between growth rate λ and the doubling rate μ). The difference in macromolecular composition across growth rates speaks to Haldane's assertion: with the change in size comes a change in form. Faster growing cells are not simply enlarged versions of slower growing ones, but differ in their composition.

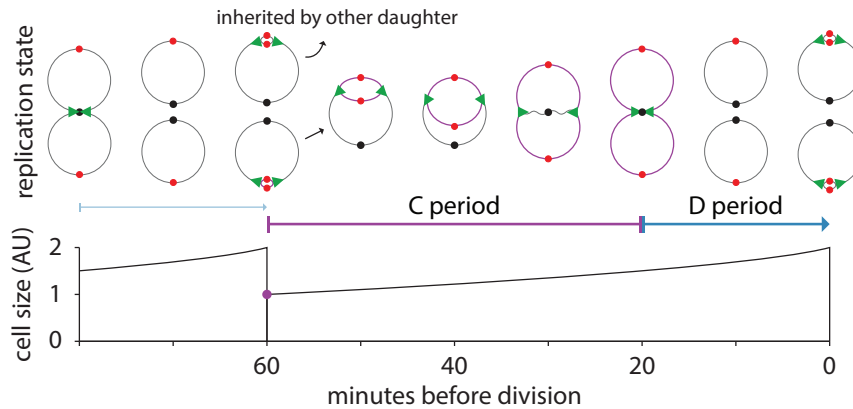
The reason for the increase in RNA is related to the increase in the fraction of active ribosomes in relation to the total proteome in fast growing cells²⁵.

Understanding why cell size and DNA increases with growth rate requires knowledge of the bacterial cell cycle (Figures 1.4 and 1.5). This was mapped out by Helmstetter and Cooper ten years later using *S. typhimurium*'s cousin *E. coli*³². By using a cell synchronization device called the baby machine, they pulse labeled cells with tritiated thymidine, which was incorporated into the nascent chromosome. By comparing the rate of DNA synthesis via thymidine incorporation to the age of the cell, they were able to deduce the timing of the start and duration of chromosome replication. They observed that chromosome replication (C period), and the time from replication termination to division (D period), were constant at about 40 and 20 minutes, respectively, for growth rates faster than one doubling per hour.

As the C+D period can be longer than the doubling time, they developed a model which calls for daughter cells to be born with chromosomes which are already partially replicated. This means that instead of increasing the speed of DNA replication, cells increase the frequency of

A Helmstetter-Cooper model of the bacterial cell cycle

$\tau = 60$ minutes, no overlapping cell cycles



B Chromosome and size at initiation

ori = 2, size = 1

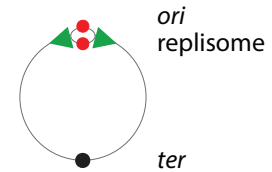


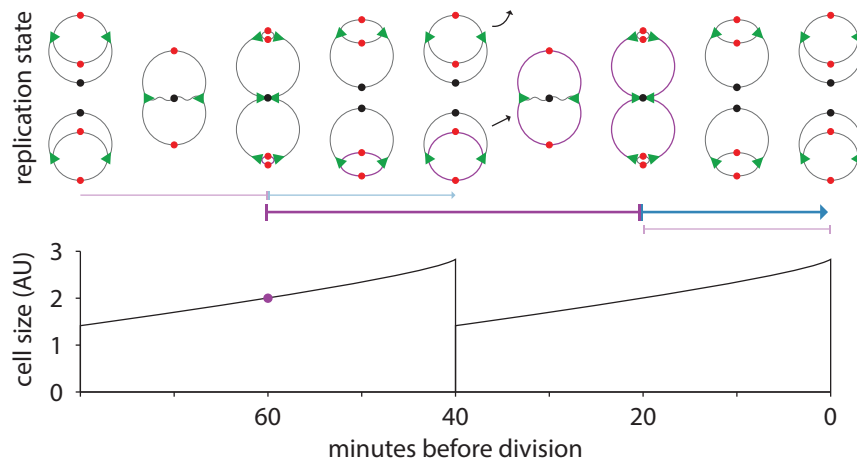
Figure 1.4: The bacterial cell cycle (slow growth). (A) The Helmstetter-Cooper model of bacterial cell division dictates when chromosome replication initiation begins assuming constant C (40 minutes) and D (20 minutes) periods. Cell size is given in arbitrary units but follows relationship of the Schaecter line such that $S \propto 2^{\mu}$. When $\tau = C+D = 60$ minutes, replication initiation (purple circle) and cell birth are coincident. The chromosome replication occurs during the first 40 minutes of the cells life. Daughter cells each inherit one complete and non-replicating chromosome. (B) The cell size per *ori* at initiation is the same as in faster conditions shown in Figure 1.5.

replication initiation. Intuitively, to keep replication and division in one-to-one correspondence, both events occur every τ minutes. When τ is less than $C+D$, the number of overlapping cell cycle n_{oc} is defined by $\text{floor}(C+D/\tau)$. This scenario of overlapping cell cycles leads to multifork replication. In this complex state, the circular chromosome simultaneously accommodates multiple sets of replication forks, all traversing from the replication origin (*ori*) to the terminus (*ter*).

Soon after the publication of what would become known as the Helmstetter-Cooper (H-C) model, William Donachie realized a striking feature connecting the cell cycle with cell size^{15,36} (Figure 1.6). In his letter to Nature, Donachie uses a graphical method calculate the cell size at chromosome replication initiation. The two major ingredients are the constant cell cycle duration $C+D$ and the exponential dependence of cell size on growth rate such that cell size is proportional to 2^{μ} . Under these assumptions, the size at initiation per replication origin is constant across

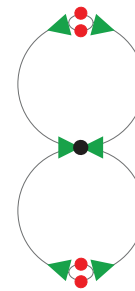
A Helmstetter-Cooper model of the bacterial cell cycle

$\tau = 40$ minutes, 1 overlapping cell cycles

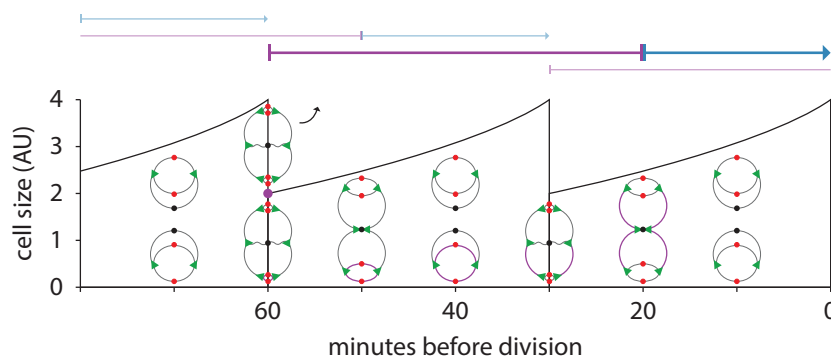


B Chromosome and size at initiation

ori = 4, size = 2



$\tau = 30$ minutes, 1 overlapping cell cycles (multifork replication)



ori = 4, size = 2

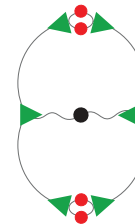


Figure 1.5: The bacterial cell cycle (fast growth). (A) Diagram same as in Figure 1.4. When $\tau = 40$ minutes and is less than $C+D$, replication initiation corresponding to a division event occurs halfway through the mother's life. Daughter cells are born with one partially replicated chromosome. When $\tau = 30$ minutes, replication initiation occurs as the grandmother divides and the mother is born. Because $\tau < C$ period, cells are born with a replicating chromosome that contains two sets of replication forks (6 total replisomes). (B) The cell size per *ori* at initiation is the same in all three conditions.

growth conditions. I refer to this normalized size at the initiation size.

This concept of the constant initiation size, or critical mass, has been the subject of debate over the last 50 years³⁸⁻⁴⁰. But recent high-throughput approaches at both the population and single-cell level have proved the strength of this principle (Figure 1.7)^{13,37,41}. In fact, the Schaechter line was found to be a special case of a more general principle³⁷. In this “growth law

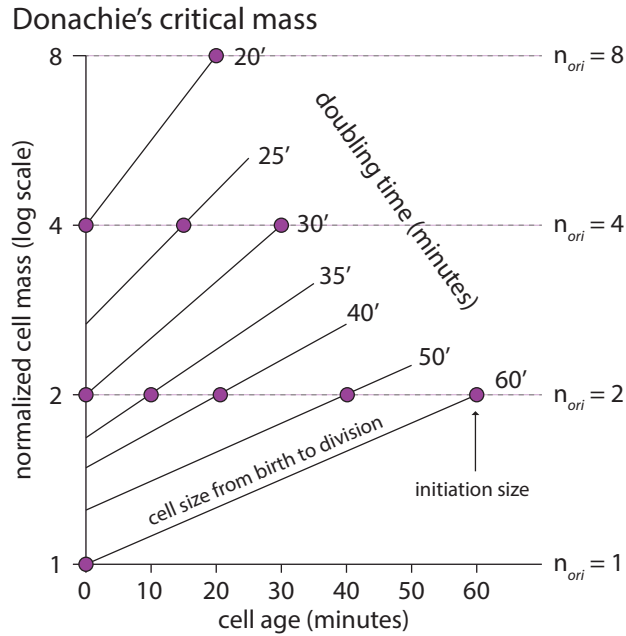


Figure 1.6: Donachie's critical mass. In this recreation of Donachie's original figure, the dual observations from the Schaechter line and the H-C model are combined to reveal constant initiation size, or critical mass^{15,16,32}. Each diagonal line represents the growth in size from birth to division for an average cell in seven growth conditions which bestow doubling times between 20 and 60 minutes. Cells double in size between birth and division, and the absolute birth size is determined by the relationship $S \propto 2^\mu$. Sizes are normalized to the birth size of cells growing with a doubling time of 60 minutes. The initiation size (purple circles) for each condition is determined simply by counting $C+D = 60$ minutes before division. For growth conditions where τ is a multiple of $C+D$, two initiation sizes are presented, one at birth and one at division. This reveals that the size at initiation is constant (times a power of two) in all conditions. When considering to the number of *ori* n_{ori} at initiation, the normalized initiation size $s_i = S_i/n_{ori}$ is invariant across conditions.

of unit cells," the average cell size is a function of a unit cell size (proportional to the initiation size), the growth rate, and the cell cycle duration:

$$S = S_0 \cdot e^{\lambda \cdot (C+D)} = S_0 \cdot 2^{(C+D)/\tau}$$

In this formulation, the exponential relationship of size on growth rate in the Schaechter line is because under nutrient limitation conditions, $C+D$ and S_0 is constant, so S is solely a function of λ . However, under a different inhibition conditions, including sublethal doses of

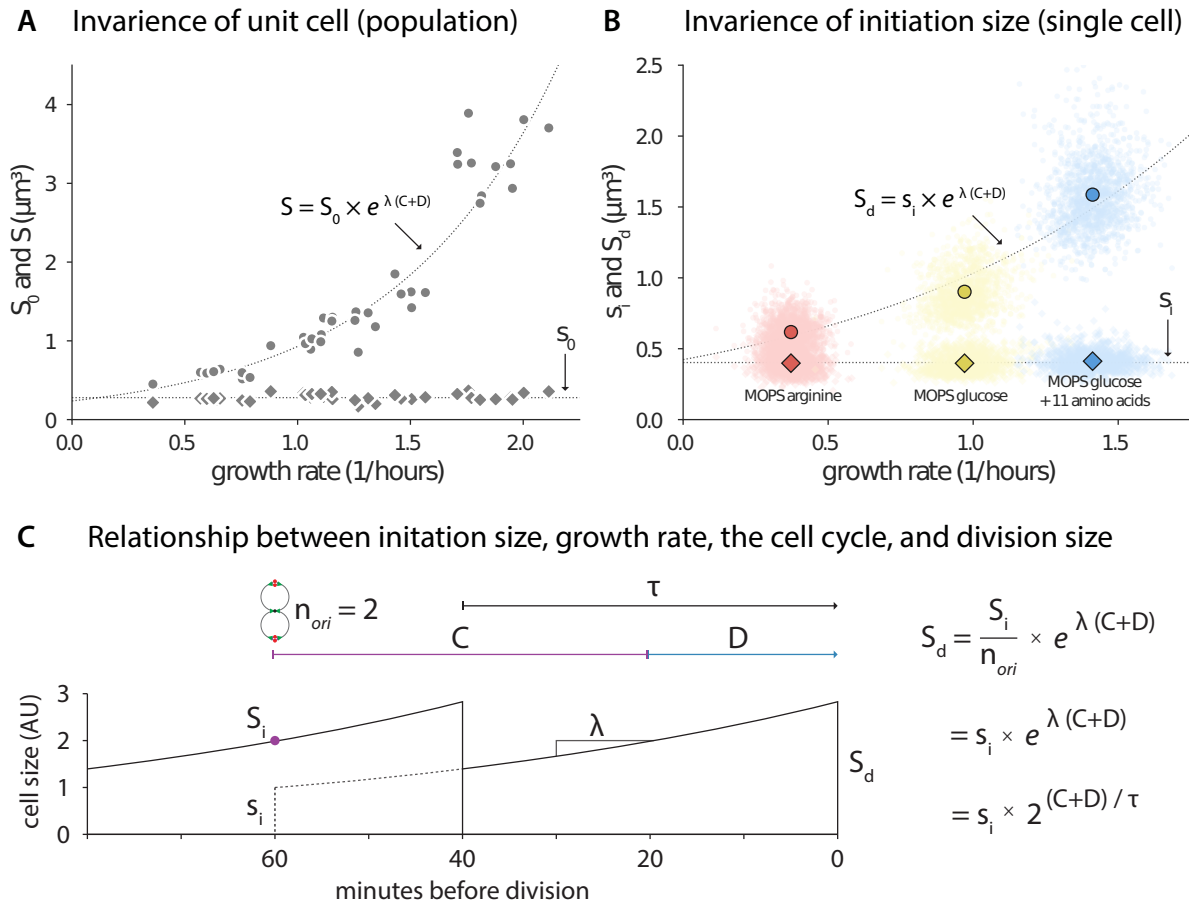


Figure 1.7: Modern confirmation of the invariant initiation size. (A) Population measurements of cell size (circles) and the unit cell size (diamonds) for many nutrient limited conditions confirms the foundational observations in bacterial physiology³⁷. (B) The invariant initiation size is maintained at the single-cell level¹³. Data from A and B is for *E. coli* NCM3722. (C) Schematic of a single cell relating the initiation size, growth rate, cell cycle duration, and the division size. $n_{ori} = 2$ (counted right before initiation).

antibiotics and genetic perturbation, all three parameters can vary. Yet S_0 was still invariant in all conditions tested except in genetic constructs where the replication initiation machinery was specifically targeted. This shows that the constant initiation size, intuited so many years ago, is an important principle in which to view bacterial size and cell cycle control.

While the aforementioned study was at the population level, it is useful to think of the initiation size in terms of individual cells (Figure 1.7). In this manner, the growth law of unit cells

can be rewritten:

$$S_d = S_i/n_{ori} \cdot e^{\lambda \cdot (C+D)} = s_i \cdot e^{\lambda \cdot (C+D)}$$

Note that the relationship between average population cell size and division size is $S = \ln 2 \cdot S_d$. This is derived from the age distribution of an exponentially growing population, and also means that the unit cell size and initiation size per *ori* are related by $S_0 = \ln 2 \cdot s_i$

This form may be easier to conceptualize, but it also reveals some issues. One is that, upon closer inspection, the relationship is tautological because it must be true based on the definitions of the inputs. This is due to the fact that the definition of D does not have a strong biological origin; it simply defines the time between replication and termination and division. This leads to a second problem in that the formula inherently suggests a strict pairing between replication initiation and division³³. This gives a false pretense for regulation which is ultimately not accurate, and discussed in the following chapters.

Finally, it is unclear what precisely defines the invariant initiation size. I speculate that at this size the cell has enough resources, either in reserves or through autophagy, to complete chromosome replication even if it were rapidly lose available resources after initiation.

1.3.4 Background on size and cell cycle homeostasis

Size homeostasis is a basic feature of life. Consider a group of newly born cells which exhibit a distinct distribution of sizes due to biological stochasticity. Without underlying coordination of growth and division, this distribution would diverge over generations, leading to cell sizes that span many orders of magnitude. Evolution has instead selected for organisms which do not take this gambit. Most microorganisms change their size by only twofold between birth and division, with the variability of the size distributions being much smaller than their mean⁴². This fidelity in the cell size maintenance points to the existence of size control mechanisms.

We now know the mechanism in which size homeostasis in bacteria is achieved. This

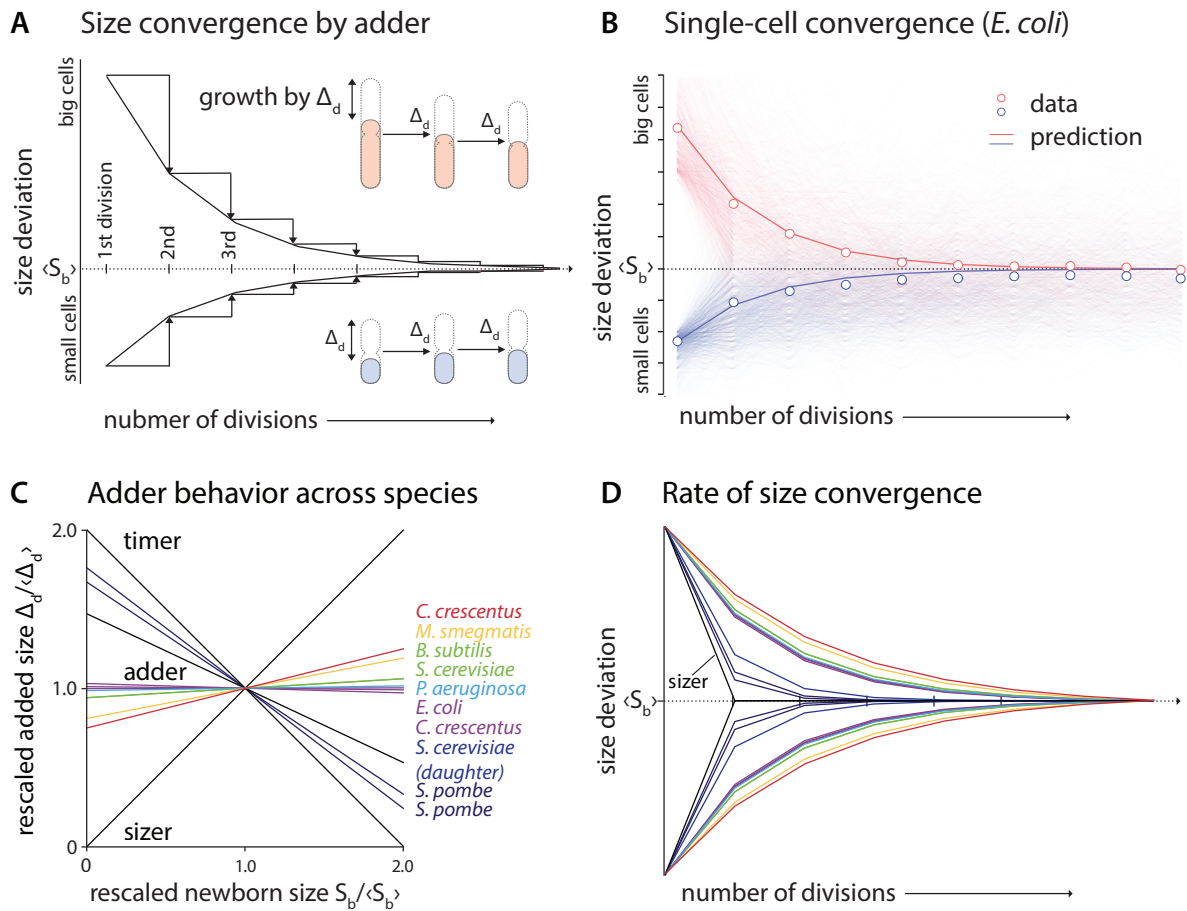


Figure 1.8: Size homeostasis by the adder principle. (A) Adder dilutes out deviations in size generation by generation following a geometric series. Cells born bigger (red) and smaller (blue) than average approach the population average division by division. The average birth size of the population is equivalent to the average added size. (B) Following the trajectories of a subset of large (red) and small (blue) cells confirms size convergence via adder. single cell traces (faint line) and average size agree with the prediction of the model. (C) Size homeostasis in many bacterial species is well described by the adder principle. (D) The rate of size convergence is a function of the slope of the lines in panel C. The more negative the slope, and closer to sizer the species behaves, and the faster it corrects deviations in size.

paradigm is called the adder, and simply states that cells add a constant size between birth and division Figure 1.8^{8,42}. This discovery was enabled by high-throughput single-cell experiments. These experiments allowed for correlation analysis of single-cell physiological parameters, which in turn proved the existence of the adder principle.

The etymology of adder comes in contrast to historical size homeostasis mechanisms

known as sizer and timer^{30,42}. With sizer, cells divide when they reach a preferred size. Sizer is intuitively attractive, as all deviation from the correct size would be corrected in a single generation. For timer, they divide a set amount of time after birth.

While both sizer and timer are obvious models for size control, they fail to explain single-cell growth data^{8,43-50}. The failure of these models is not apparent from the distributions, but requires correlations among the growth parameters. That is, if a cell divided at a critical size (sizer), then its size at division would be constant despite its birth size. If the cell instead divided after a constant time has elapsed since birth (timer), then generation time would be independent of the birth size. Neither the division size nor the generation time are constant relative to the birth size, inconsistent with either models (Figure 1.2).

In contrast to sizer or timer, cells following adder simply add on average a constant size, Δ_d , between birth and division regardless of their birth size. This alone ensures size homeostasis. To see this, consider a cell born exactly at Δ_d . This cell grows by Δ_d , doubling its size. When it divides in the middle its two daughters are born at the same size as the previous generation. However, a cell born smaller than Δ_d will more than double its size, and its daughters will be born slightly bigger than it was. Over successive generations, the difference between the initial newborn cell size and Δ_d progressively diminishes. Analogously, cells born larger than Δ_d also dilute out their size deviations with every division. The size of all newborn cells will converge to Δ_d after several consecutive divisions irrespective of their initial size. Consequently, the average newborn size of a steady-state population is identical to Δ_d , which is determined by the growth condition.

The adder principle has been shown to dictate size homeostasis for several evolutionarily divergent bacterial species such as *Caulobacter crescentus*, *E. coli*, *Bacillus subtilis*, and *Pseudomonas aeruginosa*^{8,42,45,48-50}. Importantly, adder describes cell size homeostasis without feedback. Cells employing adder passively converge their size within a few generations without the need to actively measure their absolute size. This is in stark contrast with the checkpoint-based

models in eukaryotes for coordinating growth and the cell cycle, which implies each cell actively control its own size. Dilution of size deviation through adder is conceptually similar to the dilution of molecular memory discussed earlier.

Adder was discovered in the context of division control, but it also the driving forces behind cell cycle control¹³. Deviations in the replication initiation size discussed above are corrected by an adder mechanism. In this case, it is the added size between two initiation events that is uncorrelated with respect to the initiation size.

It is important to note that the average initiation size is constant across growth conditions, but the division size scales with the growth rate. Yet within one condition, homeostasis for both is achieved through the adder principle. The mechanistic origins of adder are described in detail in relation to the threshold model and balanced growth in Chapter 4.

Chapter 2

Review of the Study of Replication and Division Coordination

2.1 Introduction

In this chapter we review the literature and models associated with replication and division coordination. We emphasize and favor the threshold model, tracking its history from the early days of bacterial physiology to its modern understanding. This chapter provides a more in depth background for the research presented in Chapters 3 and 4.

As discussed in Chapter 1, coordination of DNA replication and cell division is the fundamental feat bacteria accomplish in order to propagate. How they achieve this with such fidelity is one of the central questions of bacterial physiology and a major focus of research since the 1950s. It was also the target of pioneering work in quantitative biology, whereby researchers combine precision measurements and theoretical modeling to test rules that could govern biological systems. We will begin with a review of an important work in this vein from Arthur Koch, a meticulous thinker with a wide knowledge of microbiology (Section 2.2).

Koch's piece frames our main question of whether division is a consequence of replication

or if they are two separate processes. We then cover the history and description of the initiator threshold model and its application triggering replication and division (Section 2.3). We end that history with a deterministic description of the threshold model and its equivalency with the adder principle.

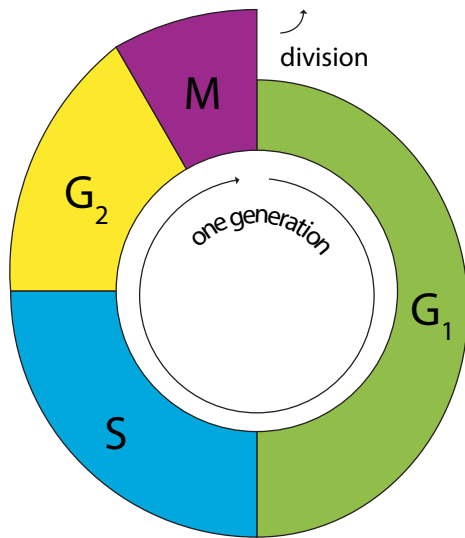
In addition to the threshold model, many molecular players and mechanisms have been discovered which influence the two processes. We will review some of these phenomena and the associated molecules, chief among them DnaA for replication initiation and FtsZ for cell division (Section 2.4).

2.2 Does replication initiation regulate division?

Whether replication initiation dictates division has been a central question of cell biology^{33,51–56}. For eukaryotic systems, it is universally taught that eukaryotic cells grow and replicate their DNA during interphase, and then segregate their chromosomes and divide during mitosis (M) (Figure 2.1A). Interphase is further divided into periods dedicated to growth (G₁ and G₂) and one where DNA synthesis occurs as well (S). Despite some recent questioning of the canon, strict ordering of these cell cycle phases is sacrosanct^{57,58}. Indeed, a central theme of the eukaryotic model is that cells employ control checkpoints before transitioning from one phase to the next.

For bacteria, diversion from the eukaryotic view was early, and the debate on if and how the cell co-regulates replication and division has carried on until the modern day^{13,41,59–61}. The fundamental issue is whether division is consequence of initiation, or if it has separate controls. The initial indication that the bacterial cell cycle differed from the eukaryotic sequence is that DNA synthesis occurred throughout the growth, not during a dedicated phase⁶² (Figure 2.1B). As discussed in Subsection 1.3.3 the field adopted the Helmstetter-Cooper (H-C) model as a basic framework in which to discuss the bacterial cell cycle³². However, while this model differs from

A Eukaryotic cell cycle



B Prokaryotic cell cycle (fast growth)

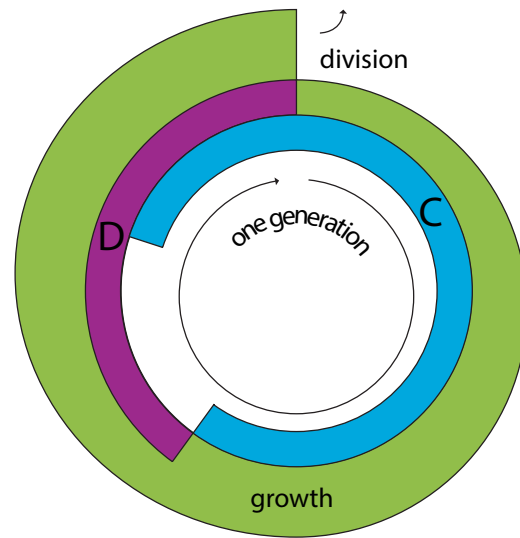


Figure 2.1: Eukaryotic and prokaryotic cell cycles. (A) The eukaryotic cell cycle is defined by discrete phases which do not overlap. Growth occurs during G₁, S, and G₂ (collectively known as interphase). DNA synthesis occurs during S. Mitosis, when the chromosomes are segregated and division occurs, is M phase. (B) Prokaryotes grow continuously throughout the cell cycle. Chromosome replication occurs during C period, and can start in the previous generation. D period defines the time between replication termination and division. Chromosome segregation begins before termination, concurrent with replication.

eukaryotic systems in that ongoing replication cycles can overlap, it still promulgates that the order of events are sequential. This sequence begins with replication initiation and ends with division, passing through intermediate steps such as nuclear segregation. This implies that, like with the eukaryotic cell cycle, one event must follow another in strict order. But is it fair to assume that division is simply a downstream consequence of initiation?

The remarkable constancy of C+D, and Donachie's insight that the size at initiation per origin is similarly invariant (at least in fast growth), increased the appeal of a replication centric viewpoint based on the H-C model. But while it is a useful conceptual framework, researchers questioned whether it explains the actual mechanism cells use to coordinate replication and division^{12,33}. The debate was fueled from many sources, including competing measure-

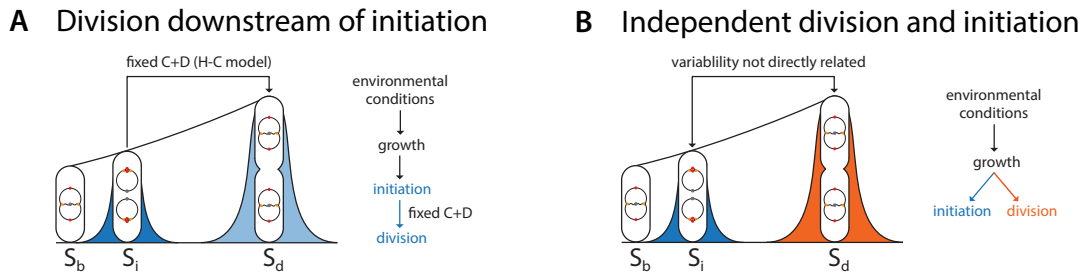


Figure 2.2: Classification of replication and division coordination models. Models describing the coordination of replication and division can be grossly grouped into two categories: models where division is directly regulated by initiation (A), and models where division and initiation are triggered by separate mechanisms tied to growth (B). In the first type of models, the variability in division size S_d should be explained by the variability in initiation size S_i plus noise. In the second type of model, the variability of the two measures should only be related insofar as they are both downstream of growth. Note that the birth size S_b is considered only as a function of S_d .

ments^{15,37,40,63}, the discovery of molecular mechanisms which regulate either process or mediate between them^{64–66}, and a general lack of quality of single cell data^{30,67}. As a result of this research, there are no shortage of models which attempt to explain replication and division coordination^{60,68–74}. Most models can be grouped into two major camps (1) those which hold that division is a down-stream process of replication initiation, and (2) those which treat replication and initiation as two independent processes (Figure 2.2). There is a third class of models in which initiation is triggered by division, but they are not widely held. One major drawback is that this class of models cannot describe initiation in cells which are waking from stationary phase as the previous division event is temporally distant.

Arthur Koch addressed this question directly in an extremely thorough work from which this section derives its name: *Does the Initiation of Chromosome Replication Regulate Cell Division?*³³. While this work represents just one approach, we review it in detail to introduce models and modes of thinking. Koch had a wide knowledge of bacterial physiology and comfort with quantitative approaches. The year in which this work was published influences its scope and insights. It is late enough that the insights of the Copenhagen school and other classic studies

of bacterial physiology, i.e., the principles outlined in Chapter 1, are established. Koch also had access to a computer capable of simulations which were not previously possible. However, it is early enough that many major discoveries made possible by molecular biology, particularly those concerning the proteins that regulate the cell cycle and their mechanisms, have not yet been made. Thus, Koch's approach was statistical and logical in nature, as he tested models to see how well they agree with the data. Specifically, he used the available data to calculate the coefficient of variation (CV) of physiological parameters and compared them to the predictions of various models.

Koch first outlines his assumptions about cellular growth. The foundational idea is that cells are chiefly concerned with growth, which he considers a continuous event. He believed the CV of growth rate should be small. He based this on the premise that the number of molecules involved in metabolism and biosynthesis are large, and those molecules are evenly divided amongst the two daughters. Ironically, single-cell growth rate is one of the main parameters for which he had little reliable data. Despite this, Koch's intuition was good; the CV of growth rate is one of the smallest of the physiological parameters, and the positioning of the septum is extremely precise (Figure 2.3).

While growth is continuous, the events of the cell cycle are discrete. This includes replication initiation, termination, nucleoid segregation, and division. Since in Koch's view growth is king, he postulates that the cell would never limit growth for the discrete events. This is supported by the fact that protein production requires the majority of cellular resources, compared to the modest amounts required for DNA synthesis or division⁷⁵. If replication and division are subservient to growth, he thinks they should be somehow triggered by cell size (the result of growth). A size based trigger is conceptually distinct from triggering an event at a certain time relative to another event.

In fact, a strict timer between birth and division would lead to cells of quickly diverging sizes. Since cells grow exponentially, a cell born large, growing for a fixed amount of time, would

Single-cell physiological parameter distributions

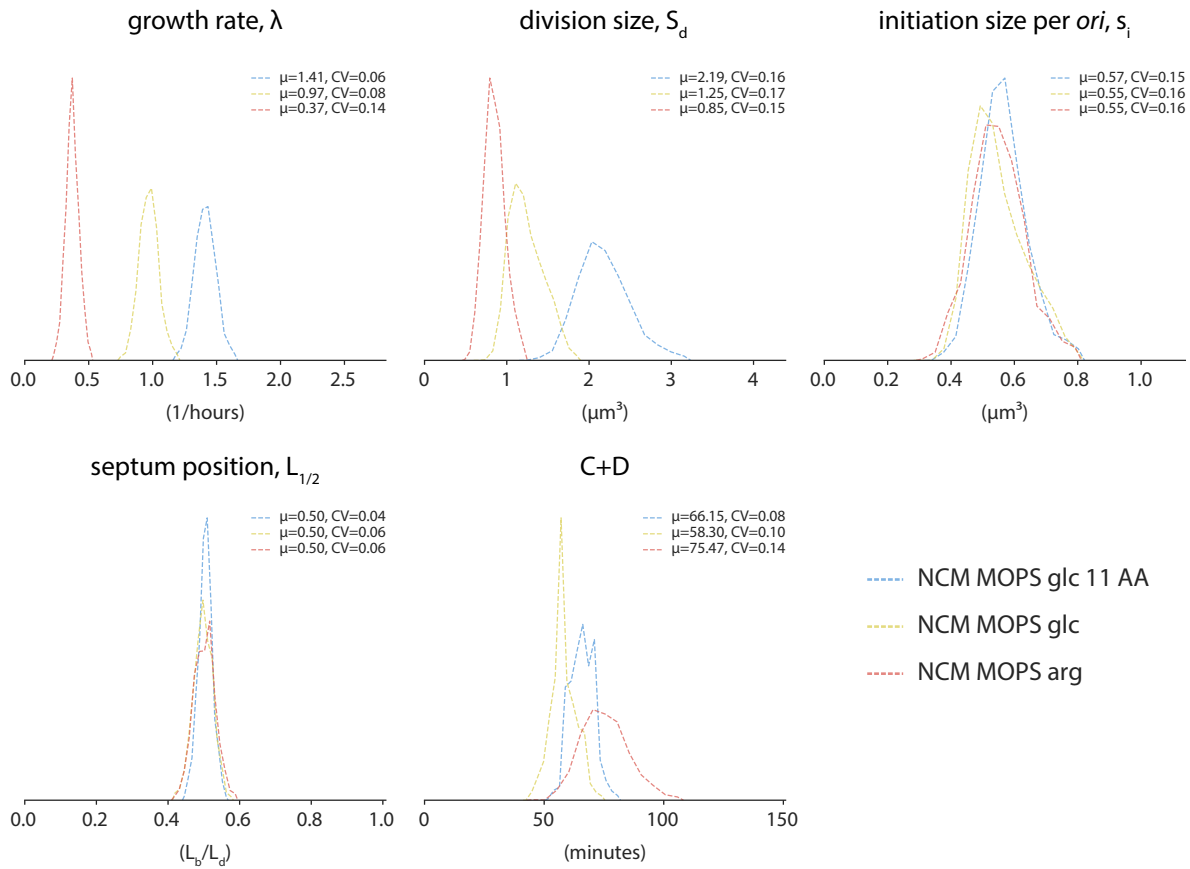


Figure 2.3: Comparison of CVs of discrete cell cycle events. The distributions and CVs of physiological parameters Koch used to show that 1) cell cycle events were subservient to growth and 2) initiation and division were triggered by independent events. NCM is *E. coli* NCM3722. Data is from Si and colleagues¹³

make daughters that are born larger than it was. The same applies for cells born small. Thus a pure timer cannot explain size homeostasis, but timer in conjunction with another mechanism could. For example, timer of length C+D (based on the H-C model) attached to Donachie's critical mass could potentially described cell size control and homeostasis.

Settled on the idea that size, the product of biosynthesis, is the key trigger for the events of the cell cycle, Koch narrows his question to how many triggers there are. Is replication initiation the only independent event, in which division inevitably follows? Or are there two (or more)

separate triggers for initiation and division (and nucleoid segregation and others).

Koch's further arguments are based on simulations of cellular growth using parameters from available data. This data comes from experiments which mostly use synchronization techniques to calculate the distribution of cell sizes at particular events, specifically birth, division, initiation, termination, and nucleoid segregation^{51,76-78}. His most used data comes from slow growth ($\tau = 120$ minutes). This is key, because at generation times greater than 60 minutes, we now know that C+D is not constant, and is in fact correlated with growth rate at both the population and single cell levels^{13,37}. Moreover, the initiation size also increases at the population level in slow growth.

In the first model tested, Koch modeled cellular growth simply by stating cells grow with growth rate λ (with no variability) from birth to a critical division size, which has a CV of 10-15%. Not surprisingly, this simulation (which accounts for the age distribution of cells), is able to reproduce the distribution of sizes in an exponentially growing population. This is his first piece of evidence that division is controlled by a size trigger (i.e., a sizer). Koch did not have access to single cell correlations among physiological parameters. If he had, as discussed in Subsection 1.3.4, he would have concluded that a sizer model does not fit the experimental data.

He then tested a model in which initiation is triggered at a fixed size, and division follows a fixed time later. For the above test, he just compared size distributions, but for this and subsequent tests he incorporated labeling data which gives an indication of when DNA synthesis is ongoing as a function of cell size. For this H-C style model, the distribution of sizes and the replication state of simulated cells does not match the experimental data. This is because at slow growth C+D is no longer constant and instead scales with generation time in individual cells^{13,41}. If he had modeled fast growing cells, where C+D is constant, the H-C model would better reproduce the observed distributions in sizes and replication state.

Instead, he rejected the H-C model and then tests an independent trigger model. In this model, both initiation and division are triggered at a critical size, and each given their own CV.

This model can reproduce both the distribution of sizes and the replication state of cells as a function of their size. However, to do so requires simulation CV parameters of 10-15% for division size and a 25% for initiation size. For Koch, this indicates that initiation cannot logically control division. This is because a noisier process cannot control a less noisy process due to the propagation of error.

Our single-cell single data at fast growth actually shows that the CV of initiation size is comparable to that of division size (15%), but Koch's logic still holds (Figure 2.3). For division to have such a relatively small CV, and be a direct downstream consequence of initiation, would require that the intermittent events occur with precision in time that is not reflected in the data.

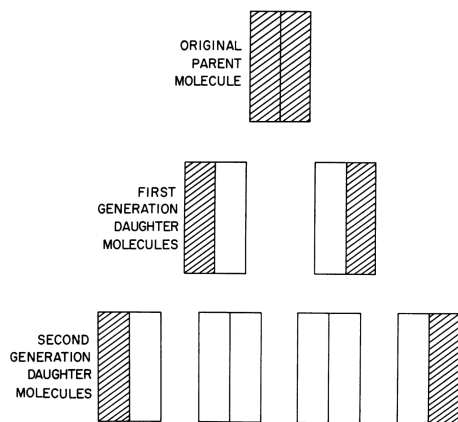
Importantly, Koch's simulations treat each cell as memoryless individuals (that is, a Markov process). This means that the parameters chosen for each daughter cell, i.e., initiation and division size, are drawn randomly from a Gaussian distribution without regard to the parameters of the mother. However, this does not reflect the biology. Instead, "memory" between consecutive generations leads to non-trivial auto-correlations in physiological parameters between mothers and daughters. The lack of auto- and cross-correlation data greatly limits Koch's analysis. Unfortunately, he simply did not have access to this data and he mentions correlations only briefly in his work. Nonetheless, Koch's clear identification and formulation of the problem is a solid stepping stone in addressing whether replication initiation controls division or if the two are independent events.

2.3 The initiator threshold model

We will now cover the history and development of the initiator threshold model. This model was initially conceived and developed in the context of replication initiation.

A Semiconservative replication

Meselson and Stahl, 1958



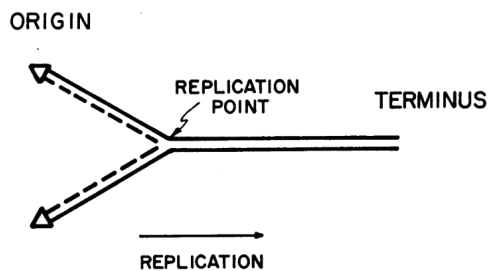
B Circular, closed chromosome

Cairns, 1963



C Unidirectional replication

Yoshikawa and Seuoka, 1963



D Replicon model

Jacobs, Brenner, and Cuzin, 1963

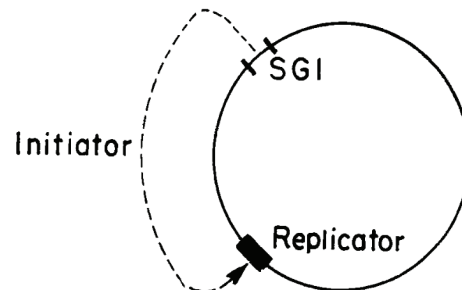


Figure 2.4: Early experiments and models of DNA replication in bacteria. A wave of discoveries following determination of the molecular structure of DNA led to the introduction of the replicon model 10 years later. (A) Watson and Crick famously hinted that the double helix suggests that one DNA strand can serve as a template for another⁷⁹. Meselson and Stahl showed that indeed each daughter cell inherits half the DNA of the mother, leading to the semiconservative model of DNA replication⁸⁰. (B) Cairns showed microscopically that the bacterial chromosome is a closed, circular ring⁸¹. (C) Using marker frequency analysis, Yoshikawa and Seoka devised a model, also suggested by Cairns, that replication proceeds from one point, the origin, to another point, the terminus, on the chromosome. (D) The replicon model maintains that a chromosome produce an initiator from a structural gene (SGI) which triggers replication for that chromosome at a specific origin (replicator)⁸².

2.3.1 The replicon model

In the previous section we identified a central question in whether division is a downstream result of initiation or if it is controlled by an independent trigger. But in either case, we must identify a mechanism by which at least initiation is triggered once per cell cycle. This question was of central importance in the early '60s after a series of insights into the nature of the bacterial chromosome.

In the 10 years after the realization of the structure of DNA, research into the bacterial chromosome and its replication resulted in a number of observations (Figure 2.4). This includes that the bacterial chromosome was a closed ring, replication was nearly continuous throughout the division cycle, and that replication proceeds linearly on the chromosome^{62,79-81,83}. Based on this foundation, along with significant insight from the replication of F plasmid and phage, François Jacob, Sydney Brenner, and François Cuzin proposed the replicon model for DNA replication⁸². In this model, a genetic element contains an origin of replication (*ori*), and the element must be replicated as a whole. In addition, the genetic element must contain a system which signals the control of its own replication.

This last point concerning a signal is a bit obscure, and is influenced by the authors' experience with the *lac* system and phage λ . Controls for those two genetic systems are epitomized by a repressor molecule which negatively controls expression via an operator until some signal releases the repressor^{84,85}. However, they did not believe that negative regulation can explain DNA replication in some lytic phage mutants. So they instead argued for an active control of replication, proposing an activator element (a protein) known as an *initiator*. This vocabulary has survived through today.

2.3.2 Beginnings of the initiator threshold model

The paper by Jacob and colleagues introduced the influential replicon and initiator models. However, it did not address how replication initiation may be connected to growth. Five years later, Helmstetter, Cooper, Pierucci, and Revelas synthesized the recent breakthroughs in conceptualizing the bacterial cell cycle to formally introduce a threshold model for initiation¹².

The threshold model for replication for initiation represents a conceptual breakthrough which ties together the major aspects of bacterial physiology: growth, cell size, and the cell cycle. While it has oscillated in and out of the scientific consciousness, we now know that it explains cellular behavior under a huge range of growth conditions and perturbations^{13,37}. We will more formally define our iteration of this model in Subsection 2.3.5, but here we will outline the original authors' understanding.

In their formalism, they recognize a number of tenets. The first is that for cells growing with doubling time τ , replication initiation also occurs every τ minutes. This is a necessary requirement to ensure the one-to-one pairing between replication and division. The second is that the accumulation of an initiator protein for a period of τ minutes allows for initiation to commence. This statement is based on experiments in which protein synthesis is inhibited for a period of time and then restored, which delays initiation by an equivalent time⁵². Though subtle, this is an extremely important point because it implies that the initiator molecule is indeed a protein, and not some other genetic element or macromolecule. They also incorporate the observation of Donachie that initiation occurs at the same cell size per *ori*, and state that the amount of initiator required to begin replication is the same in all conditions.

The beauty of the initiator threshold model is that it elegantly explains the contemporaneous data without invoking complex regulatory mechanisms. Though they recognize that they do not have a handle on the kinetics of initiator accumulation, the most basic assumption is that it increases in proportion to growth rate. They also do not know the mechanistic action of the initiator, and what happens to it after initiation. Those details, while the subject of significant

future debate, are not necessary to understand the basic framework of initiation control.

In their model, cells grow and accumulate initiators until a critical size per *ori*, at which point all cells divide C+D minutes later from that moment. This ensures a one-to-one correspondence between initiation and division. In the meantime, cells still continue to grow and accumulate initiators. When $\tau = C+D$, cells are haploid, and initiate at birth. When τ is smaller than C+D, overlapping cell cycles ensue. The cell size increases because cells still grow for C+D minutes from the initiation size, but they are growing faster (Figure 1.6). The absolute initiation size increases by factors of two while the initiation size per *ori* stays the same, as cells become diploid or higher ploidy.

Importantly, the influence of the H-C model means that the threshold model is only applied to initiation (hence the initiator threshold model), and division is a downstream consequence. Part of the motivation for this belief were experiments in which replication is stopped part way through, which often inhibits division^{86,87}. In either case, the authors give a note of caution in reference to the issue of how replication and division are connected:

While the accumulation of a unit of initiator may ‘cause’ the inception of a new round of replication, the possibility of a causal relationship between the completion of a round of replication and cell division should be treated with caution. The evidence indicates only that termination of a round or replication is a necessary condition for cell division, and not necessarily a ‘trigger’ of division¹².

2.3.3 Development of the initiator threshold model

This subsection covers further developments to the initiator threshold model. We do so only briefly, as this topic has been covered extensively elsewhere⁸⁸⁻⁹⁰.

The initiator threshold model became the basis for the conversation around replication initiation control in the field and in turn the focus of additional research. At the same time as the model described above was suggested, Prichard and colleagues formally introduced a variation known as the inhibitor titration model^{36,91}. In this model, it is not an initiator molecule which

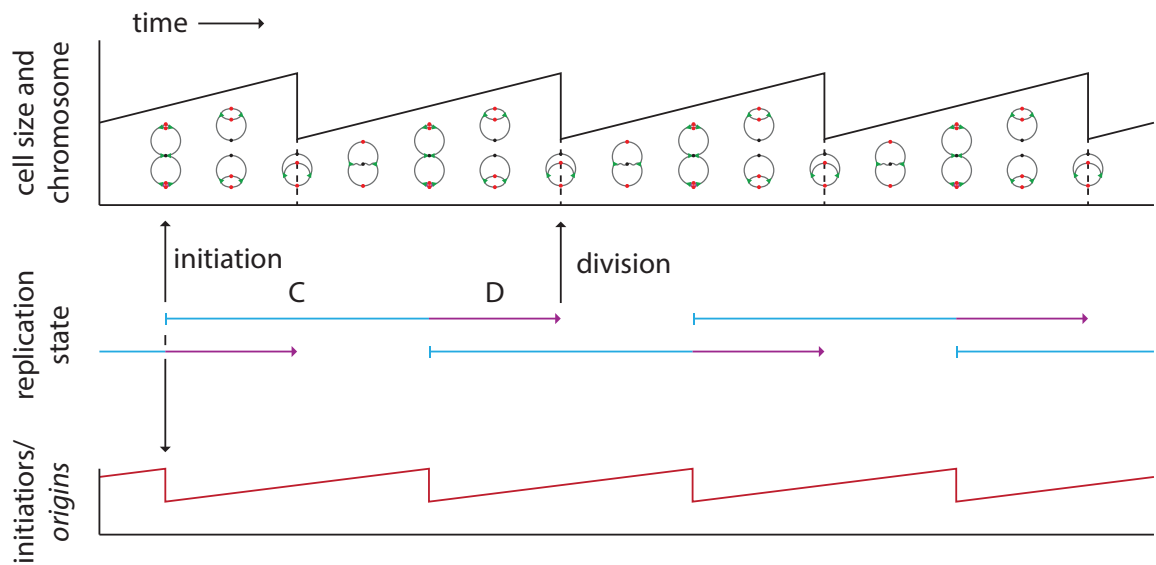
accumulates to a certain level to trigger division, but an inhibitor molecule which dilutes to a certain level. There exists a subtle but distinct difference between these two models in terms of the quantity of initiator or inhibitor molecule over the cell cycle. The initiator threshold model assumes that the initiator is maintained at a constant concentration, increasing its total number with volume. The inhibitor titration model assumes that the inhibitor is maintained at a constant copy number per *ori*, decreasing its concentration with volume. However, no inhibitor molecule which fits the model's description has been found, and later theoretical work showed that an inhibitor titration model cannot attain the observed CV in initiation size.^{90,92}

In line with an initiator molecule which accumulates with growth and triggers initiation at a certain level, Sompayrac and Maaløe introduced the autorepressor model³⁸. This model describes how the concentration of such a molecule could remain constant throughout the cell cycle despite fluctuations in growth. Simply put, the molecule represses its own transcription. When it is in overabundance its production is reduced, and when it is at a dearth its production is increased.

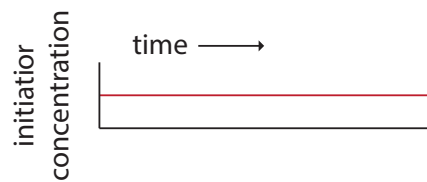
The autorepressor model formally states that it is the number of initiator molecules per origin that is the trigger for initiation. When initiation commences, the number of origins doubles by an integer number, causing a discrete halving of the ratio of initiators to origins. As the cell grows in volume, the ratio increases until the next initiation is triggered. This is so even though the initiators maintain a constant mass fraction of the proteome (Figure 2.5).

Developments on the initiator threshold model from this point were heavily influenced by the identification of DnaA, which is the replication initiator^{94,95}. A key discovery was that of DnaA-boxes. These are genetic elements near *oriC* and elsewhere that bind DnaA^{96,97}. This provides a mechanistic explanation of how the cell can plausibly measure the ratio of DnaA to the number of origins. The number of DnaA-boxes increase when the chromosome replicates, and the cell is effectively filling those boxes with DnaA until they are saturated, triggering initiation. Hansen and colleagues extended this notion to explain how cells avoid reinitiation in what is

A Threshold model for initiation



B Autorepressor model



C Initiator titration

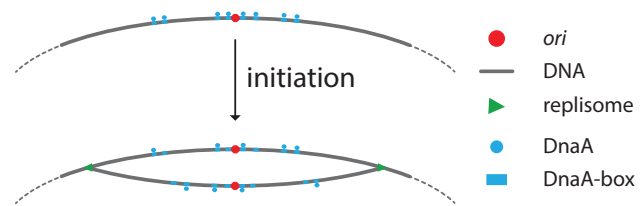


Figure 2.5: Threshold model for initiation. (A) In Helmstetter and colleague's threshold model for initiation, an initiator molecule is accumulated at the growth rate and thus remains a constant fraction of the total proteome¹². At a certain fixed amount, initiation is triggered. Replication and division follow during the C and D periods, at which the cell divides. While this model holds that division is downstream of initiation, the authors caution that this does not mean initiation triggers division. (B) The autorepressor model describes how a protein could be kept at a constant concentration and states that initiation could occur when the number of initiators per origin reaches a threshold³⁸. (C) The discovery of DnaA-boxes and the initiator titration model give evidence for how the cell can monitor the DnaA to origin ratio⁹³.

known as the initiator titration model^{93,98}. Further discussion on DnaA and its role as the initiator are covered in Subsection 2.4.1.

2.3.4 The threshold model in application to division

This subsection covers the inception of the threshold model in the context of division as opposed to initiation.

In the '70s and '80s, molecular biologists committed considerable resources to identifying genes and their protein products. In this era, the holistic approach to bacterial physiology faded as excitement about new genetic tools allowed researchers to uncover the molecular players on which they had previously speculated. Despite this shift of focus, members of the previous generation kept the physiological questions in mind as they developed new skills and trained new students.

In Section 2.4, I will cover some of the major molecular discoveries of this time and how they relate to replication and division coordination. In this section however, I will elaborate specifically on a school of thought that sees division as a parallel process to initiation. In this viewpoint, division is controlled by a threshold mechanism akin to initiation.

I believe this thinking originated from none other than Donachie himself, and later championed by his student Joe Lutkenhaus and others. The hint that division was controlled by a “division factor” which must accumulate came in a 1974 paper by Teather and colleagues, but predated the discovery of any such molecule⁹⁹. Using a division mutant, Teather hypothesized that cells have a limited capacity for division that normally couples one division to a certain amount of cell growth. The mutant that they used, which was the as-of-then unidentified *min* mutant, does not divide just at the midcell but also at the cell poles, producing anucleate minicells¹⁰⁰. A characteristic of this mutant is that the population contains not only nonviable minicells, but also that the viable cells are longer than normal. They reasoned that minicell divisions come at the expense of normal divisions, resulting in these long cells. They then calculated the theoretical size distribution of cells which can at every generation either divide in a normal location or at the cell poles, and it matched well with the experimental data (Figure 2.6).

The conclusion of Teather and colleagues was tied up with the chromosome-membrane

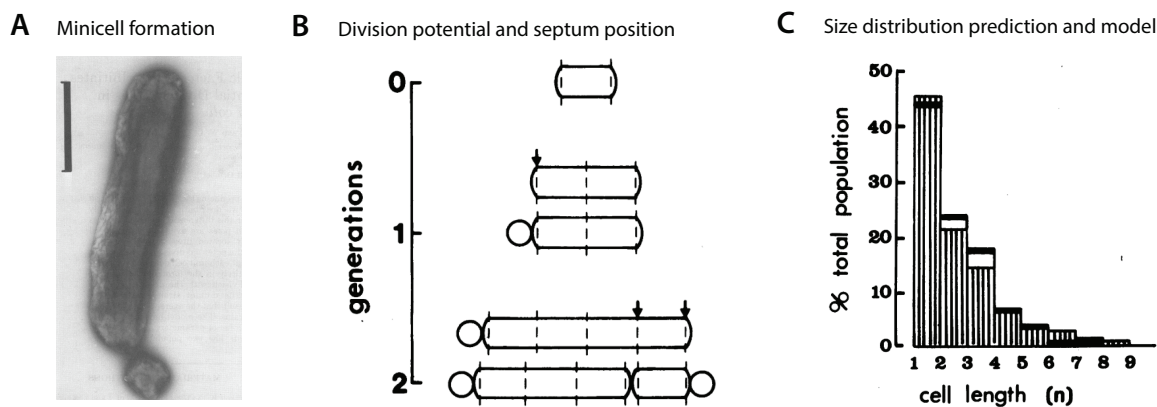


Figure 2.6: Division potential model by Teather and colleagues. (A) The mutant used by Teather and colleagues could divide at a normal position or at the cell pole, producing a minicell. Scale bar is $1\mu\text{m}$. (B) In their model, each division event is associated with the growth of the cell by one unit of length equal to the birth length. The cell could then spend this division potential at the cell poles or at any multiple of the unit length along the cell body with equal probability (dashed lines are potential division sites, arrows show where division occurred). Note that the adder principle is implied in this model though it had not yet been discovered. (C) The distribution of cell lengths at birth (excluding minicells) was calculated based on the model (thick horizontal bars) and compared to the experimental distribution (vertically shaded area). Cell length is presented in number of unit lengths n . All panels reproduced from the article⁹⁹.

tethering hypothesis and the idea that the division factor only accumulated after termination. But behind this speculation, the central idea that division requires its own protein factor whose accumulation is attached to growth provided a foundation for the threshold model to be applied to division.

The idea that synthesis of specific proteins, independent of replication, was required for division was supported by studies with thermosensitive *ftsA* (previously called *divA*)^{101,102}. But it was the discovery and investigations of *ftsZ* that gave more traction to this idea^{103,104}. This was based on observations that increasing the gene dosage of *ftsZ* delays filamentation during stress response. In fact, overexpression of *ftsZ* caused minicell formation in otherwise normal cells¹⁰⁵. That is, additional *ftsZ* increases the division capacity of the cell, leading to smaller cells. This is akin to the overexpression of *dnaA*, which causes cells to initiate at a smaller size as they attain the requisite threshold more quickly. In a return to Teather's original work, it was shown that

overexpression of *ftsZ* (and especially overexpression of both *ftsZ* and *ftsA*) rescues *ftsZ* mutants to produce wildtype cell size distributions^{106–108}.

The above works consider a protein required for division, but they do not clearly attach the accumulation of that protein to cell size or growth rate. Some of the papers connect it to cell size implicitly, yet there is not a direct link between growth and accumulation. This may be because they do not necessarily believe that accumulation is proportional to the instantaneous elongation rate. Instead the papers tend to support arguments that, while you need to accumulate a division factor to trigger division, the accumulation of that division factor is cell cycle dependent^{99, 107, 109}.

Weart and Levin show that contrary to this view, FtsZ, the likely division threshold molecule, has a constant concentration during the cell cycle (this supported by experiments detailed in Chapter 4). This is congruent with the idea that FtsZ is produced in proportion to the instantaneous growth rate, similar to DnaA. In a later review, Chien, Hill, and Levin argue that accumulation and FtsZ assembly are both continuous throughout the cell cycle, resulting in the formation of a complete ring that triggers division⁵⁹. This model disconnects division triggering from replication and gives it its own, independent threshold controlled primarily by growth.

2.3.5 The threshold model, balanced growth, and the adder principle

Based on measurements of FtsZ accumulation and division in single cells, we support the notion that division is controlled by a threshold mechanism analogous but independent of replication initiation. Moreover, this threshold mechanism, paired with balanced biosynthesis, is the driving force behind the adder principle¹³. This subsection formally defines this model. This is a simple deterministic version of this model to demonstrate the unity between a threshold mechanism and the adder principle. Variations of this formulation have been produced previously^{13, 38, 110}. For a more in-depth mathematical treatment of the adder principle, see Taheri-Araghi et al.⁸ and Jun et al.¹⁴.

For this demonstration, we will consider the triggering of division, but the same system

applies to initiation. We make the following assumptions.

1. (Threshold) There is a protein or group of proteins which triggers division, which we will call FtsZ for simplicity and directness. FtsZ triggers division when it reaches a threshold number.
2. (Balanced growth) FtsZ is produced according to balanced growth, meaning that its production is proportional to volumetric growth.

At steady-state, the concentration of a protein under balanced growth is constant. Consider the mass fraction of FtsZ ϕ_{FtsZ}^* , where the asterisk indicates it is at steady state. The total mass of FtsZ m_{FtsZ} is related to the total mass of the cell M by:

$$\frac{dm_{\text{FtsZ}}}{dt} = \phi_{\text{FtsZ}}^* \frac{dM}{dt}$$

We convert mass to copy number of FtsZ N_{FtsZ} , by way of the individual mass of one FtsZ $m_{1\text{FtsZ}}$, the density of the cell ρ_c , and the cell volume V . The steady-state concentration of FtsZ is c_{FtsZ}^* and is equal to:

$$c_{\text{FtsZ}}^* = \phi_{\text{FtsZ}}^* \frac{\rho_c}{m_{1\text{FtsZ}}}$$

On the left hand side, FtsZ concentration is defined as:

$$c_{\text{FtsZ}} = \frac{N_{\text{FtsZ}}}{V}$$

The mass of all FtsZ is defined by:

$$m_{\text{FtsZ}} = N_{\text{FtsZ}} \cdot m_{1\text{FtsZ}}$$

And the cell mass is:

$$M = V \cdot \rho_c$$

This allows us to rewrite the relationship between FtsZ and cell mass to be between copy number and cell volume:

$$\frac{dN_{\text{FtsZ}}}{dt} = c_{\text{FtsZ}}^* \frac{dV}{dt}$$

We now take into account the threshold assumption to stipulate that division occurs when FtsZ reaches the copy number N_{FtsZ}^d . The cell accumulates these FtsZ over its generation time $\tau = t_d - t_b$, and when a cell is born inherits half of these FtsZ such that:

$$N_{\text{FtsZ}}^d = N(\tau)$$

$$N_{\text{FtsZ}}^b = \frac{N_{\text{FtsZ}}^d}{2}$$

Recall that cells grow exponentially from birth to division:

$$V_d = V_b e^{\lambda \tau}$$

We can then consider the added volume between birth and division, $\Delta_d = V_d - V_b$ in terms of accumulation of FtsZ:

$$\frac{dN_{\text{FtsZ}}}{dt} = c_{\text{FtsZ}}^* \frac{dV}{dt}$$

$$N_{\text{FtsZ}}^d - N_{\text{FtsZ}}^b = c_{\text{FtsZ}}^* (V_d - V_b)$$

$$N_{\text{FtsZ}}^d - \frac{N_{\text{FtsZ}}^d}{2} = c_{\text{FtsZ}}^* (V_d - V_b)$$

$$\frac{N_{\text{FtsZ}}^d}{2c_{\text{FtsZ}}^*} = \frac{N_{\text{FtsZ}}^b}{c_{\text{FtsZ}}^*} = \Delta_d$$

Which states that between birth and division cells must on average accumulate the amount of FtsZ with which they are born. This is the adder principle.

2.4 Molecular players and associated models

In this section, we discuss some of the molecular players and other mechanisms thought to pair replication initiation with division.

Cell cycle coordination was often born out of studies of mutant cells in which either replication, division, nucleoid segregation, or some other critical aspect of the cell cycle was disrupted^{87,94,111}. Identification of the culprit molecules were backed by increasingly powerful genetic and microscopy techniques of the '90s and '00s. Consequently, there is no shortage of mechanistic models which account for replication and division fidelity.

The coordination between replication and division from a molecular perspective is the subject of a large number of reviews^{66,74,87,112–115}. I will not attempt to reproduce this work, but instead focus on the two key molecules of replication (DnaA) and division (FtsZ), as well as a few systems for which I have relevant data. I want to emphasize that this means I will not address important and well studied mechanisms such as the Min system^{65,100,116}. In addition, a number of intriguing and unique systems have discovered in diverse prokaryotes^{74,117}. However, I will focus on those active in *E. Coli*.

2.4.1 *dnaA* and replication initiation

In this section we will briefly cover DnaA and the molecular underpinnings of initiation.

The discovery of the DnaA protein gave a molecular face to the replicon model, which calls for both an initiator and a replication origin. In fact, Jacob and colleagues' 1963 paper mentions a mutant that contains an (unidentified) thermosensitive DnaA, which is incapable of initiation at non-permissive temperatures⁸². Kohiyama, of Jacob's lab, identified that mutant, and over the rest of the decade multiple labs found similar mutants and they were eventually ascribed to the *dnaA* locus⁹⁴. Follow up work further characterized the *dnaA* gene locus and its vicinity^{118,119}.

At a similar time, the nature and location of the replication origin was being investigated^{120,121}. Both *dnaA* and *oriC*, as the origin was named, were found to be located near the *ilv* locus. Biochemical, genetic, and microscopic experiments confirmed that DnaA does indeed bind to *oriC*, cementing its position as the initiator molecule⁹⁵⁻⁹⁷. While the exact mechanisms of initiation by DnaA is not totally understood, generally it is believed that DnaA forms filaments at *oriC*, melting the local DNA structure and allowing the replication forks to assemble^{88,89}.

There are many regulatory systems that modulate the binding of DnaA to *oriC* and thus regulate the timing of initiation¹²². To prevent re-initiation, DnaA is sequestered to additional binding sequences⁹⁸. DnaA is an ATP/ADP binding protein, and as it is active in the ATP bound state, cycling between either state provide an additional level of control¹²³. The concentration of DnaA is kept tightly controlled as it negatively regulates its own expression as predicted by the autorepressor model^{38,124,125}.

However, for our purposes it is sufficient to regard these molecular mechanisms as auxiliary systems which increase the precision of replication initiation. The primary method of regulating replication is accumulating DnaA to a certain threshold, at which initiation is triggered. The accumulation is tied directly to the instantaneous growth rate. Importantly, many studies have shown that, within a certain range, increasing or decreasing the concentration of DnaA inversely affects the initiation size^{13,37,39,93,95,126}.

2.4.2 *ftsZ* and division

I will now provide some historical and molecular background on FtsZ and its role in division.

Above, we discussed FtsZ in relation to a threshold model for division. However, much of the work on this influential protein was and is concerned with its spatial organization, molecular behavior, and binding partners. In the '60s, parallel to work discovering temperature sensitive initiation mutants, some labs were also isolating mutants deficient in division^{127,128}. Because

FtsZ forms a ring at the midcell

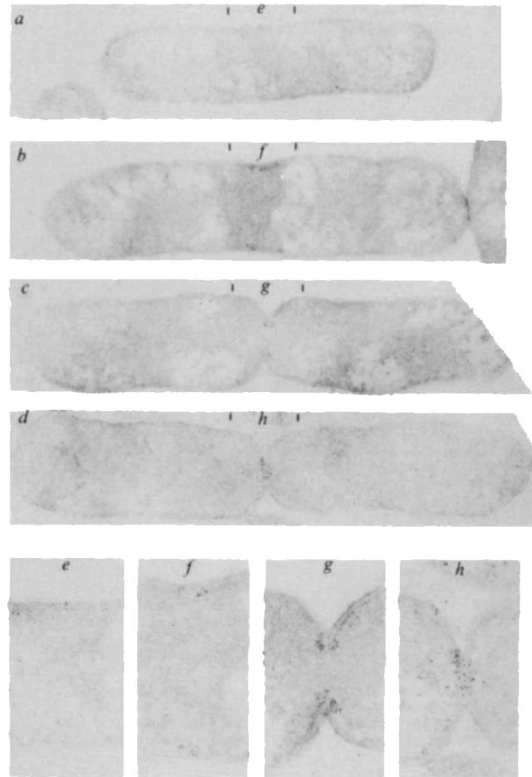


Figure 2.7: First image of FtsZ localization. First image from Bi and Lutkenhaus showing FtsZ forming a ring at the midcell during division¹³². FtsZ was tagged and imaged via gold-labelled antibodies and electron microscopy, and appear as small dark dots on the micrographs. Fluorescent immunolabeling and fluorescent fusion proteins were later used to image FtsZ^{133–135}.

aborted DNA replication often leads aborted division, it can be hard to identify mutants which contain genes specifically associated with the division machinery. Nevertheless, Piet van de Putte and colleagues identified such mutants, giving them the name *fts* for “filamentous growth is thermosensitive”¹¹¹. Additional work in this area often revolved around the delay of division due to DNA damage, known as the SOS response, resulting in discoveries of the *lon* and *sul* genes^{129–131}.

As mentioned previously, it was Joe Lutkenhaus in Donachie’s lab that truly identified the locus that contained *fts* mutants, naming both *ftsA* and *ftsZ*^{102,103}. These two genes covered many of the previously discovered mutant strains. Later, in his own lab, and aided by new tools

in imaging, he showed that FtsZ forms a ring structure at the midcell in association with the pinching septum (Figure 2.7)¹³². This marked an important turning point in the field. Many labs, excited by the prospect of a prokaryotic cytoskeleton, put serious effort in understanding FtsZ's biochemical and localization characteristics^{133,134,136,137}. The result is a formidable body of research concerning FtsZ. I will group the discoveries into two major (though interrelated) categories.

The first category of FtsZ research concerns its highly dynamic nature¹³⁸⁻¹⁴⁶. Generally, FtsZ is can be thought of as a monomer that polymerizes to form filaments, the result of which is the Z-ring^{137,142}. Biophysical work and increasingly powerful imaging has most recently determined that FtsZ polymers in fact treadmill, perhaps directing peptidoglycan synthesis¹⁴⁷⁻¹⁴⁹.

The second category are studies which looked into the assembly of the Z-ring. Here, researchers learned that the ring is actually a highly complex structure containing more than a dozen proteins¹⁵⁰⁻¹⁵⁵. For example, while FtsA fell out of the spotlight during the '90s, it and many other *fts* proteins colocalize with FtsZ at the midcell to form what is known as the divisome. Assembly of the divisome in relation to the cell cycle provided more clues about the regulation of division^{133,151}.

Many investigations were also aimed at FtsZ's regulatory binding partners, which affect both its dynamic and spatial properties. For example, SulaA, which delays division during SOS, was found to inhibit FtsZ polymerization, giving a molecular mechanisms to long-studied stress response¹⁰⁴. Other proteins were found to help bundle FtsZ, or connect it with other aspects of the cell cycle^{66,74,115,142}. Some of these proteins are discussed in the following sections.

When considering the threshold model, and similar to how we treat DnaA, it is not important to consider all the individual molecular players of the divisome and the various binding partners. We will simply treat the accumulation of FtsZ at the midcell as a representative of the division apparatus, which must reach a critical amount to trigger division. This assembly happens at a pace and location which is the sum result of all of FtsZ's various binding partners. We thus do

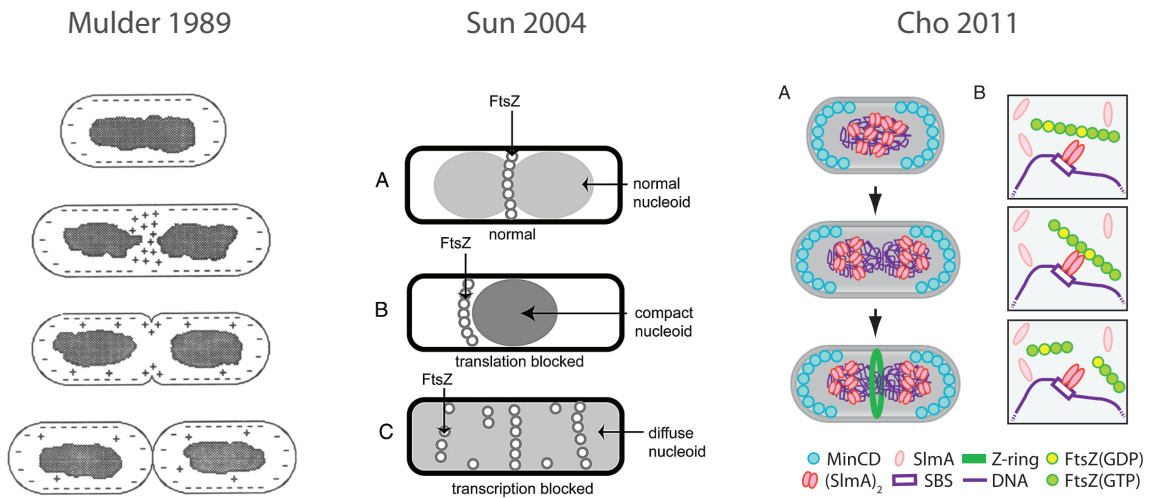


Figure 2.8: Nucleoid occlusion development. Development of the nucleoid occlusion model from observation to mechanism^{156–158}. Mulder posited that a positive signal (+) for division is made at termination, and then directed to the constriction site by the absence of the negative nucleoid signal (-). Sun showed that in abnormal nucleoids caused by blocking translation or transcription, FtsZ positioning was also abnormal. Cho build on Bernhardt’s work with SlmA to form a more complete model. In it, SlmA beaks polymerized FtsZ, only allowing the Z-ring to form near the center of the cell near the *ter* domain. MinCD disallows Z-ring formation at the poles.

not want to lose the forest for the trees when considering these molecular mechanisms. However, because the discovery of molecular systems which act upon FtsZ and the divisome stimulated significant discussion about the coordination between replication and division, we will discuss some of those systems below as well as explore them experimentally.

2.4.3 Nucleoid occlusion

In this section we review the nucleoid occlusion model, in which the nucleoid prohibits septum formation in its vicinity.

It was recognized early that the two major spatial undertakings of the cell were extremely precise: segregation of the replicated nucleoids and positioning of the septum¹⁵⁹. Through the ‘90s, until more powerful imaging experiments showed a less definite connection, it was

almost taken for granted that segregation was achieved through a membrane to chromosome tether^{56,82,160,161}. But how did the septum form in the middle of the cell? A number of models were developed to explain the spatiotemporal control of the division plane. Of particular note are the Min system and the nucleoid occlusion hypothesis, the latter of which we will cover here.

The idea that the nucleoid positioning could determine the location of the septum was first put forth by Woldring and collaborators in 1985^{156,162-164} (personal communication). The basis for the idea was that even in minicell mutants in which septum position was aberrant, or in filamentous cells with high ploidy, the division plane did not form over nucleoids. In temperature sensitive mutants in which DNA replication had been inhibited, septation occurred in locations that were devoid of nucleoids^{87,156}. This led to the idea that the nucleoid provided a negative signal for septum formation. Along with a system to avoid septation at the poles, this would favor divisions between segregated nucleoids. From the outset, nucleoid occlusion was paired with the idea of a positive regulator for division being produced at termination (based on work from Donachie's lab discussed above). Taken together, the cell would produce the capacity to divide, and nucleoid occlusion would direct that capacity towards the midcell in the space between the replicated chromosomes (Figure 2.8)⁹⁹.

At this time, the nature and importance of FtsZ in setting the location of division was not yet appreciated, nor were any molecular players known that could be responsible for nucleoid occlusion. But during the '90s, the realization that FtsZ forms a ring at the midcell to direct division pushed FtsZ to the forefront of division regulation¹²⁸. Then, in 2005, Bernhardt and Boer identified *slmA* (synthetic lethal with *min*), a protein which both binds to the nucleoid and inhibited the local polymerization of FtsZ⁶⁴.

Briefly, SlmA is a DNA binding protein whose binding sequences are concentrated towards the upper part of the chromosome, closer to *ori*. It can bind FtsZ, and when doing so inhibits its ability to form polymers and associate with the membrane^{158,165}. As the chromosome replicates, the new *ori* domains move towards the cell poles¹⁶⁶. This frees the midcell of SlmA,

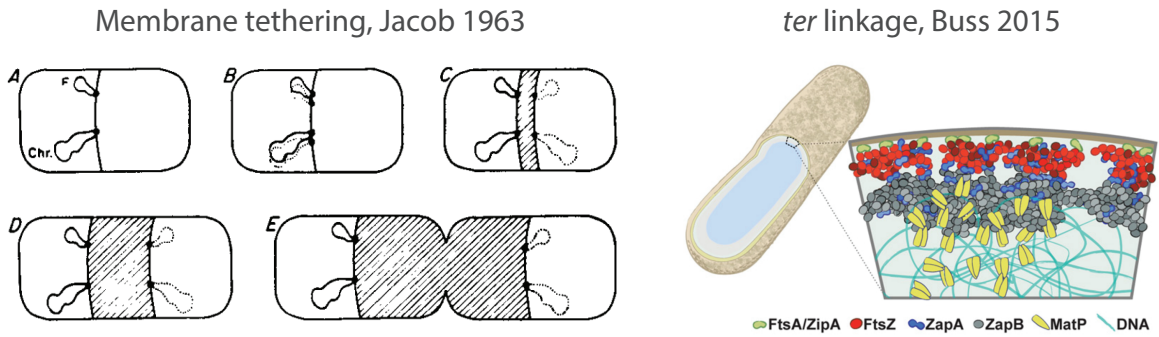


Figure 2.9: Chromosome-membrane attachment models. The discovery of *ter* linkage harks back to the chromosome-membrane tethering hypothesis suggested by Jacob and perennially popular despite scant evidence^{82,171}. However, the models are fundamentally different. In chromosome-membrane tethering, the replicated chromosome is segregated into the daughter cells by an anchor point which moves due to the synthesis of new cell wall. The exact purpose of *ter* linkage is unclear, but it is likely pertains to the positioning of the septal plane relative to *ter*, and perhaps ensures that the replicated chromosomes are separated before cell division.

presumably allowing the Z-ring to form.

Yet the importance of *slmA* is questionable. At the outset, its discovery was based on its conditional essentiality, as it is only necessary in cells with deficient *min* systems. Numerous later papers show that even without it, the cell can accurately place the division plane at the midcell and away from nucleoids, or inhibit division when the nucleoids remain unsegregated^{167–170}. Nucleoid occlusion by *slmA* sets the tone for many of the replication and division coordination systems; while they may increase the precision or efficiency of division and reduce errors, they are not strictly necessary for viability⁶⁶.

2.4.4 *ter* linkage

Here, we review a model that physically links the chromosome to the cell periphery in order to coordinate replication and division.

A recent discovery shows that cells may regulate FtsZ positioning using the chromosome in a positive way via the terminus region (Figure 2.9)^{70,169,171–173}. Nucleoid occlusion and the *min* system represent negative regulators of septum formation via FtsZ. But Espéli and colleagues

found that the protein MatP physically links the terminus region of the chromosome to proteins of the divisome⁷⁰. MatP is a DNA binding protein known to condense the lower portion of the chromosome into what is called the *ter* macrodomain^{174,175}. Using a fluorescent *parS*-*parB* to mark points on the chromosome, they showed that the *ter* macrodomain localized to the midcell of dividing bacteria, and that this localization was dependent on MatP. Moreover, they showed that localization was also dependent on the divisome proteins ZapA and ZapB¹⁷⁶. These observations were supported by additional papers from the Männik Lab which found that MatP, ZapA, and ZapB contribute to Z-ring positioning in *min* and *slmA* mutants^{169,172}.

These works provide strong evidence for a physical link between the chromosome and the division machinery. It is not in the form originally imagined by Jacob and others, but it is an intriguing coordination mechanism with a molecular basis. However, it is unclear what exactly *ter* linkage is designed to accomplish. On one hand, it positively regulates Z-ring formation at the location of *ter* at the midcell (or the other way around)^{70,171}. On the other hand, it was shown to delay actual segregation of the chromosomes, perhaps in conjunction with FtsK¹⁷⁷⁻¹⁷⁹. Finally, like *slmA*, none of the genes implicated in *ter* linkage are essential^{166,179}.

2.4.5 Regulators of FtsZ assembly with growth rate

In this section I describe two known regulators of FtsZ assembly that are thought to connect division size with growth rate, OpgH and ClpX.

There are no shortage of regulators of FtsZ via its promiscuous C-terminal domain^{170,180}. Most of these regulators, such as those outlined above, are associated with spatial control of FtsZ assembly. Yet others, such as SulA of the SOS response, are associated with quick temporal control of assembly in response to stress^{131,181}. However, there are two known regulators that are thought to regulate the assembly of FtsZ more generally with growth rate on slower time scales. These models provide a molecular underpinning for how *E. coli* can modulate its average size with growth rate.

The first regulator is OpgH, referred to as a metabolic sensor, as it relays nutrient availability information to the division machinery¹⁸². OpgH is expressed by *E. coli*, but an analogous (though non-homologous) protein UgtP was first discovered in *B. subtilis*¹⁸³. In brief, the system works as follows. OpgH inhibits FtsZ assembly by sequestering FtsZ monomers in the presence of UDP-glucose. UDP-glucose is a metabolite that is two steps from glycolysis and the pentose phosphate pathway, and is itself a precursor to cell wall and membrane components. In rich nutrient conditions, when flux through UDP-glucose is high, OpgH is more active in inhibiting FtsZ assembly. This is effectively the same as decreasing the fraction FtsZ monomers which are active for division. This delays division as compared to slow growth, which results in a larger size at division⁵⁹. While the action of the metabolic sensor can plausibly work on fast time-scales, such as during a nutrient shift, the beauty of the system is that it is also coordinates the average growth rate with cell size at steady-state. This partially explains how cells grow larger in fast growth, even if FtsZ concentration is the same in different conditions¹⁸⁴. Based on knockout studies, the metabolic sensor seems to be effective in fast growth conditions, and “dispensable under nutrient-poor conditions¹⁸³.”

The second regulator is ClpX, which, along with its protease ClpP also antagonizes Z-ring assembly. Better known for its job in SsrA mediated protein degradation for quality control, ClpX was found to inhibit FtsZ assembly in both *B. subtilis* and *E. coli*^{185–188}. There is some disagreement to whether it degrades or simply inhibits FtsZ polymerization (it likely degrades in *E. coli* but only inhibits in *B. subtilis*), but the effective result is the same^{141, 189–191}. Similar to OpgH, the effective pool of active monomers is reduced, and division delayed, in conditions in which ClpX is active. Unlike OpgH, the effect of ClpX is prominent in slow growth and masked in fast growth^{13, 191, 192}. At slow growth, the balance between FtsZ production and degradation by ClpX controls the timing of division in both transient and steady-state scenarios, explored in more detail in Subsection 4.2.5¹⁹¹.

The metabolic sensor helps explain some of the foundational quantitative principles of

bacterial physiology, like the Schaechter line which states there is an exponential relationship between size and growth rate in fast growth. ClpX, contrarily, partially explains why those principles break down in slow growth^{13,41}. However, both molecules are indicative of a control framework whereby cells regulated division in a cell cycle independent manner, instead linking it directly to growth rate.

2.5 Conclusion

The study of replication and division coordination has taken a long arc to the modern day, tracing back to the beginnings of bacterial physiology and molecular cell biology. How the cell can keep these two processes in sync was a driving question and fertile ground for speculative models and molecular investigations. We now believe that both processes are independent insofar as they are dictated by growth, and connected to each other only in an auxiliary manner. As is not uncommon in biology, ultimately accurate theories had been proposed early on to explain this feat¹⁹³. Yet they would have to wait for experimental data to separate them from the pack. A collection of such experiments are the subject of Chapter 4.

Chapter 3

B. subtilis and *E. coli* Share Common

Principles to Coordinate Growth and the Cell Cycle

3.1 Introduction

In Chapter 1, we introduced the fundamental concepts and growth principles of bacterial physiology. In this chapter, we explore these principles in greater depth using the model gram-positive organism *B. subtilis*. We do so in comparison to *E. coli*, which aside from being a model gram-negative organism, has become the best known bacteria, and arguably the best known species, since the biological revolution of the 20th century. Because the phylogenetic diversity of bacteria is enormous, we ask to what degree a unified physiological regulatory framework can be applied to these two species, which diverged over a billion years ago.

Our current understanding of fundamental, quantitative principles in bacterial physiology is largely based on studies of *E. coli* and *S. typhimurium*. Several of these principles have been presented in the form of “growth laws”^{14,37,194}. For example, the “growth law of cell size” states

that the average cell size increases exponentially with respect to the nutrient-imposed growth rate¹⁶. This principle has been extended to the “growth law of unit cells,” which allows prediction of the average cell size based on the growth rate and the cell cycle duration for any steady-state growth condition³⁷.

Gram-positive *B. subtilis* is distinct from Gram-negative *E. coli* at the genetic, molecular, and regulatory level¹⁹⁵. However, despite their evolutionary divergence, *B. subtilis* and *E. coli* follow the same phenomenological principle of cell-size homeostasis known as the adder principle^{8,48}. Furthermore, both organisms share the identical mechanistic origin of the adder principle, namely, a molecular threshold for division proteins and their balanced biosynthesis during growth¹³. Based on these findings, we wanted to know to what extent *B. subtilis* and *E. coli* coordinate growth, size, and cell cycle in the same manner. A shared coordination framework would imply that, despite phylogenetic and molecular diversity, physiological regulation in bacteria is functionally conserved.

In order to create a full complement of data necessary for comparative analysis, we measured the growth and cell cycle parameters of *B. subtilis* at both the population and single-cell level under a wide range of conditions.

Previous population-level studies have found that *B. subtilis*, like *E. coli*, initiates replication at a fixed mass, establishing a regulatory bridge between cell size and cell cycle control^{15,63,196}. We extended this avenue with single-cell methods to precisely measure the cell cycle parameters in individual *B. subtilis* cells across conditions^{13,41}. These results showed that the initiation size is constant not only in steady-state conditions, but also during nutrient shifts between two steady-state conditions. This strongly supports a threshold model for initiation in both steady and dynamic environments^{12,13,37,39}.

The single-cell approach also allowed us to compare the relative variability of all growth and cell cycle parameters both among conditions and among species. These measurements reveal a strikingly similar hierarchy of physiological parameters between *B. subtilis* and *E. coli* in terms

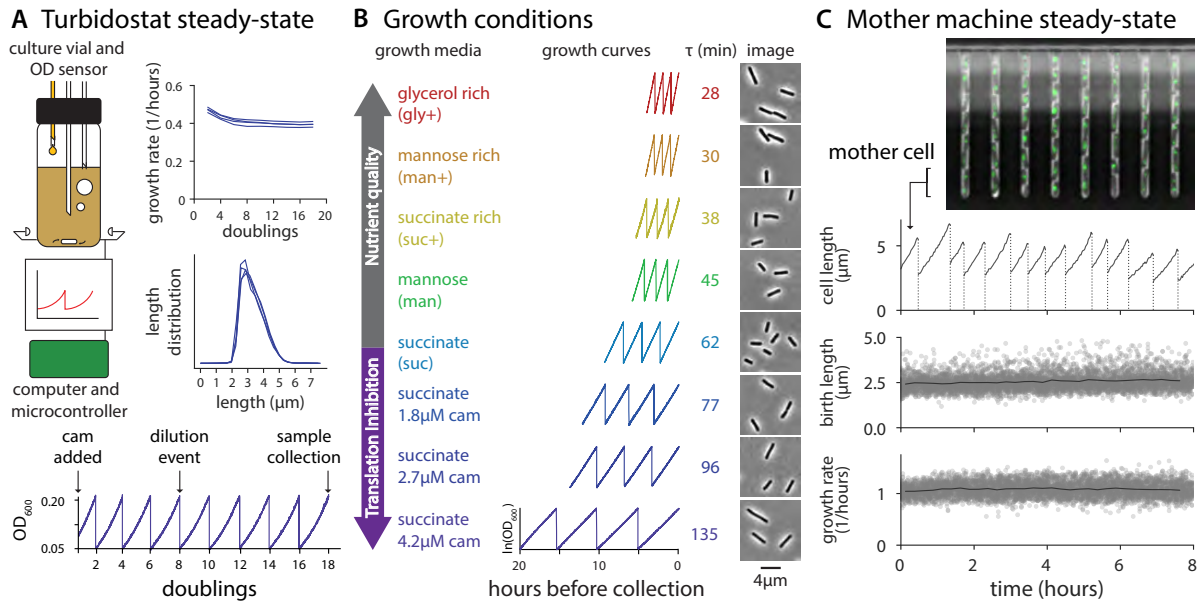


Figure 3.1: Population and single-cell methods to achieve steady-state growth. (A) Turbidostat experimental method and validation. Top left: In the multiplex turbidostat vial, the culture volume was maintained constant and cell concentration was monitored and adjusted automatically by infusing fresh medium. Aerobic conditions were ensured via bubbling and stirring. Top right: growth rate measurements were consistent between 5 and 20 doublings and cell length distributions were reproducible at sample collection. Data shown is from 4 repeats in succinate with 2.7 μM chloramphenicol (cam). Bottom: A representative growth curve showing the timing of the addition of chloramphenicol, dilution events, and sample collection. Each dilution occurred when the culture reached OD_{600} 0.2 and was diluted to 0.05, allowing for two doublings during the growth interval. (B) Overview of population growth conditions and measurements. Growth media and their abbreviations for 5 different nutrient conditions, all of which are based on S7₅₀. Glycerol rich, mannose, and succinate were selected for translation inhibition experiments (succinate shown here). Representative growth curves (final 8 doublings), average doubling time τ , and representative crops of images used for population sizing shown for each condition. (C) Single-cell experiments with the mother machine. Representative image showing cell-containing traps. Fluorescent signal is DnaN-mGFPmut2 (Figure 3.6, Materials and methods). The growth in length (black lines) and division (dotted vertical lines) of a single mother cell is shown over 8 hours. Average birth length and growth rate (solid grey lines) of the single-cell measurements (grey scatter points) are in steady-state over the course of the experiment. Data shown is from mannose. Additional measurements for all conditions are presented in Figure 3.2.

of tightness of their control.

The richness of our quantitative physiological data generated in *B. subtilis* is comparable to that in *E. coli*, providing key evidence that *B. subtilis* and *E. coli* share core phenomenological

and quantitative principles that govern their physiology, thereby providing a unified picture of bacterial growth, size, and cell cycle coordination.

3.2 *B. subtilis* physiological control

3.2.1 Ensuring steady-state growth in *B. subtilis*

Maintaining a steady-state growth is essential for reproducible measurements of the physiological state of the cell¹⁴. In steady-state growth, the total biomass of the culture increases exponentially with time and protein biosynthesis is balanced with the total biomass increase. That is, the protein production rate is the same as the growth rate of the cell. As a result, average protein concentrations are constant, whereas the total amount of proteins increases in proportion to the cell volume. This constant concentration and proportional increase also applies to other macromolecules such as DNA, RNA, phospholipids, and the cell wall.

To achieve steady-state measurements in *B. subtilis*, we grew and monitored cells over many generations using a multiplex turbidostat that we previously used for *E. coli*³⁷ (Figure 3.1A). For both population and single-cell methods, we began cultures from single colonies and pre-cultured cells using appropriate batch methods before transferring to continuous culture set-ups (Materials and methods). We ensured pre-cultures did not enter stationary phase to avoid sporulation. We used a *B. subtilis* strain which was non-motile and non-biofilm forming to facilitate single cell-size measurements. This was necessary because *B. subtilis* exhibits a temporal chaining phenotype, particularly in faster growth conditions^{197,198}. During chaining, cells are physically connected yet their cytoplasm is compartmentalized, obfuscating a definition of division^{199,200}. Our strain contained a genetic modification to abolish cell chaining, ensuring that cell separation coincided with septation²⁰¹ (Materials and methods).

To measure how long it takes for *B. subtilis* to reach physiological steady state, we measured growth rate continuously during time course experiments using our multiplex turbidostat.

Mother machine steady-state measurements from all conditions

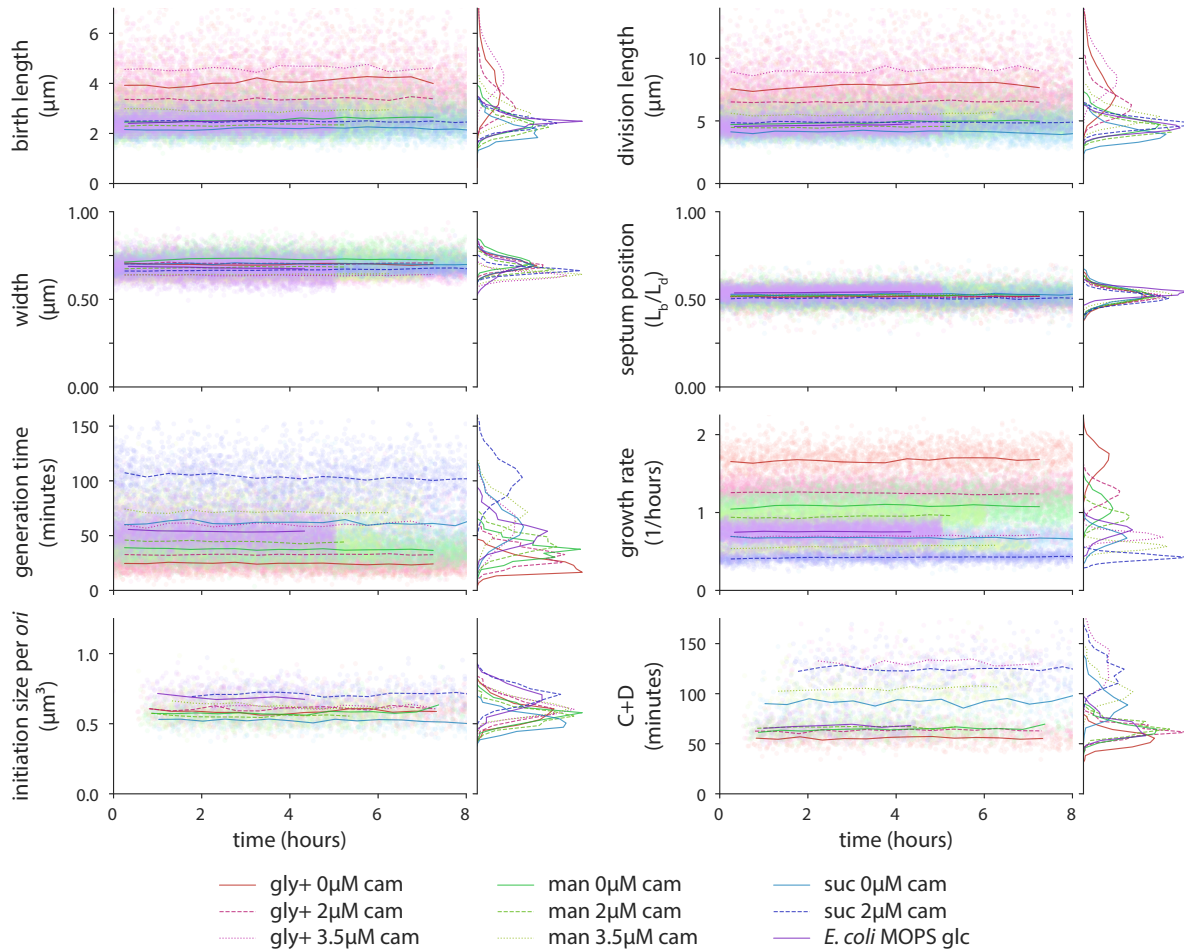


Figure 3.2: Single-cell steady-state physiological parameters for all conditions. Physiological parameters for all *B. subtilis* mother machine experimental conditions and one *E. coli* experiment. Time course is shown with single-cell measurements (scatter points) and 30 minute binned mean (horizontal lines) plotted against the birth time. Multiple consecutive generations are needed to determine initiation size, C period, and D period, thus a gap exists before those measurements are possible. Single-cell distributions are invariant in time and shown for each condition, sharing the same scale as time course. Colors are as in Figure 3.1B. Sample sizes are provided in Table 6.

Growth rate generally stabilized after 6 generations, and the cell size distribution was reproducible (Figure 3.1A). However, to be certain of steady-state growth, we typically waited for at least 14 doublings before sample collection in all our subsequent experiments. At collection, we split the culture for qPCR marker frequency and cell size measurement (see Table 5 for experimental

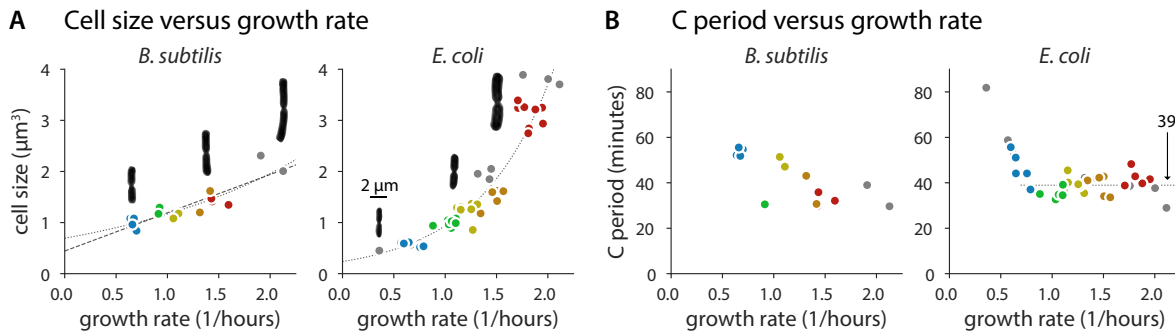


Figure 3.3: Population cell size and C period measurements in *B. subtilis* and *E. coli*. (A) Cell size increases with respect to growth rate in *B. subtilis* and *E. coli* under nutrient limitation. For *B. subtilis*, the relationship is not clearly exponential as it is for *E. coli* (dotted lines are linear regression fits of logarithm transformed data, dashed line is a linear regression fit). Representative images of cells during division show change in aspect ratio as a function of growth rate. Length and width measurements presented in Figure 3.4. (B) C period measurements with respect to growth rate in *B. subtilis* and *E. coli* under nutrient limitation. For *E. coli*, C is approximately constant at 39 minutes (horizontal dotted line) for doubling times faster than 60 minutes ($\lambda = 0.69$). That constancy is less clear for *B. subtilis*, though single-cell data shows that C+D is proportional to generation time (Figure 3.9). *B. subtilis* growth media are colored as in Figure 3.1B with additional LB data in grey. *E. coli* data is previously published work³⁷; Red is synthetic rich, orange is glucose with 12 amino acids, yellow is glucose with 6 amino acids, green is glucose, and blue is glycerol, with additional conditions in grey.

conditions).

For single-cell measurements, we used the microfluidic mother machine to collect phase contrast and fluorescent timelapse images for at least 10 generations^{9,13} (Figure 3.1C). After analyzing all cell lives, we limited our data to the time interval in which all measured parameters equilibrated (Figure 3.2). A typical experiment produced data for around 2,500 cells (see Table 6 for experimental conditions).

3.2.2 Growth law of cell size: *B. subtilis* size shows a positive but not exponential dependence on the nutrient-imposed growth rate

A foundational observation by Schaechter, Maale, and Kjeldgaard showed that the average cell size in *E. coli* increases exponentially with respect to the nutrient-imposed growth rate¹⁶.

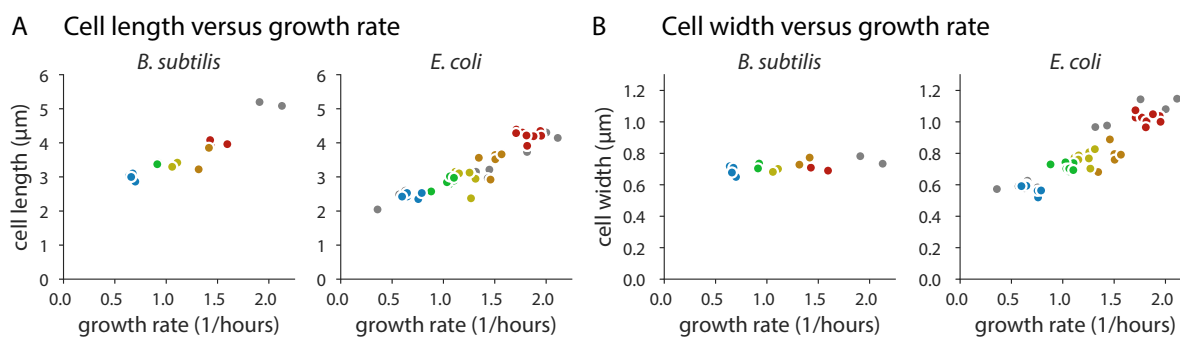


Figure 3.4: Length and width measurements in *B. subtilis* and *E. coli*. (A) Cell length in *B. subtilis* and *E. coli* increases with growth rate. (B) For *B. subtilis*, width is independent of the nutrient-imposed growth rate. For *E. coli*, width increases with growth rate in a similar manner to length. Colors and conditions are as in Figure 3.3. *E. coli* data is from previously published work³⁷.

Previously, we investigated this growth law of cell size in *E. coli* under various growth and cell cycle inhibition, and showed that the exponential relationship was a special case wherein the growth rate was the only experimental variable³⁷. In *B. subtilis*, the Levin lab recently revisited the relationship between size and the nutrient-imposed growth rate, and found that the average cell size in *B. subtilis* increased with the growth rate at the population level¹⁸³.

We extended our efforts in *E. coli* to *B. subtilis*. Using the multiplex turbidostat, we grew cells in 5 nutrient conditions with doubling times ranging between 28 and 62 minutes (Figure 3.1B, Materials and methods; Table 5). Here, we use size interchangeably with volume, and consider volume to be proportional to dry mass¹⁹.

Figure 3.3A shows the average cell size versus growth rate for the 5 different growth conditions. As expected, the average cell size increased with growth rate. However, the exponential dependence observed for *E. coli* was less clear in *B. subtilis*. This discrepancy in *B. subtilis* could be due to changes in the duration of replication (C period) and cell division (D period) in different nutrient conditions³⁷.

We thus measured the population average C period of *B. subtilis* employing qPCR marker frequency analysis^{37,63,83}. Both species exhibited a similar maximum replication speed

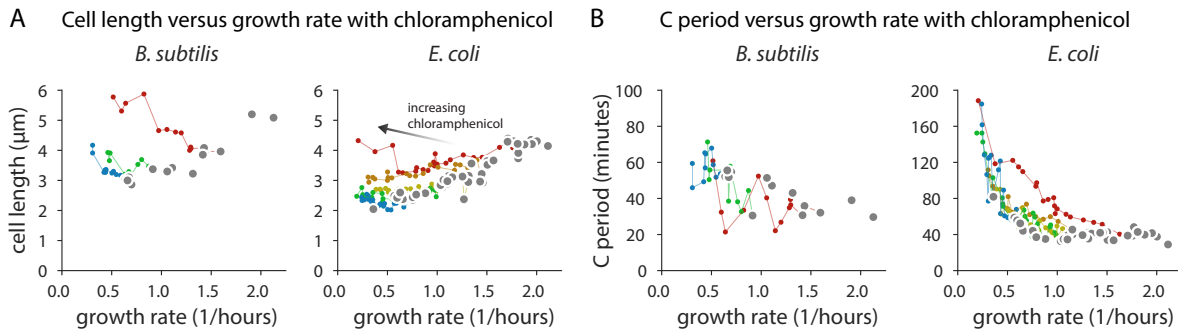


Figure 3.5: Size and C period under translational inhibition in *B. subtilis* and *E. coli*. (A) Under translation inhibition due to chloramphenicol, the relationship between cell size and growth rate under nutrient limitation breaks down for both *B. subtilis* and *E. coli*. (B) The deviation from the nutrient growth law can be attributed to the change in C period in both species under translation inhibition. Lines connect translation inhibition experiments using the same media. Colors and conditions are as in Figure 3.3. *E. coli* data is from previously published work³⁷.

(approximately 40 minutes for C period), but our data indeed do not indicate C period is strictly constant in fast growth (Figure 3.3B).

Unfortunately, despite extensive efforts, we were unable to reliably measure the D period in *B. subtilis* from the population samples as we had done previously for *E. coli*³⁷. The main issue was consistency of fluorescence labeling of the DNA required for flow or image cytometry. Our results were variable from experiment to experiment, and protocol to protocol. We therefore concluded that the measurement of D period using population methods is not as reliable as needed to test the growth law of cell size in *B. subtilis*, a cautionary reminder in interpreting previous measurements in *B. subtilis*. For these reasons, we set out to measure the *B. subtilis* cell cycle explicitly at the single-cell level.

3.2.3 Single-cell determination of cell cycle parameters in *B. subtilis*

We employed a functional replisome protein fused with a fluorescent marker, DnaN-mGFPmut2, to measure cell cycle progression in single cells^{13,202} (Materials and methods). In *B. subtilis*, the replisomes from the two replication forks of a replicating chromosome are often

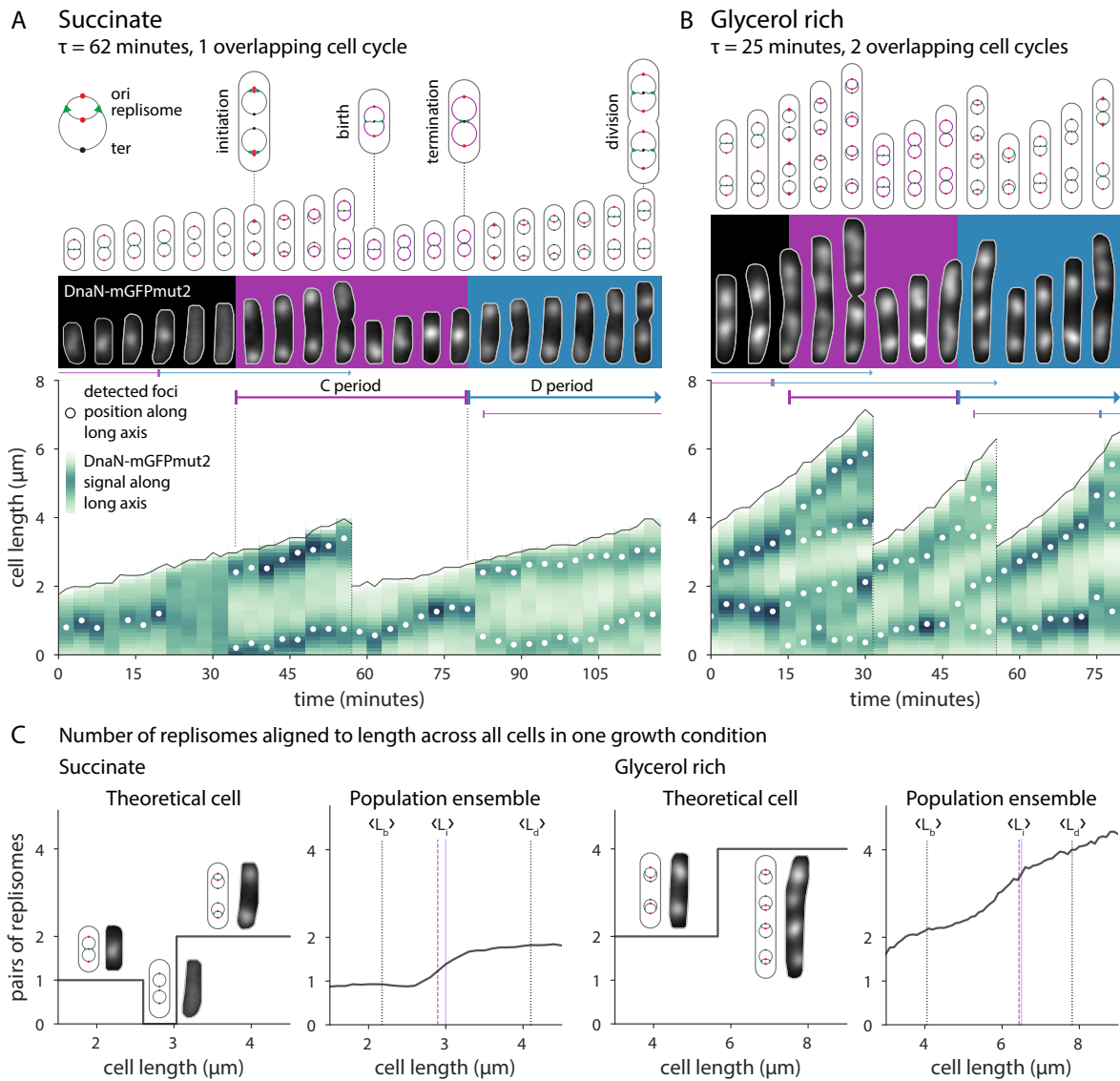


Figure 3.6: Single-cell growth and cell cycle progression in *B. subtilis*. See text for information.

colocalized, thus most foci represent a pair of replisomes²⁰³.

Figure 3.6A and B show representative cells from two growth conditions, succinate and glycerol rich, respectively. Panel A shows a typical cell cycle progression of *B. subtilis* in slower growth media. Top: Chromosome configuration. Middle: Fluorescent images of DnaN-mGFPmut2 signal. Bottom: Processed image data represented as a cell lineage trace. Vertical green bars are the DnaN-mGFPmut2 signal summed along the long axis of the cell, with white circles showing

foci position. Panel B shows a typical cell cycle progression of *B. subtilis* in faster growth media. Panel C shows the ensemble method to determine cell cycle parameters. Left: In succinate, a theoretical cell is born with one pair of replisomes. It may briefly contain no active replisomes upon termination, and then contain two pairs of replisomes as the two complete chromosomes begin replication. The length at which the number of replisome pairs increases corresponds to the initiation size. The average initiation length $\langle L_i \rangle$ as determined from the cell traces (dashed purple line) agrees with the ensemble estimate (solid purple line). The average birth $\langle L_b \rangle$ and division length $\langle L_d \rangle$ of the population are shown as dotted vertical lines. Right: In glycerol rich, cells transition from two to four pairs of replisomes

In the slower growth condition (succinate), cells were normally born with one replicating chromosome. Replication initiation begins synchronously in the mother cell for two chromosomes. At that time, the origins are located towards the cell poles. Replication proceeds through cell division, at which point the replication forks reside near the midcell of the newly born cell. Chromosome segregation is concurrent with replication. By the time the replication forks reach the terminus region, which is still at the midcell, the previously duplicated origins have already migrated to the cell poles²⁰⁴.

While overlapping cell cycles are common even at slower growth, cells rarely exhibit multifork replication. Multifork replication indicates initiation begins before the previous termination event completes. Instead, *B. subtilis* normally initiates when the cell contains complete, homologous chromosomes where the copy number is a power of two. In fact, replication initiation often proceeds immediately after the previous termination event. This may be due to the role of YabA in *B. subtilis* replication initiation control, which ties DnaA activity to DnaN availability^{205,206}. Comparatively, multifork replication is common in *E. coli*, where Hda is thought to play a similar but mechanistically distinct role in reducing initiation potential during ongoing replication^{13,207}.

In faster growth conditions (glycerol rich), cells are often born with two replicating chromosomes. However, the relative variability between division size and C+D was greater in

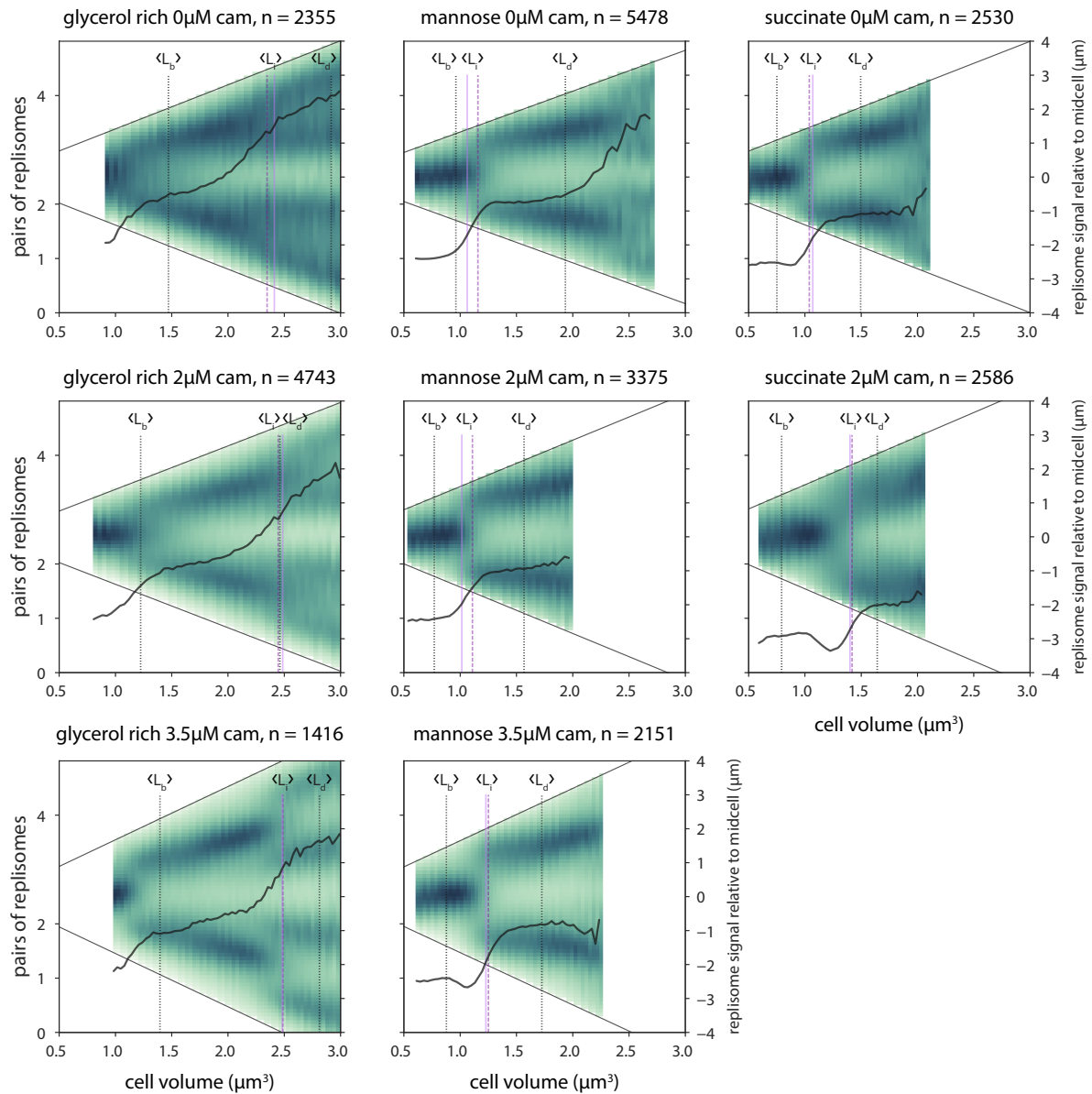


Figure 3.7: Ensemble replisome count and localization for all conditions. See text for information.

this rich condition. This means that a substantial fraction of the population were still born with one replicating chromosome (Figure 3.16). Moreover, transient filamentation and asymmetrical septation are more common in fast growth conditions, leading to cells born with a number of replicating chromosomes which are not a power of two.

3.2.4 Complementary, ensemble determination of cell cycle parameters in *B. subtilis*

The main advantage of the single-cell approach is that it allows for direct comparison of the relationships among growth parameters, providing mechanistic insights⁸. However, it can be difficult to determine the cell cycle parameters manually, particularly when the foci are clumped or the signal is weak. This is especially true in faster growth conditions. To ensure an unbiased analysis of the cell cycle, we also employed an “ensemble method” to extract cell cycle parameters⁴¹ (Figure 3.6C). We used the foci count at a given size as a proxy for the replication state (Materials and methods). This method produces data similar to the original schematics used by Helmstetter and Cooper when first elucidating the *E. coli* cell cycle³².

For all but the slowest growth conditions, the measured average number of foci monotonically increases because initiation almost immediately follows termination as discussed above. Unlike a theoretical single cell, the ensemble plots do not display a strict step-like behavior; we interpret this as variability in the initiation size. Ensemble plots for all conditions, along with the foci localization patterns, are presented in Figure 3.7. In it, ensemble plots for three media conditions tested with and without translational inhibition. Average pairs of replisomes (thick black line) are plotted against cell volume with consistent scale across conditions. Purple vertical lines show the initiation size from the average of single cells (dashed) and the ensemble method (solid). Vertical dotted black lines indicate the average birth and division size. The average number of foci may be above or below the theoretical number as replisomes can transiently dissociate, and a pair of replisomes may be counted as two foci when they are not colocalized^{203,208,209}. The normalized DnaN-mGFPmut2 signal relative to midcell (green background) shows the localization of replisomes over the cell cycle, with the diagonal solid black lines indicating the cell periphery.

This measurement is in good agreement with the average initiation size as measured from individual cells. We used these complementary methods to test whether the initiation size is

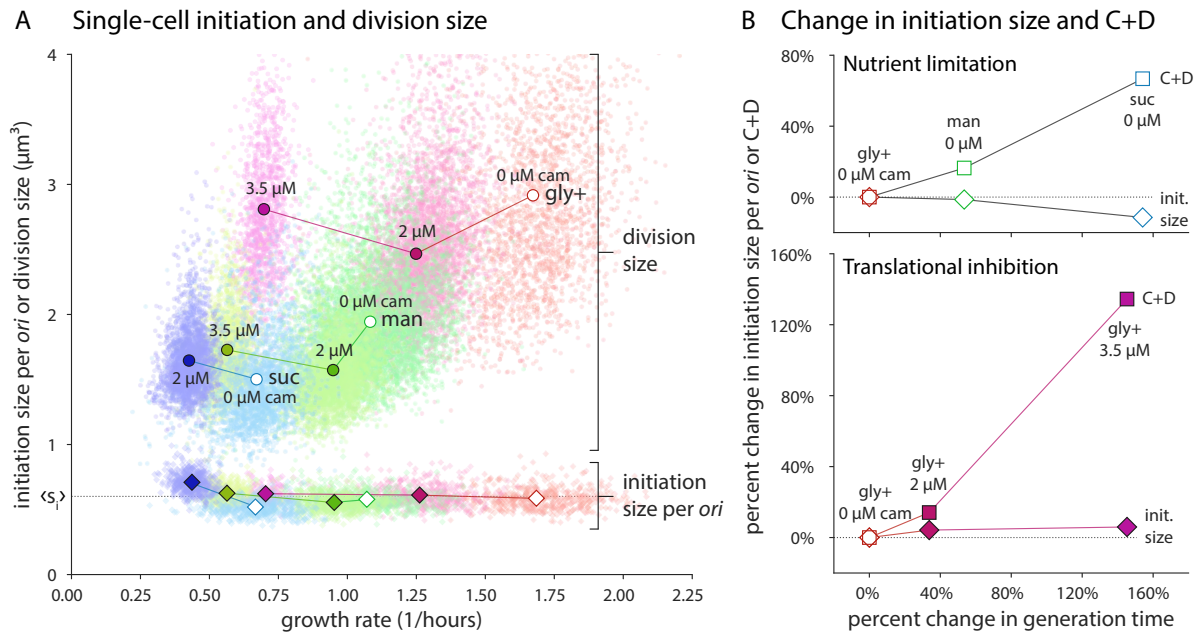


Figure 3.8: Initiation size is invariant in *B. subtilis* during steady-state growth. (A) Single-cell initiation size per *ori* s_i is condition independent. Division size (circles) changes dramatically under both nutrient limitation and translational inhibition. The corresponding initiation size per *ori* (diamonds) collapses onto a constant value, $\langle L_i \rangle$, across all conditions (dotted horizontal black line). This holds for both single cells (scatter points) and population averages (solid symbols). Growth media are colored as in Figure 3.1B with the amount of chloramphenicol indicated (0 μM chloramphenicol with empty symbols, lines connect the same growth media with and without chloramphenicol). (B) C+D is condition dependent and increases with generation time. Top: Increase in generation time under nutrient limitation causes an increase in the population average C+D (squares) while initiation size minimally changes. Bottom: A similar pattern is seen under translational inhibition. For both plots, measured parameters are compared to the fastest growth condition. Single-cell C+D data presented in Figure 3.9 and Figure 3.16.

invariant in *B. subtilis* as in *E. coli*³⁷.

3.2.5 Invariance of initiation size: *B. subtilis* initiates at a fixed cell size per *ori*

In *E. coli* and *S. typhimurium*, the concept of a conserved initiation size was first explained by Donachie as a consequence of the growth law of cell size and the constant C+D^{15, 16, 32}. The upshot is that, at a fixed size per origin (*ori*), all origins of replication fire simultaneously. Recent

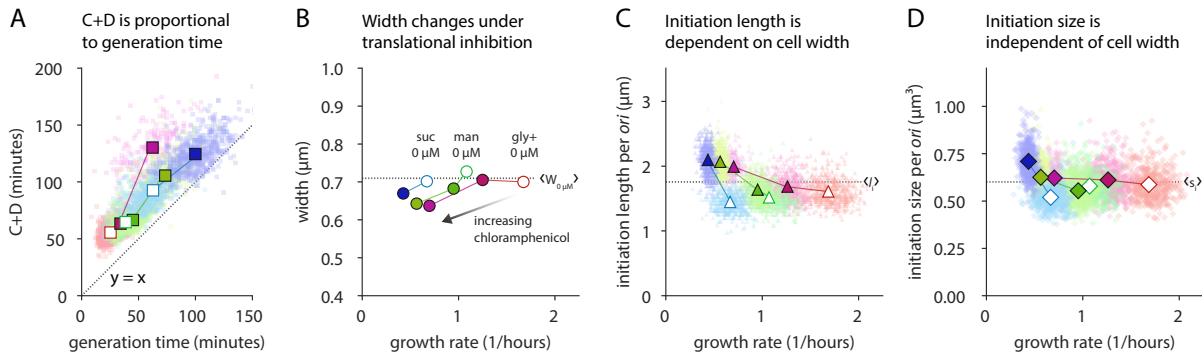


Figure 3.9: *B. subtilis* cell cycle and initiation size behavior. (A) C+D is proportional to generation time in *B. subtilis* when the generation time is modulated by nutrient condition or translational inhibition. (B) Cell width under translational inhibition decreases as compared to the average width without inhibition, $\langle W_{0\mu\text{M}} \rangle$ (dotted black line). (C) Initiation length increase with width under translational inhibition. Mean initiation length per *ori* $\langle L_i \rangle$ shown as dotted black line. (D) Initiation size from Figure 3.8 A reproduced for comparison. In all plots, colors are as in Figure 3.8, where lines connect the same growth media with and without chloramphenicol. Scatter points are single-cell data and solid symbols are population averages.

high-throughput works at both single-cell and population levels have conclusively shown that the early insight by Donachie was correct^{13,37,41}. In fact, the initiation size per *ori* is invariant not only across nutrient conditions, but also under antibiotic inhibition and genetic perturbations³⁷.

The constancy of initiation size in *B. subtilis* has previously been tested by several groups at the population level under nutrient limitation conditions^{63,196,210}. We further measured the initiation size using single-cell methods under nutrient limitation and translational inhibition. We found that the initiation size per *ori* in *B. subtilis* is indeed invariant across conditions, even for individual cells (Figure 3.8A).

This constant initiation size is in stark contrast to the varying C period under different growth conditions (Figure 3.9A). In fact, initiation size is one of the least variable physiological parameters along with septum position and width (Figure 3.16). The single-cell approach also allowed us to measure the correlations among all growth and cell cycle parameters. The initiation size is only weakly correlated with other measured parameters (Figure 3.17).

These observations are consistent with a threshold model for replication initiation^{13,37,125}.

Within that framework, initiator molecules accumulate proportional to the growth rate. This mechanism is enacted in single cells and is in turn apparent at the population level.

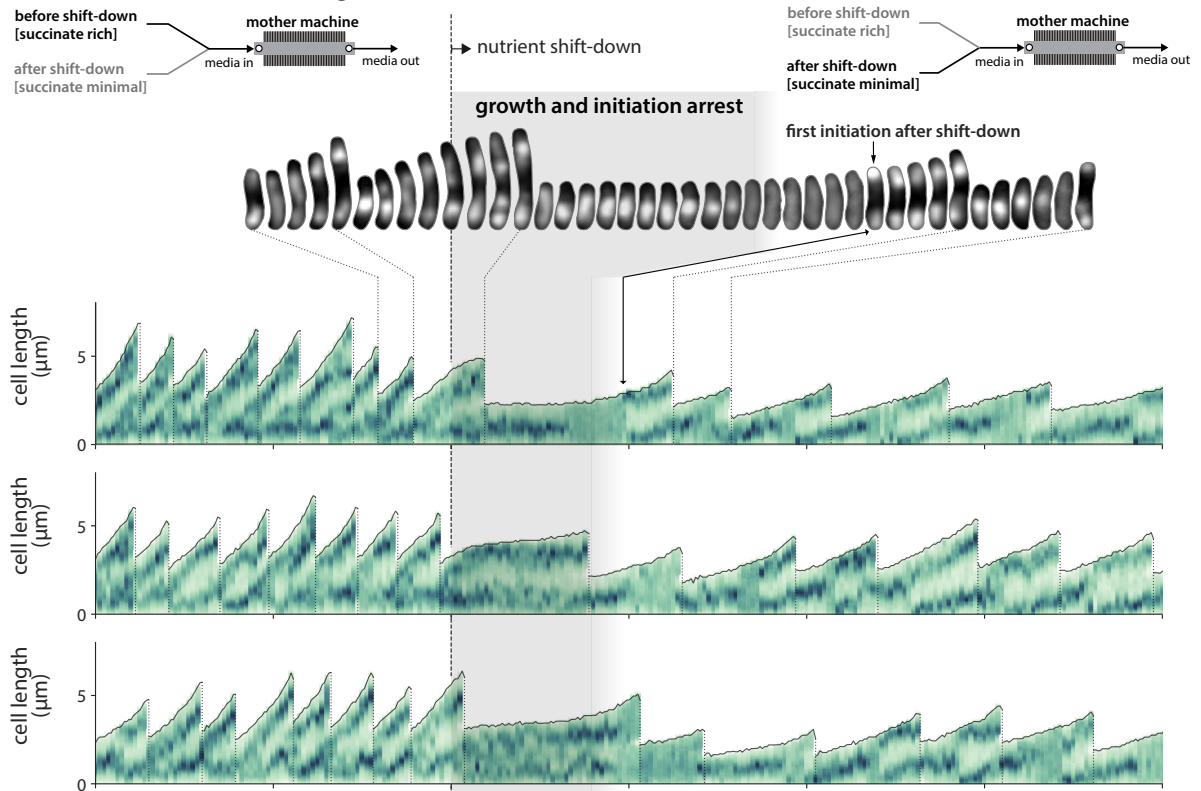
3.2.6 Initiation size is invariant even during nutrient shifts at the single-cell level

Because the constant initiation size was implemented by individual cells in the previous steady-state experiments, we wondered how cells would behave in a changing environment. Nutrient shift experiments have provided important insight into the coordination of biosynthesis and the cell cycle^{22,211,212}. We revisited this paradigm at the single-cell level, shifting cells from minimal media ($\tau = 65$ min) to rich conditions ($\tau = 30$ min) and back again (Figure 3.11). By using the mother machine, we could add and remove nutrients immediately while measuring the cell cycle and all other physiological parameters (Materials and methods).

The most drastic results occurred upon shift-down (Figure 3.10). When nutrient supplements were removed, growth immediately paused. The crash in growth rate caused a drastic increase in generation and cell cycle time for cells which experienced the shift-down. Replicating chromosomes were stalled and division ceased. Strikingly, the growth pause led to an absence of initiation events until after cells restarted elongation and attained the requisite initiation size. Thus individual cells maintained a constant initiation size through the transition. Division also resumed after growth recommenced, but at a smaller size commensurate with the post-shift-down growth rate. A constant C+D period is not maintained during this time (Figure 3.11).

The decoupling of initiation and division supports the idea that they are controlled by independent threshold mechanisms¹³. That is, the cell builds up a pool of dedicated molecules for each task to a certain level^{12,13,53,59,99}. For initiation, this threshold and the accumulation rate is conserved across growth conditions. For division, the threshold or the accumulation rate is set by the growth condition¹⁸⁴. In the generation after shift down, cells grow much more slowly and therefore accumulate threshold molecules at a similarly depressed rate. As a result, both initiation

A Nutrient shift-down and single-cell behavior



B Population average

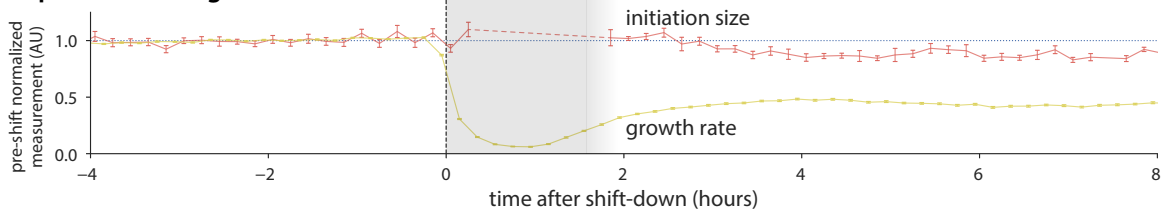


Figure 3.10: Initiation size is invariant in *B. subtilis* during shift-down. (A) Behavior of single cells undergoing shift-down from succinate rich to succinate minimal at time zero. Upon shift-down, cells pause growth and initiation for 1-2 hours. Media shift is achieved via a Y-valve upstream of the mother machine inlet. Top: Fluorescent images of cell lineage during shift-down. Bottom: Representative traces of 3 lineages. Representation is as in Figure 3.6, with the density of the vertical green bars representing the intensity of the DnaN-mGFPmut2 signal along the long-axis of the cell. (B) Population average behavior during shift-down. Growth rate is the instantaneous elongation rate (6 minute time step). Initiation size per *ori* is plotted against the initiation time. Each measurement is normalized by their respective mean in the 4 hours before shift-down. Lines connect the 12 minute binned mean, and error bars are the standard error of the mean. Minimum bin size is 5. Dashed line in average initiation size signifies gap in initiation events after shift-down. $n=3,160$ cells (752 with initiation size). Entire time course showing shift-up and shift-down is available in Figure 3.11.

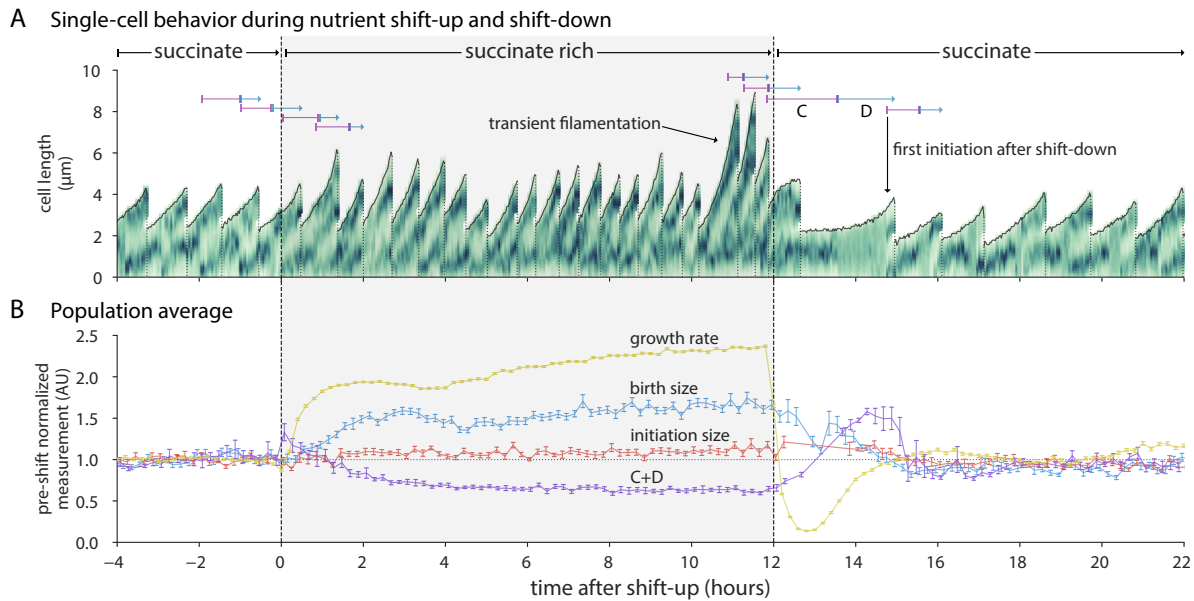


Figure 3.11: Initiation size is invariant during shift-up and shift-down. (A) Representative lineage trace for cells undergoing shift-up at time zero followed by shift-down 12 hours later. Note that this particular trace exhibits transient filamentation before and unrelated to shift-down. (B) Population average behavior for all cells. Mean lines are calculated as in Figure 3.10, except that the measurements are normalized by their respective mean in the 4 hours before shift-up. Additionally, birth size is plotted against the birth time and C+D is plotted against the corresponding division time. Upon shift-up, growth rate immediately increased, simultaneously resulting in an increase in birth size. C+D proportionally decreased. After shift-down, all parameters return to their pre-shift-up average. Despite complex dynamics in these parameters during nutrient shifts, the initiation size showed less than a 10% change during the entire time course. $n=7,671$ cells (1,695 with initiation size and C+D).

and division are delayed. For division, active degradation or antagonization of FtsZ could further hinder the triggering of constriction^{187,191}.

3.2.7 *E. coli* and *B. subtilis* change cell shape differently under different growth conditions but maintain a constant initiation size

One of the major differences between *E. coli* and *B. subtilis* is their shape under different nutrient conditions. Data from our lab and others have shown that the aspect ratio of *E. coli* is nearly constant (approximately 4) under different nutrient-imposed growth rates^{31,37}. By contrast,

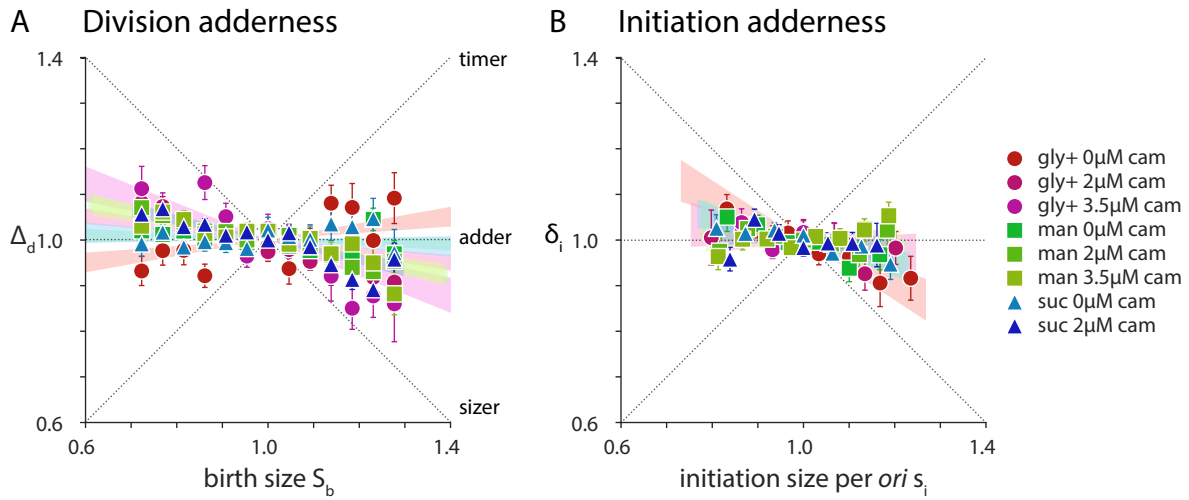


Figure 3.12: *B. subtilis* is an initiation and division adder. (A) In steady-state growth under nutrient limitation or translational inhibition, *B. subtilis* Δ_d is not strongly correlated with the S_b , consistent with the adder principle. Theoretical correlation between Δ_d and S_b for the timer, sizer, and adder models of size homeostasis are shown as dotted lines⁸. Symbols are binned data and error bars are standard error of the mean. Shaded wedges are the 95% confidence interval of a linear regression line fit to the underlying data. Data are rescaled by their respective means. (B) *B. subtilis* is an initiation adder such that δ_i is uncorrelated with s_i . However, in the fastest growth condition, added initiation size per *ori* behaves sizer-like.

the average width of *B. subtilis* remains relatively constant (Figure 3.4)^{196,213}.

Nevertheless, for initiation control in *B. subtilis*, we find that volume per *ori* is more conserved than the length per *ori* at initiation. While we find length to be a good proxy for initiation size under nutrient limitation, our data show that chloramphenicol treatment decreases cell width in *B. subtilis*. Thus, when comparing across all growth conditions, only the initiation volume is constant (Figure 3.9B-D).

3.2.8 *B. subtilis* is both a division adder and an initiation adder

As previously reported, *B. subtilis* achieves size homeostasis by following the adder principle⁸. We recently showed that *B. subtilis*, along with *E. coli*, are also initiation adders; the size added per *ori* between successive initiation events is constant with respect to initiation size¹³. We further tested those results here under additional growth conditions and translational

inhibition (Figure 3.12). We find that, for division, our data is best described by the adder principle. However, we note that when going from faster to slower growth condition, the slope becomes slightly negative. This may be due to active degradation or inhibition of FtsZ assembly or other key division proteins^{13,187,191}. For initiation, we again find that our data is best described by the adder principle. Importantly, the added size between initiation and added size between division are uncorrelated (Figure 3.17), consistent with initiation and division being controlled by separate threshold mechanisms¹³. While both processes are tied to global biosynthesis, this indicates minimal crosstalk between the two in steady-state conditions.

3.2.9 *B. subtilis* and *E. coli* share the same hierarchy of physiological parameters

The coefficient of variation (CV) of a distribution of a physiological parameter is often interpreted as the tightness of the underlying biological control⁵¹. We extended previous analysis to include the cell cycle related parameters C period, D period, initiation size, and added initiation size for both *B. subtilis* and *E. coli*. We found that both evolutionarily distant organisms share the same order of their physiological parameters in terms of CV (Figure 3.13). Width, septum position, initiation size, and growth rate are the tightest of the parameters. D period is significantly more variable than C period, and they are inversely correlated. In fact, the CV of a particular physiological parameter is extremely similar across growth conditions, species, and strains (Figure 3.14).

Ultimately, the CV of the physiological parameters is the manifestation of molecular regulatory mechanisms. Classically, *B. subtilis* and *E. coli* provide excellent examples of both homologous and non-homologous versions of such mechanisms. For example, major protein players controlling replication and division, such as DnaA and FtsZ, are conserved in these and most other prokaryotes^{88,214}. However, the regulation of those molecules in *B. subtilis* and *E. coli* is unique^{74,117,215}. More generally, the two species often use unrelated mechanisms to

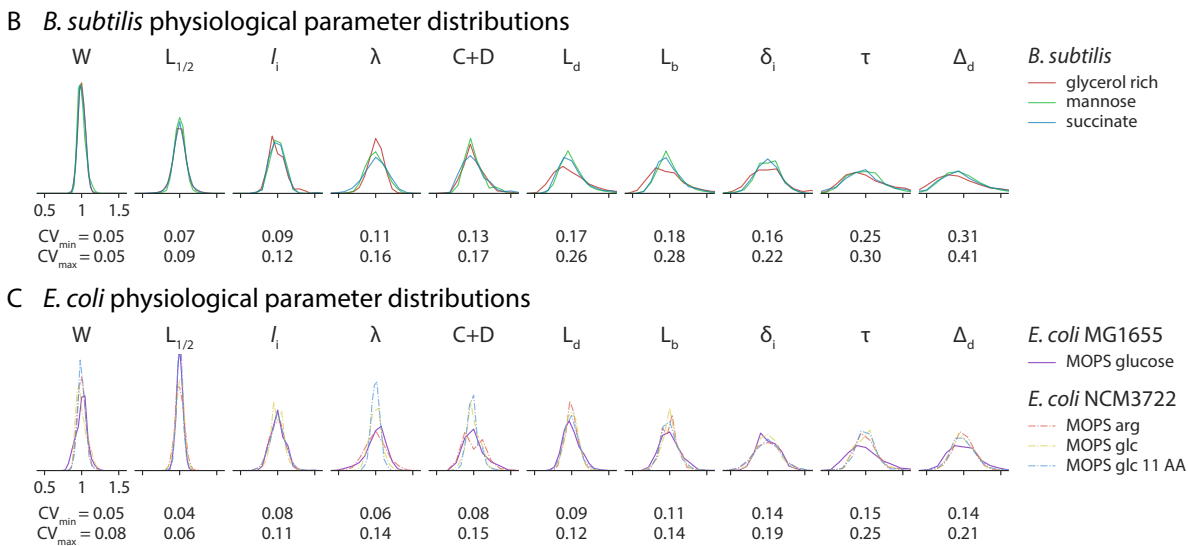
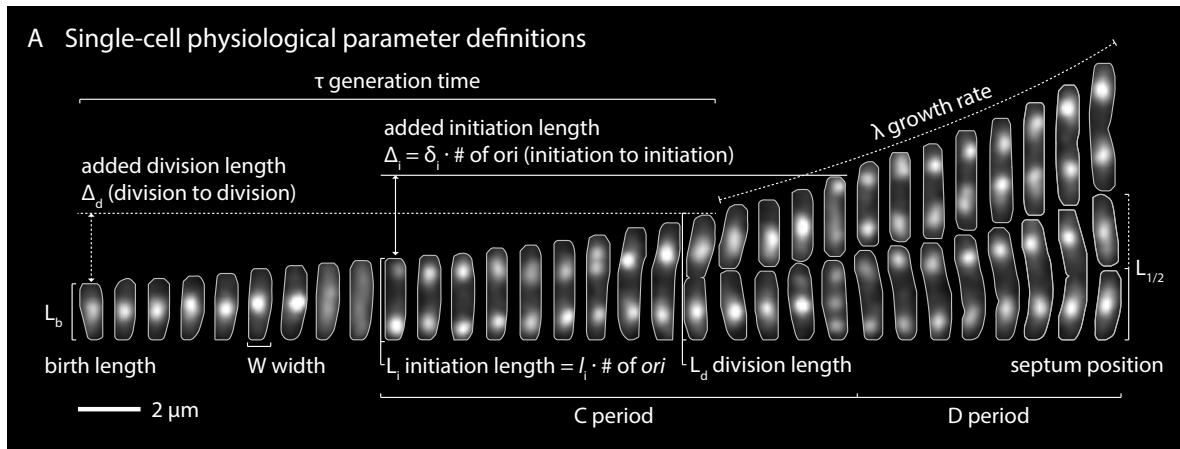


Figure 3.13: *B. subtilis* and *E. coli* share the same hierarchy of physiological parameters.

(A) Single-cell physiological parameter definitions as determined from time-lapse images. Cells are *B. subtilis* growing in mannose ($\tau = 38$ minutes). Fluorescent signal is DnaN-mGFPmut2 and grey outlines are from the segmented phase contrast image. Picture interval is 3 minutes. (B) *B. subtilis* parameter distributions are shown in order of ascending coefficient of variation (CV). Parameters are normalized by their mean. The range of CVs for each parameter is shown below the distributions. Note that length based parameters are shown here; their volume equivalents have slightly higher CVs due to variability in width. (C) Distribution of the same measurements in *E. coli* display the same CV hierarchy. Data from *E. coli* NCM3722 grown in MOPS arginine (arg), glucose (glc) and glucose + 11 amino acids (glc 11 AA) are from previously published work¹³.

achieve the same regulatory goal^{117,182}. Because of their phylogenetic distance, the uncanny agreement among the CVs of their physiological parameters suggests an evolutionary ancient

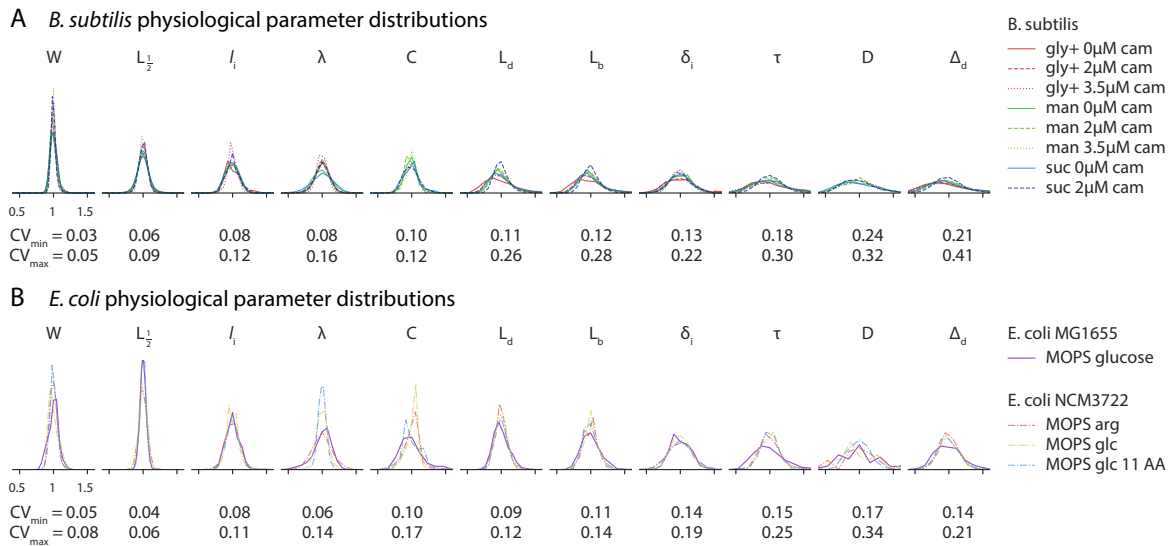


Figure 3.14: Normalized physiological parameter distributions for all conditions. (A) *B. subtilis* parameter distributions from perturbation experiments are commensurate with nutrient limitation conditions. C period has a smaller CV than D period. (B) In *E. coli*, the CV of C period is smaller than D period. The CV of C+D is smaller than each individually as they are inversely related. Data from *E. coli* NCM3722 grown in MOPS arginine (arg), glucose (glc) and glucose + 11 amino acids (glc 11 AA) are from previously published work¹³.

control framework shared by these organisms.

3.3 Conclusion

We have shown that *B. subtilis* and *E. coli*, despite their historical separation across the Gram stain divide, share extremely similar fundamental physiological behavior (Figure 3.15). Under a wide range of nutrient and growth inhibition conditions, both species base their chromosome replication in a constant initiation size. Impressively, this constant initiation size is imposed even during dynamic growth transitions. This is consistent with a threshold mechanism and constant production of cell cycle initiator proteins for initiation and division timing control, thus maintaining size homeostasis with the adder principle¹³.

As with *E. coli*, DnaA and FtsZ are among the key proteins responsible for the initiation and division threshold mechanisms in *B. subtilis*, respectively^{13,39,106}. The view that global

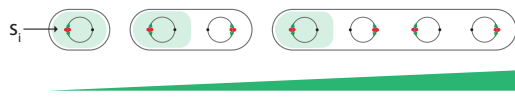
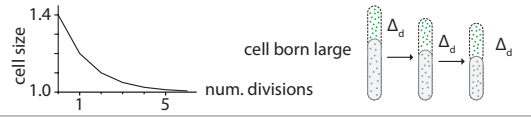
Shared?	Physiological principle	<i>B. subtilis</i>	<i>E. coli</i>
Shared	Invariant initiation size	Initiation size is constant in both nutrient limitation and antibiotic inhibition conditions.	
Shared	Initiation and division size homeostasis	Initiation and division size homeostasis is achieved via the adder principle.	
Shared	Parameter hierarchy	CV of physiological parameters retains same order. CVs are independent of growth condition.	$W, L_{1/2}, s_i, \lambda, C$ L_d, L_b, δ_i τ, D, Δ_d $5\% < CV < 10\%$ $10\% < CV < 20\%$ $CV > 20\%$
Partially shared	Cell size and shape behavior	Cell size increases with growth rate due to extension in length. Constant width.	Cell size increases <i>exponentially</i> with growth rate. Proportional increase in length and width.

Figure 3.15: *B. subtilis* and *E. coli* comparative summary.

biosynthesis fundamentally controls their production, and thus the replication and division rate, is still compatible with the idea that additional levels of regulation modulate or coordinate their activity in certain situations^{66,74}. It is unclear whether these additional mechanisms have evolved to increase replication and division fidelity during steady-state or are more important in dynamic environments. More single-cell shift experiments with mutant or even minimal genome cells will help reveal the importance of redundant regulatory systems.

These deep similarities between *B. subtilis* and *E. coli* speak to a conserved control framework which both species use to coordinate growth, DNA replication, and division. In doing so, they ensure life's essential demand of physiological homeostasis. In the end, it is unclear if this framework is the result of parallel or convergent evolution. In order to better address this question, more quality single-cell data is needed from diverse prokaryotes. In either case, the existence of a shared control framework underscores its efficacy, providing an intriguing avenue for the development of synthetic organisms.

Chapter 3, in full, has been prepared for submission for publication of the material. Sauls, John T; Cox, Sarah E; Do, Quynh; Castillo, Victoria; Ghulam-Jelani, Zulfar; Jun, Suckjoon. The dissertation author was the primary investigator and author of this material.

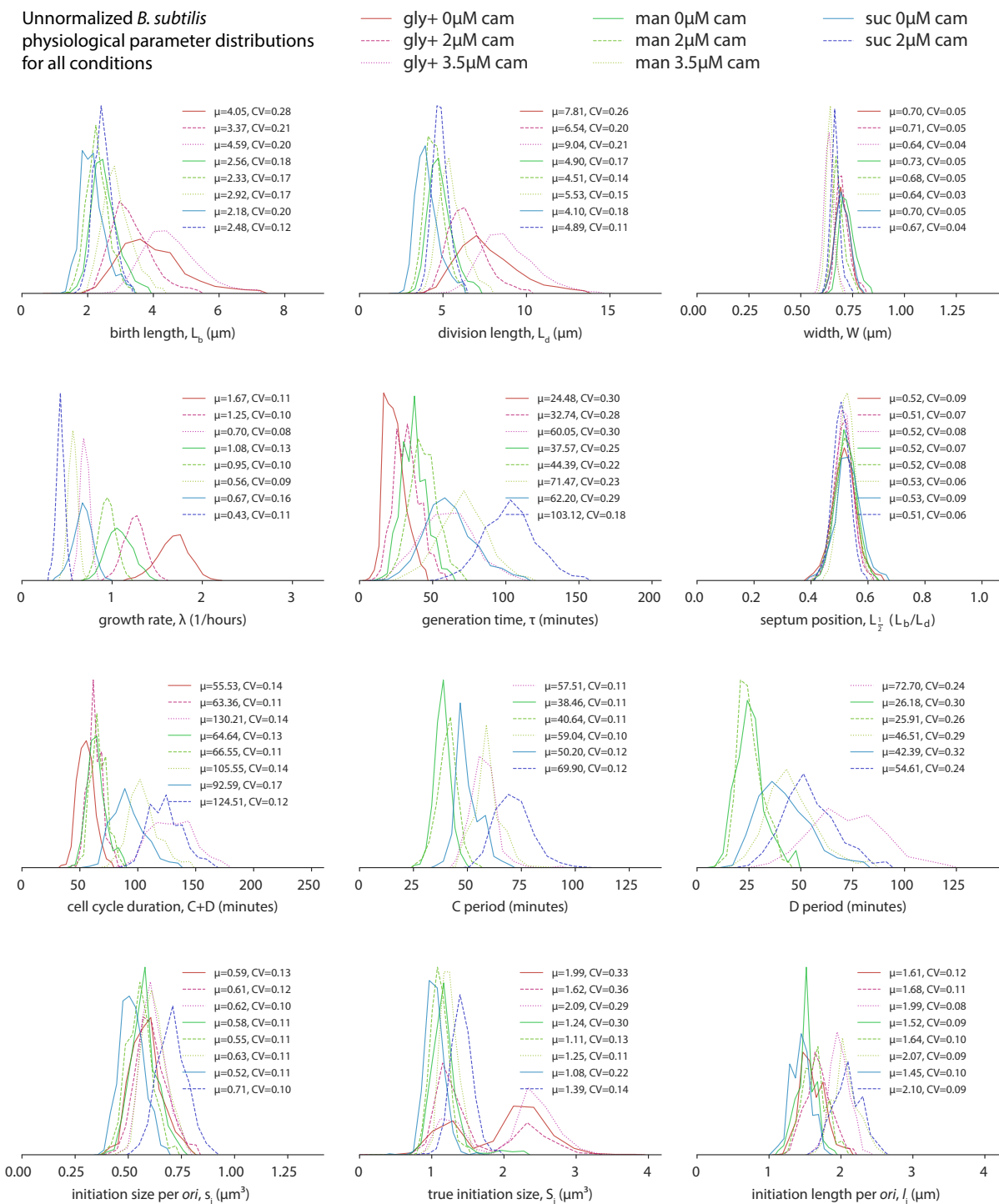


Figure 3.16: Unnormalized physiological parameter distributions for all conditions. *B. subtilis* physiological parameter distributions for all conditions. True initiation size S_i is not corrected for the number of *ori*. For conditions in glycerol rich, cells may be born with 1 or 2 replicating chromosomes.

Normalized cross correlations of
physiological parameters for all conditions

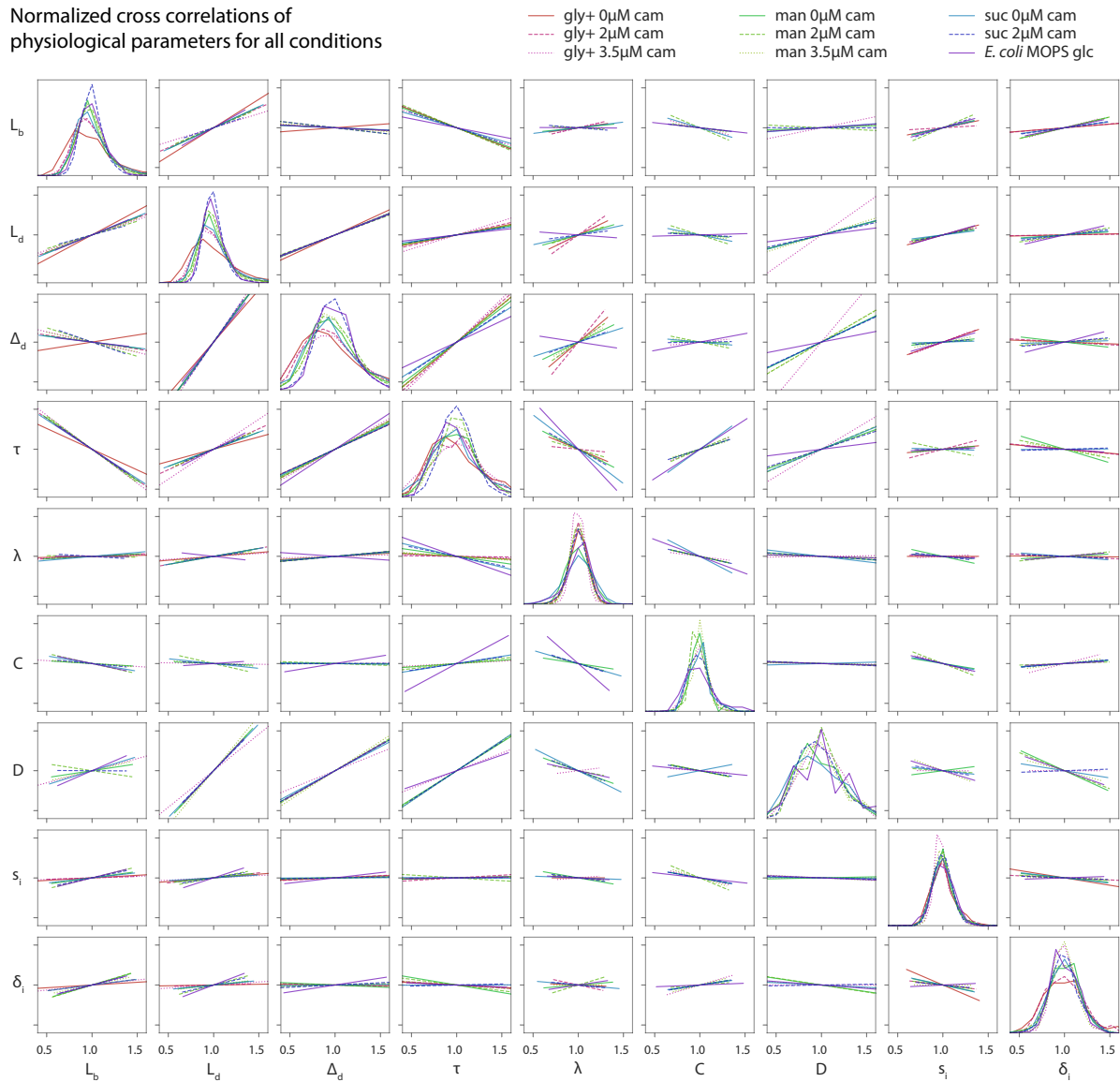


Figure 3.17: Normalized cross-correlations. Normalized cross-correlations for all *B. subtilis* conditions and one *E. coli* condition. Lines are linear regression fits to the single-cell data. Symbols are as in Figure 3.13. Normalized distributions are plotted along the diagonal.

Chapter 4

Replication and Division Coordination

During Physiological Shifts

4.1 Introduction

In this chapter I describe a collection of single-cell imaging experiments where I measure replication and division control in order to understand the extent of their coordination. These experiments rely on fluorescent fusion proteins, which in addition to phase contrast imaging, allow me to track these processes directly. This includes replication via DnaN, divisome assembly via FtsZ, and nucleoid segregation via HU.

Many of these experiments also exploit the nutrient shift paradigm, in which cells growing at steady-state in one condition are abruptly switched to another condition. This second condition may be more (shift-up) or less (shift-down) favorable than the initial condition. The manner in which cells respond to this change has historically shed light on their physiological regulation. I will cover relevant cases in the literature as needed, as many many of my experiments are simply modern renditions of classic studies.

Macromolecular accumulation and rate maintenance during nutrient shift-up
Kjeldgaard, Maaløe, and Schaechter (1958)

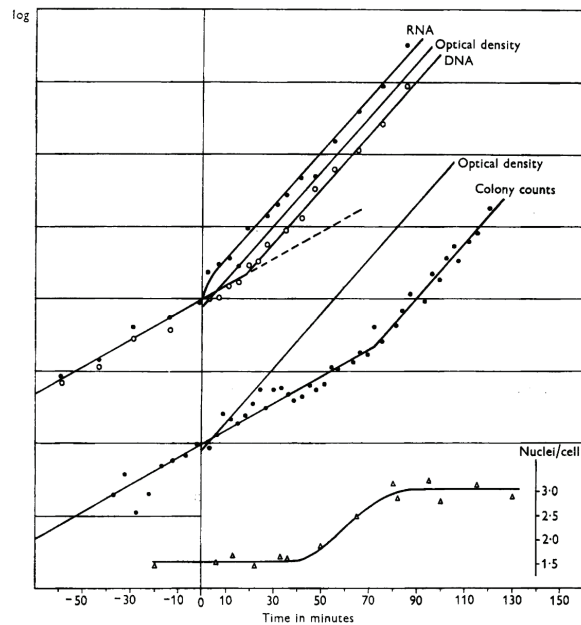


Figure 4.1: Macromolecular accumulation and rate maintenance during nutrient shift-up. RNA and optical density increase quickly upon a shift to richer medium, while DNA synthesis and cell number are delayed by 20 and 70 minutes, respectively. Reproduced from Kjeldgaard et al.²¹¹.

4.2 Imaging replication and division coordination in *E. coli*

4.2.1 A constant initiation size is conserved during nutrient shift-up

In this section we review experiments that show a constant initiation size is obeyed even in dynamic environments. This strongly supports the threshold model for initiation.

At steady-state, the pioneering work by Schaechter, Kjeldgaard, and Maaløe demonstrated how faster growing cells in rich medium were larger, and contained a higher concentration of RNA and DNA than slower growing cells in minimal medium (Figure 1.3)¹⁶. The same authors in the same year also measured how these quantities changed in a shift from minimal to rich medium (Figure 4.1)²¹¹. They found that while RNA and cell mass increased their rate

Tracking cell cycle parameters during nutrient shift-up

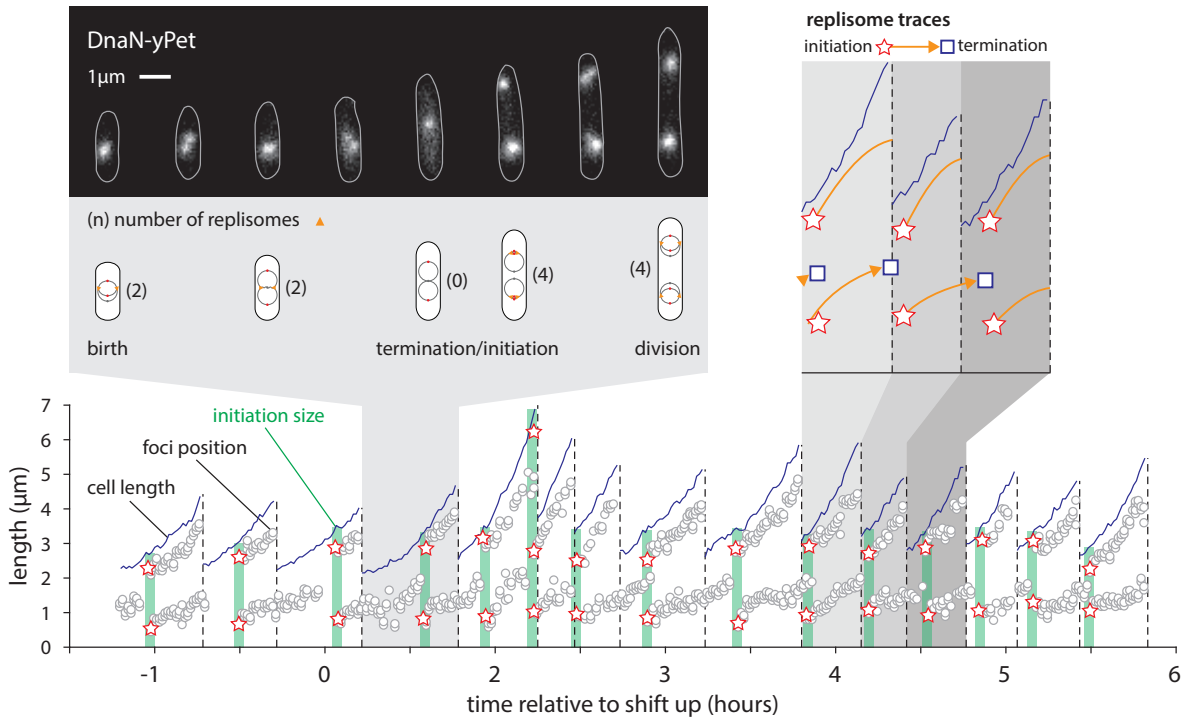


Figure 4.2: Single-cell nutrient shift-up. DnaN-yPet can be used to track active replisomes and determine the cell cycle parameters in single cells. Images of fluorescent images are shown with the corresponding chromosome conformation for the highlighted cell. During nutrient shift-up, cell size increases but the initiation size stays constant, moving the timing of initiation closer to the birth of the cell.

of accumulation instantly, an increase in DNA and cell count was delayed. They coined this phenomenon “rate-maintenance.”

Stephen Cooper later explained rate-maintenance as a consequence of the constant $C+D$ of the H-C model²¹². When cells enter a richer medium, they immediately upregulate the production of RNA (of all types), as well as protein production, which is reflected in the increase in mass (growth rate). However, they cannot increase their rate of division because initiation events that occurred before the shift-up must still wait $C+D$ minutes before cells divide. In fact the increase in cell count was measured by Kjeldgaard and colleagues to be 70 minutes after shift up, close to the 60 minute duration for $C+D$ measured by Helmestetter and Cooper. They delay in DNA

Single-cell parameters during shift-up

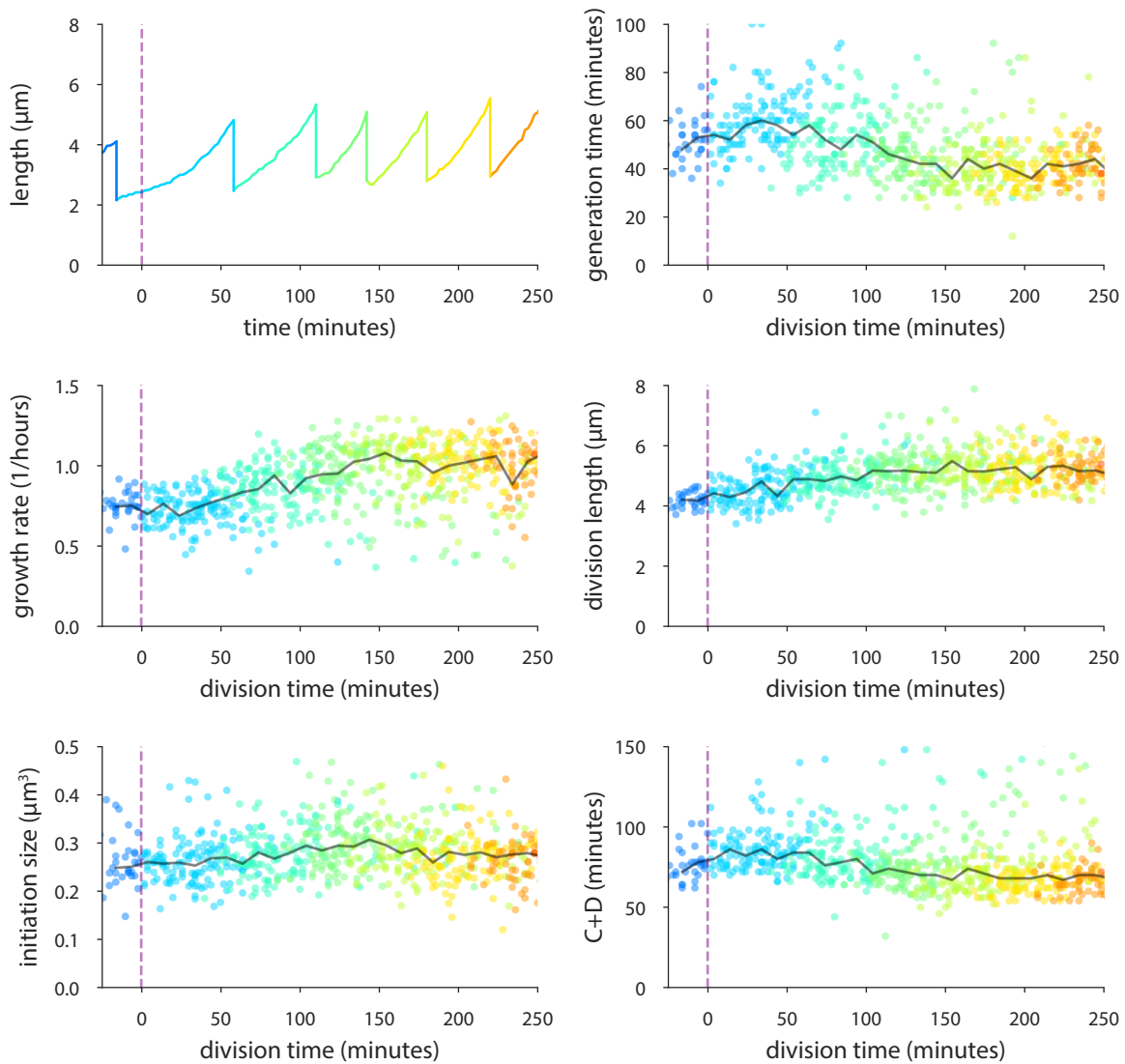


Figure 4.3: Single-cell parameters during shift-up. Single-cell parameters during nutrient shift-up. Scatter plot colors correspond to the generations relative to the shift-up in the top left single cell trace, i.e., light blue dots are cells born before shift-up but divide after. Rate maintenance is seen in the top right plot as these cells have a generation time of 60 minutes, which only decreases for cells born after the shift-up. Note that parameters are plotted against the division time of each cell.

synthesis of 20 minutes can be attributed residual D periods overlapping with the shift.

I repeated this experiment at the single-cell level, shifting cells from glucose minimal

media to the same media with a supplement of 11 amino acids, changing the doubling time from 40 to 60 minutes. To measure the cell cycle parameters, I used a fluorescent protein fused to DnaN, the β -clamp of DNA polymerase III²¹⁶. When the replisome is active and polymerizing DNA, the local concentration of DnaN increases such the location of the replisome can be resolved as a diffraction limited spot. The spatiotemporal location of these foci can be used to manually determine the cell cycle parameters. Figure 4.2 shows an example image of the DnaN signal and resolving the single-cell cell cycle dynamics during shift-up.

My data supports the classic observations to a large degree (Figure 4.3). I find that while the elongation rate increases immediately, the generation time is maintained in the generation of cells that experience the shift up. While C+D is not strictly constant between the two growth rates, the shift-down supports the notion that the division rate cannot be greatly increased before C+D minutes after the initiation rate has increased.

The initiation rate however increases immediately with the growth rate. This is reflected in the initiation volume, which is constant throughout the shift-up. This supports a model in which the replication initiator molecule accumulates in proportion to cell volume, and triggers initiation at a constant number per *ori*. This naturally leads to an initiation time that occurs earlier in the cells life, as the shift-up is accompanied by a corresponding increase in birth and division size.

4.2.2 A constant initiation size is conserved during nutrient shift-down

In this section we extend the previous measurement to nutrient shift-down. We observe that the initiation size is still conserved through the transition, but that the timing of division is not well explained by the H-C model.

Kjeldgaard and colleagues also measured the reverse of their shift-up experiment by growing cells in nutrient broth, then filtering the cells and resuspending them in minimal glucose media (Figure 4.4)²¹¹. In this scenario, RNA synthesis and optical density do not increase until at

Macromolecular accumulation and division during nutrient shift-down
Kjeldgaard, Maaløe, and Schaechter (1958)

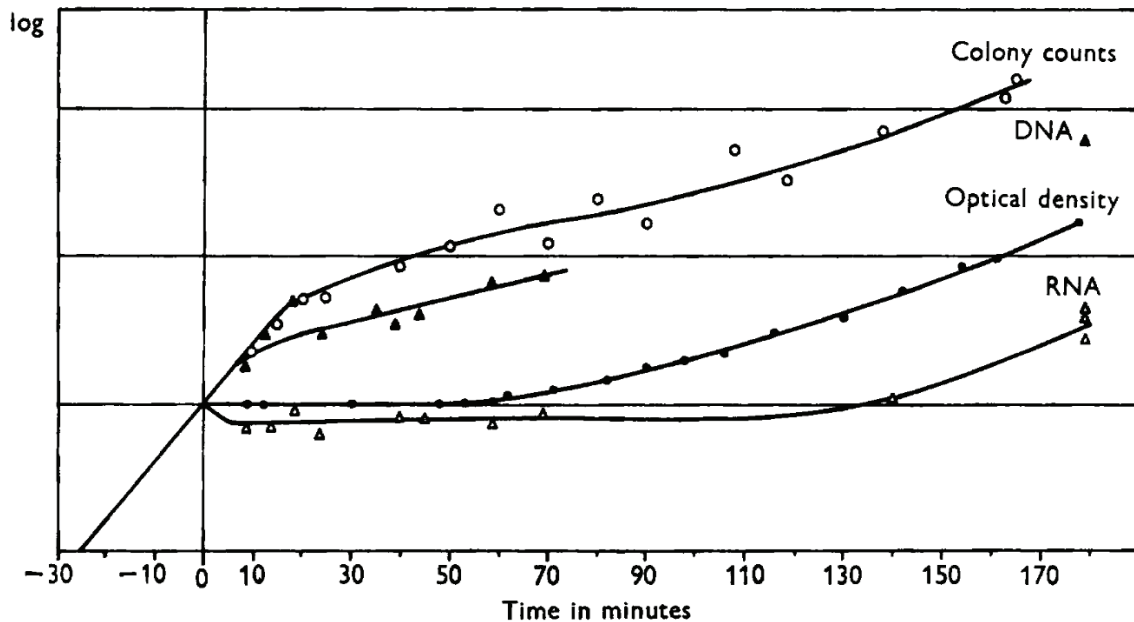


Figure 4.4: Macromolecular accumulation and division during nutrient shift-down. RNA accumulation and cell mass cease increasing upon shift-down, while DNA synthesis and division occur at the pre-shift rate for a short time. Reproduced from Kjeldgaard et al.²¹¹

least an hour has passed, indicating growth is inhibited. However, DNA synthesis and cell count maintain their preshift rate for approximately 20 minutes, and then reduce the rate to something closer to the post-shift steady-state value.

The authors recognized that if cell count continues to increase while cell mass does not, the average cell decreases during shift-down. However, it was not clear to them the source of the discrepancy between RNA and protein synthesis, versus DNA synthesis and the division rate. Tellingly, Cooper did not attempt to explain this data when he addressed the shift-up data as outlined above²¹².

The H-C model does not describe shift down, because if the constant $C+D$ was obeyed, colony counts should have increased for 60 minutes from the shift down, not 20. Instead, the data implies that only cells already close to division executed the task, while others waited. Indeed,

Single-cell cell cycle parameters during nutrient shift-down

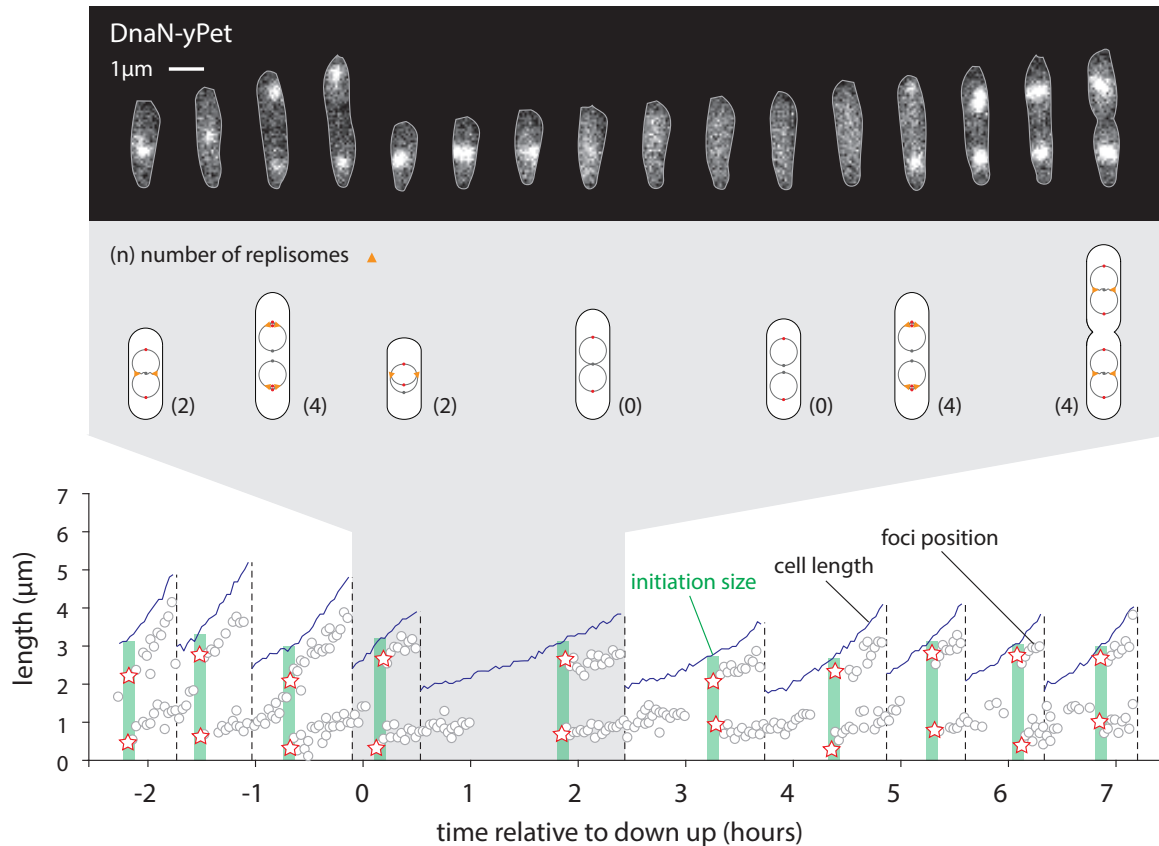


Figure 4.5: Single-cell nutrient shift-down.. Determining replication dynamics in single cells during shift down. (Top) Replication foci are visible by DnaN-Ypet. (Middle) The replication state of the cell is deduced from the foci. (Bottom) A single lineage undergoing shift down (at time zero). The red stars show the initiation time and the green bars are the initiation size. Termination is at the end of the line created by the foci positions. The top and middle panels show the two cells in grey. The first cell experiences the shift down at time zero. While C period does not appreciably increase, the second cell has a delayed division (and hence delayed D period).

this is what I observed when revisiting in this experiment with the mother machine (Figure 4.5). In the generation during and after shift down, a cell may divide, and then it is followed by a cell with an extremely long generation time and low growth rate (Figure 4.6). Interestingly, the C period of cells during this time does not appreciably increase. That is, if replication starts, it will finish “on time.” Since division is delayed, there is instead a large increase in the D period.

Impressively, the size at replication initiation is unperturbed during these changes. Cells

Single-cell parameters during shift-down

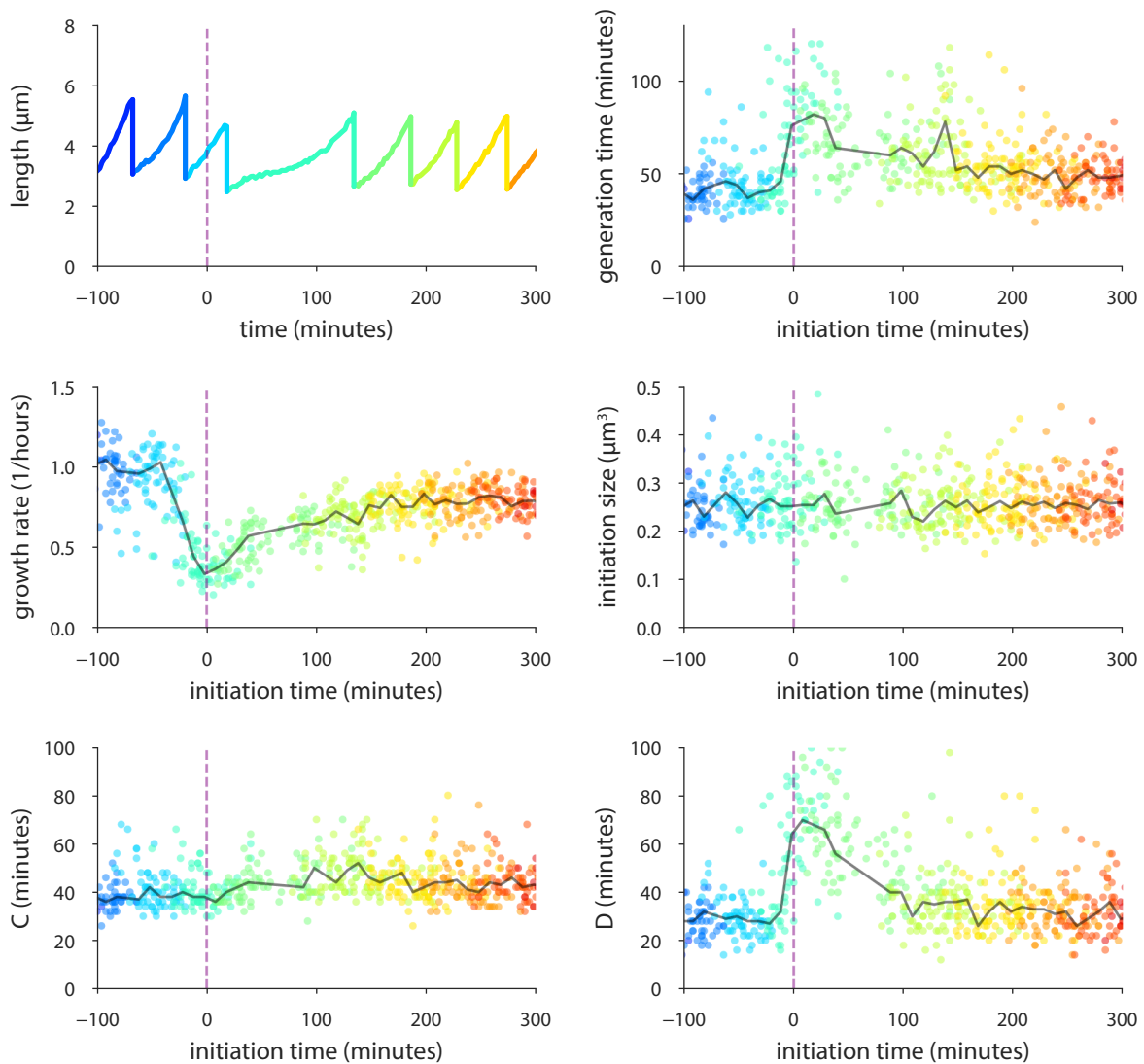


Figure 4.6: Single-cell parameters during shift-down. Single-cell parameters during nutrient shift-down. Scatter plot colors correspond to the generations relative to the shift-up in the top left single cell trace, i.e., light blue dots are cells born before shift-up but divide after. Note that parameters are plotted against the initiation time of that cell. This emphasizes that cells which initiate before the shift down can still increase their generation time (via the D period), greater than what is prescribed by the H-C model.

simply wait until they have reached the requisite size, which manifests itself as a dearth of initiation events after shift-down. This comports with the idea that replication initiators accumulate

FtsZ accumulation in *E. coli*

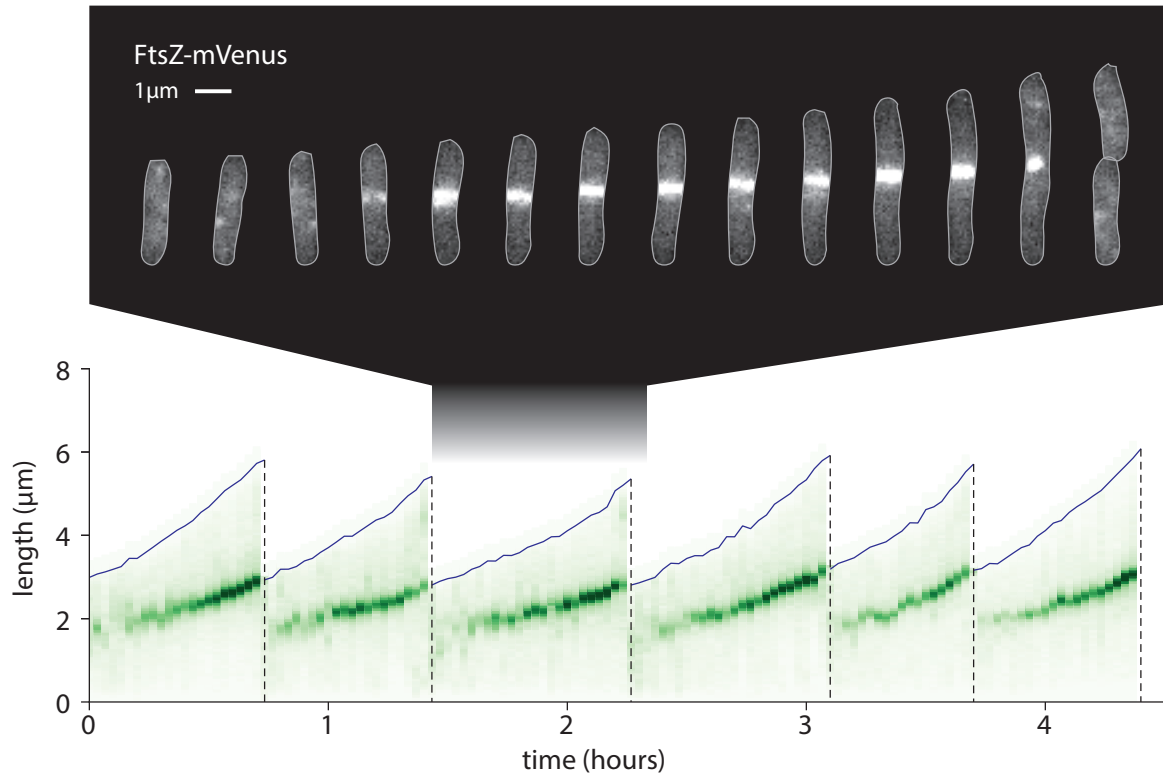


Figure 4.7: Measuring FtsZ ring formation in single cells. (Top) Time lapse images of the mVenus channel of the cell indicated. (Bottom) The cell length and fluorescent signal from FtsZ-mVenus for a single lineage at steady state. The green color is the sum of the fluorescence intensity along the long axis of the cell. The formation and location of the Z-ring are clear at the midcell. Cells are growing in MOPS glucose.

proportionally with growth rate, thus retaining a constant concentration regardless of if cells are in steady-state or not. Indeed, the added size between initiation events is also constant. The fact that division is delayed relative to these initiation events indicates that the former is not strictly coupled to the latter. An explanation for this delay is covered in the next section.

4.2.3 Division is controlled by FtsZ accumulation at the midcell

During nutrient shift-down the canonical time interval between replication and division is broken. Instead, division proceeds when FtsZ accumulates to the proper level, supporting a

model in which division is controlled by a separate threshold mechanism.

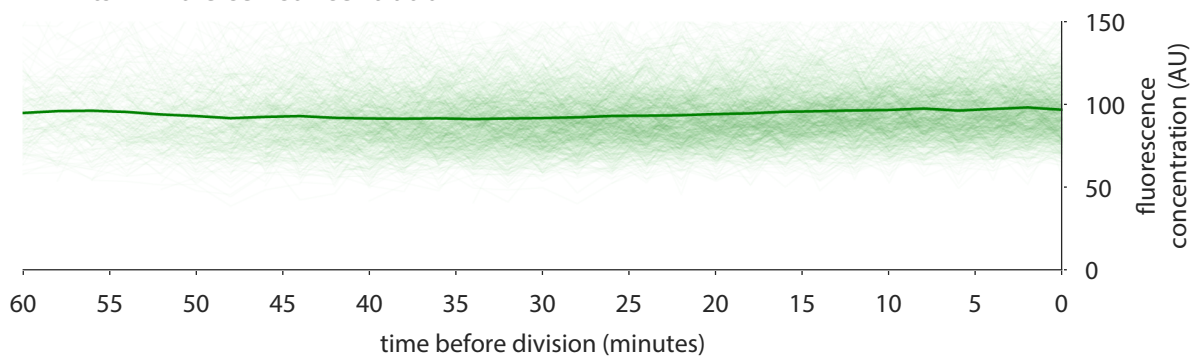
To understand why division is delayed during nutrient shift-down, we should first consider how division is triggered in steady-state conditions. As described in Subsection 2.3.5, I hold that the cell divides when it attains a requisite number of FtsZ. More specifically, I believe that it commits to division when the number of FtsZ molecules have assembled in the Z-ring at midcell. This commitment happens before the actual division event, likely right before the onset of visible constriction. This is around 10 minutes before division in faster growth rates²¹⁷.

To test this theory, we used a near-functional FtsZ-mVenus fusion protein and tracked its amount and localization over the division cycle (Figure 4.7)¹³⁵. The FtsZ-mVenus marker is the sole copy of FtsZ in the cell. From this data we first recognize that FtsZ concentration is constant throughout the cell cycle. This means it satisfies the requirement of balanced biosynthesis, as its production is tied directly to instantaneous growth rate of the cell. We also recognize that the formation of the Z-ring occurs very early in the cell's life, usually only a few minutes after birth. Once the Z-ring forms, the fraction of FtsZ in the ring versus the cytoplasm is stable at around 30%, increasing slightly towards division, and then decreases during constriction as the ring disassembles^{154, 178}. Because the FtsZ concentration is constant, and the fraction of FtsZ in the ring is stable save for right around a division event, the number of FtsZ in the ring steadily increases as the cell grows (Figure 4.8).

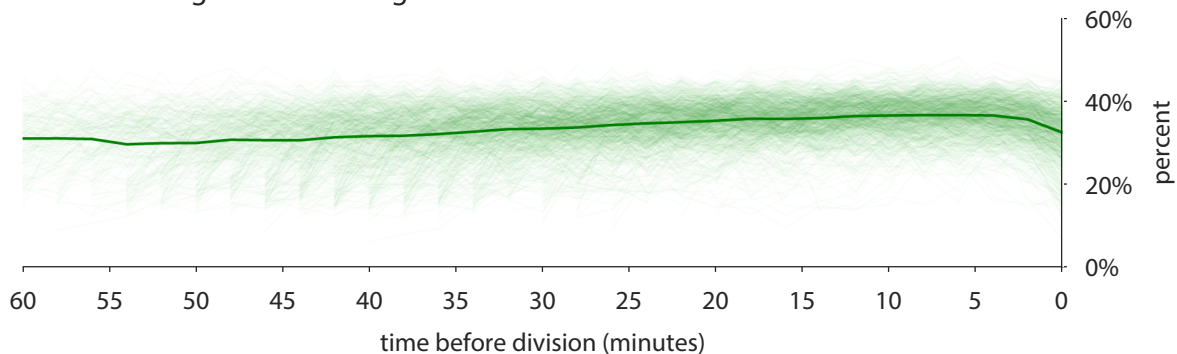
If division is triggered when FtsZ reaches a critical level in the ring, then the intensity of FtsZ-mVenus in the ring at that time should be independent of the division size. This is indeed the case (Figure 4.9). The top left panel shows the amount of FtsZ in the ring at the time of constriction is independent of the eventual division. This supports a model where the cell commits to division at constriction, which is triggered by this amount of FtsZ. The top right panel shows the FtsZ in the whole cell at this time correlates with the division size, indicating that it the amount in the ring which is critical. That is to say, cells which divide large may have more FtsZ at constriction, but they do not have more active FtsZ. The bottom left panel shows the division

Accumulation of FtsZ over the division cycle

A FtsZ whole cell concentration



B Percentage of FtsZ in ring



C FtsZ intensity at midcell and quarter position

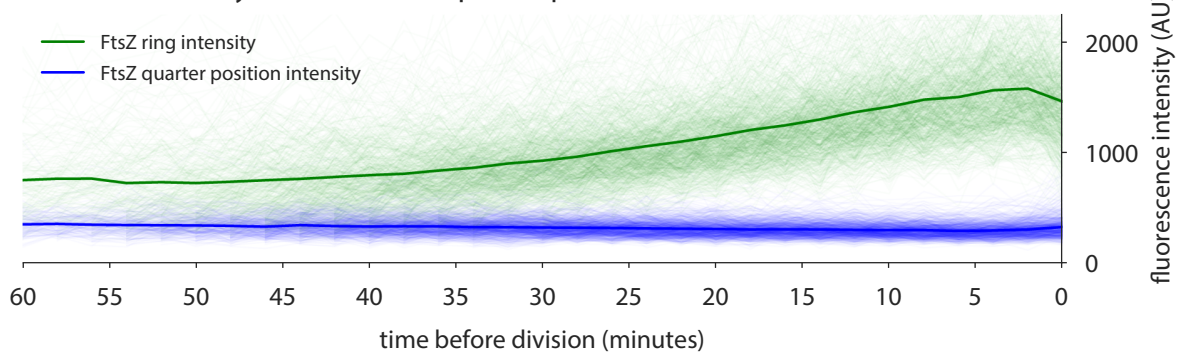


Figure 4.8: FtsZ accumulation over the division cycle. (A) Thin traces show the concentration of FtsZ of many cells aligned to their division time. FtsZ concentration is constant throughout the division cycle. The thick line is the population average. (B) The percentage of FtsZ in the ring is mostly constant over the division cycle. (C) The intensity of the Z-ring increases throughout the division cycle until the moment of constriction, at which point the ring disassembles. The intensity of the Z-ring was calculated by integrating the intensity of a box surrounding the midcell. The intensity of quarter position, like the total concentration, remains constant.

FtsZ ring intensity at constriction

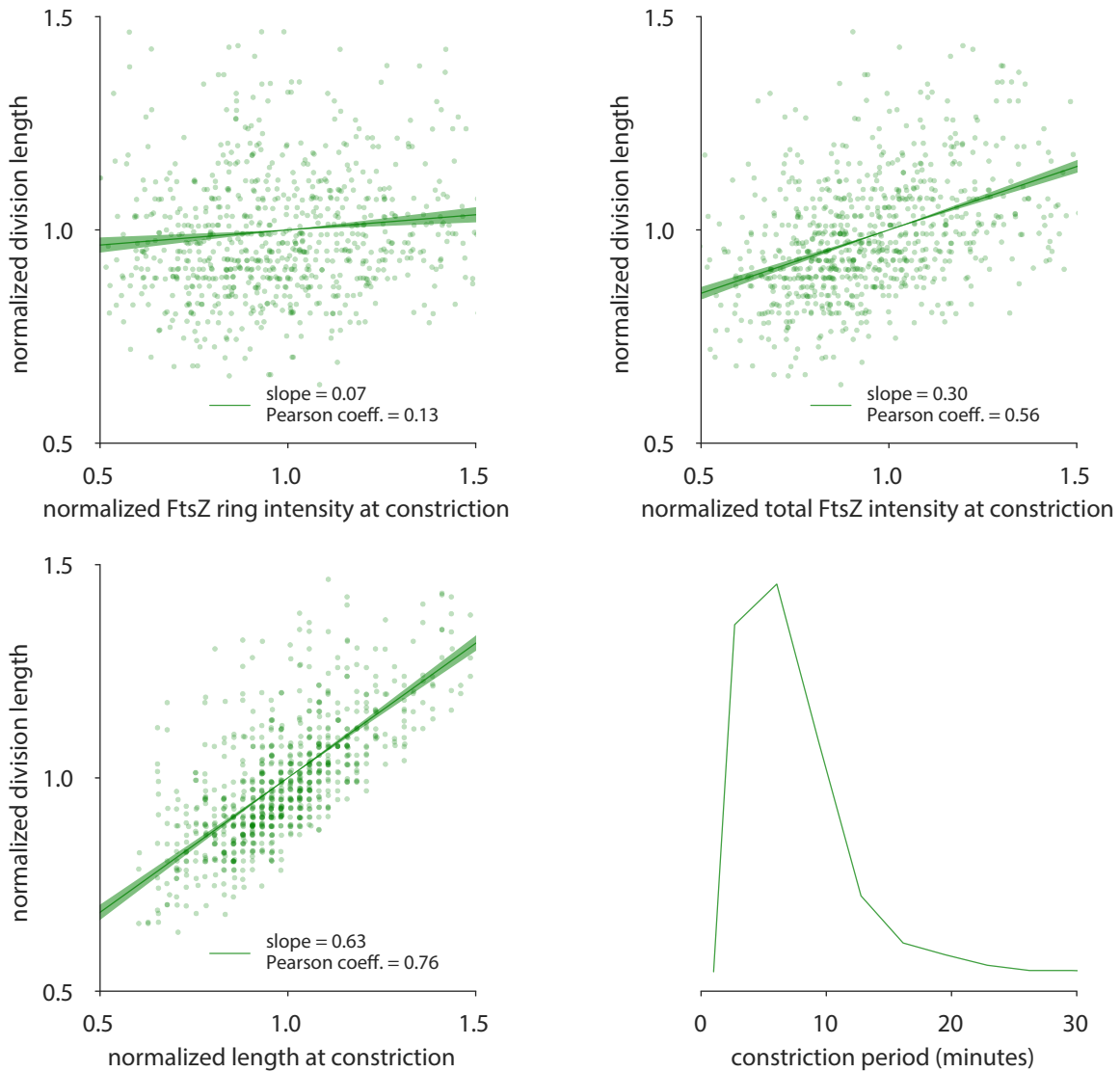


Figure 4.9: Division is triggered when the Z-ring contains a critical amount of FtsZ. See text for information.

length correlates highly with the constriction length. This indicates that once constriction begins, division follows shortly after. The bottom right panel shows the distribution of the time period between constriction and division.

Whether a cell is small or large at a particular moment is irrelevant to the timing of division, it only matters if they have assembled a functional Z-ring. Of course, larger cells will naturally

have more FtsZ than smaller one due to balanced biosynthesis, but the stochasticity in division size can be attributed in part due to stochasticity in the timing of reaching the FtsZ-in-the-ring threshold.

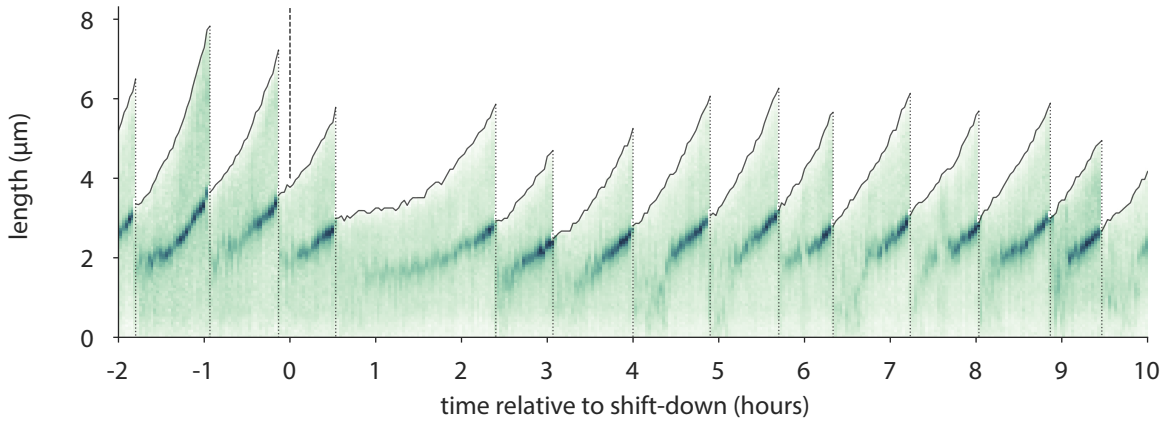
This argument is strengthened in experiments in which FtsZ levels are oscillated by way of an exogenous signal¹³. In these experiments, and in accordance with previous research, division size decreases with higher FtsZ expression and increases with lower expression. However, despite an almost two-fold change in division size, the maximum intensity of the Z-ring (usually around 10 minutes before division) is independent of the division size (See Si et al. Figure 6¹³).

During shift-down, what then are the dynamics of ring formation? In Figure 4.10, we see that the Z-ring still forms and that division is triggered upon the intensity of the Z-ring reaching a critical amount. FtsZ concentration remains roughly constant during the shift down, indicating that it is made in proportion to the instantaneous growth rate. Since the division size decreases, the total number of FtsZ in the cell at division also decreases. In order to divide at a smaller size, while maintaining the same critical threshold for FtsZ in the ring and the same FtsZ concentration, the cell increases the fraction of FtsZ in the ring. It is not clear how the cell achieves this, but it is likely due to changes in the activity of FtsZ regulators such as ClpX and OpgH.

The differential regulation of FtsZ with growth rate, both its expression and assembly, makes it distinct from DnaA and is the essential reason for how *E. coli* changes its size. For DnaA, we observe a constant concentration in all growth rates. Additionally, we posit that the same fraction of DnaA is active for initiating replication, and the same number of active DnaA molecules per *ori* are needed for initiation (i.e., the threshold is the same). The result of this is that the initiation size is the same across all growth conditions.

For FtsZ, at least one of these tenets must be false. Otherwise, the cell would divide at the same size across growth rates, at odds with the foundational Schaechter line. If division is controlled by a threshold model, and assuming balanced biosynthesis (i.e., FtsZ is not regulated in a cell cycle dependent manner), three possible aspects division triggering can change with

A FtsZ dynamics during shift-down



B Population behavior of FtsZ during shift-down

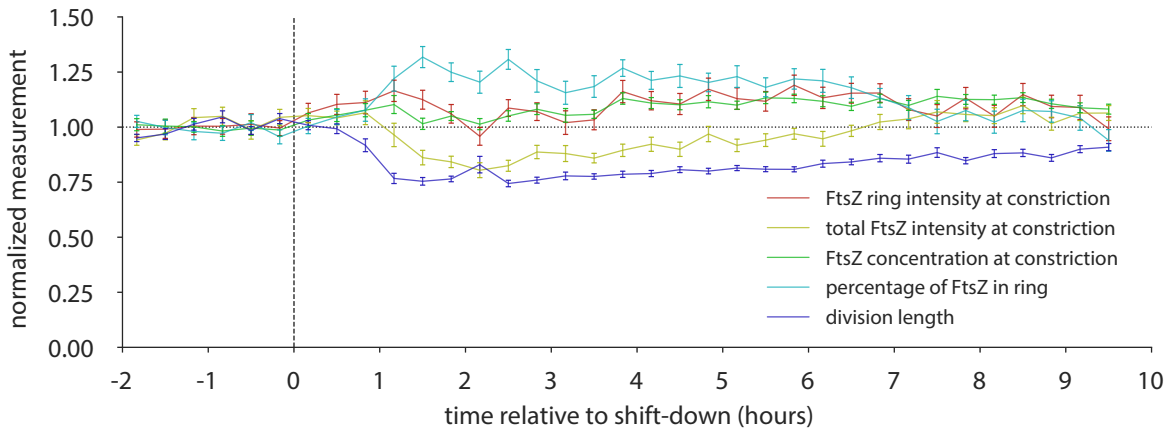


Figure 4.10: Division is determined by FtsZ accumulation in the Z-ring. (A) During shift-down, growth-rate crashes and division is delayed. In single cells, FtsZ still accumulates at the midcell during the division cycle, while the total concentration of FtsZ in the cell stays roughly constant. (B) The divisions after shift-down are still triggered when the cell attains a critical amount of FtsZ at the midcell. Because the concentration stays the same, the fraction of FtsZ in the ring transiently increases.

respect to FtsZ.

1. The threshold amount of FtsZ can change with the growth rate.
2. The concentration of FtsZ can change with the growth rate.
3. The ratio of active FtsZ to total FtsZ can change with the growth rate.

Unfortunately there is conflicting data on which of these aspects of FtsZ regulation changes with growth rate to produce the Schaechter line, and it is possible that all three are in play.

For the threshold to change, the most intuitive evidence is that the cell width also changes with growth rate. It is conceivable then that faster, larger cells with greater width require more FtsZ to trigger division. However, because the mechanisms of triggering constriction is not fully understood (i.e., how the cell measures if the threshold number of FtsZ molecules has been attained), this avenue of thought is mostly speculation. In addition, cell width does not change with growth rate in *B. subtilis*.

For the differential expression of FtsZ, there are conflicting reports stating that the concentration of FtsZ is constant and that the copy number of FtsZ is constant at different growth rates^{109,184}. If the copy number were constant, that would provide a tidy solution to the problem. It means that faster growing cells down-regulate the expression of FtsZ, such that its concentration is lower in larger cells. If the same number of FtsZ is required to reach the division threshold in all growth conditions, then fast growing cells would indeed divide at a larger size as they would grow more between successive division events.

However, if the concentration does not change during with growth rate, then it is the amount of FtsZ that is competent for activating division which must change. Arguably, there is the most evidence for this method of regulation. FtsZ has many binding partners, most of which antagonize the assembly of FtsZ into the ring. As discussed above, if the activity of these Z-ring assembly inhibitors is coordinated with growth rate, then the cell can effectively control its division size by changing the active fraction of FtsZ. My shift-down data also supports this strategy as it is the fraction of FtsZ in the ring that changes most when the cells change environments. However, to fully understand how absolute cell size is coordinated with growth rate, a more systematic treatment of FtsZ expression and assembly dynamics are required.

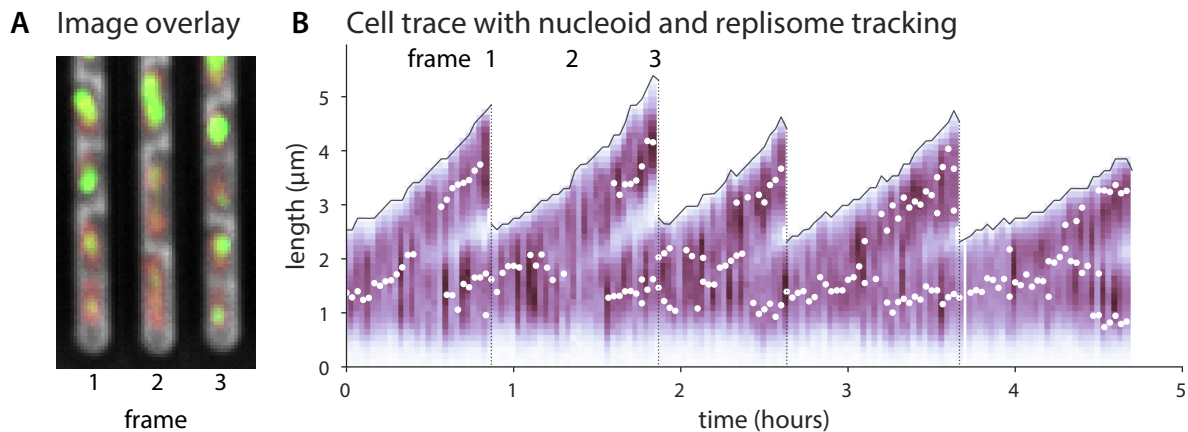


Figure 4.11: Tracking nucleoid segregation and replication. (A) Representative images for cells expressing HU-mCherry (red) and DnaN-yPet (green). (B) Example trace of cells in A used to determine the size and timing of initiation, termination, and nucleoid segregation. Purple signal is Hu-mCherry fluorescence summed along the long axis of the cell. White circles are the position of replisomes as determined from the DnaN-yPet foci.

4.2.4 Nucleoid segregation occurs at a fixed size unrelated to ring formation

The timing of nucleoid segregation in relation to the cell cycle and cell size provided fertile ground for speculation about coordination mechanisms in the past. Here, we show that segregation occurs at a fixed size as opposed to certain time after initiation. Nucleoid segregation is spatially but not temporally correlated with Z-ring formation. Note that by nucleoid segregation I mean the physical separation of the nucleoid. This is distinct from chromosome segregation, in which new replicated DNA is separated. Chromosome segregation is known to happen concurrently with replication¹⁶⁶.

In *Does the Initiation of Chromosome Replication Regulate Cell Division*, Arthur Koch investigates if, like initiation, division is controlled by its own independent signal. He also speculates that nucleoid segregation could itself be linked to its own size-related trigger. This theory had roots in earlier work, including some from Schaechter and colleagues based on quantitative imaging experiments showing that segregation happened at a certain time before

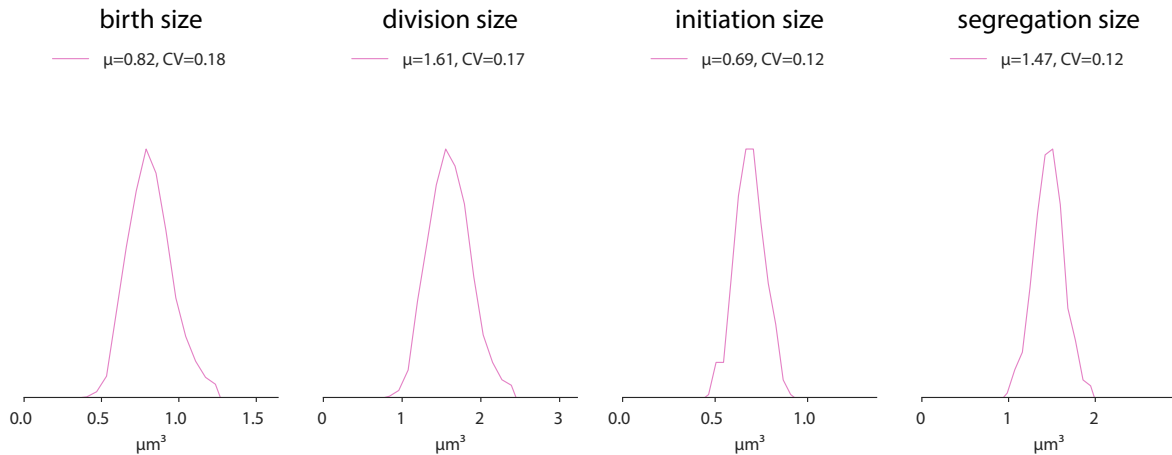


Figure 4.12: Distribution of cell cycle event sizes. As previously reported, the CV of the initiation size is significantly smaller than birth or division size. Here we also show that the size and segregation is similarly small.

division and with a similar CV¹⁵⁹.

Using a fluorescent marker for the DNA associated protein HU in conjunction with a replisome marker, I measured the single-cell growth and cell cycle parameters, including the segregation size (Figures 4.11 and 4.12). Impressively, the CV of the size at segregation is extremely small at 12%, the same as the initiation size. In addition, this size seems to be conserved in additional growth rates and during nutrient shift-down.

It is unclear to me what the significance of the segregation size is. Donachie and others produced a number of papers speculating that nucleoid segregation occurred at a size that was twice the minimal cell length (as extrapolated from the Schaechter line and equivalent to the initiation length) and commensurate with the termination time²¹⁸. My data for *E. Coli* growing with a doubling time of 55 minutes, indicates that the segregation time is always after termination by around 7 minutes, but with a large CV (63%). My segregation size is slightly greater than twice the minimum cell length (4.11 vs 1.93 μm), consistent with Donachie's work (personal communication).

This may mean that the cell must reach a minimum size before segregation can occur.

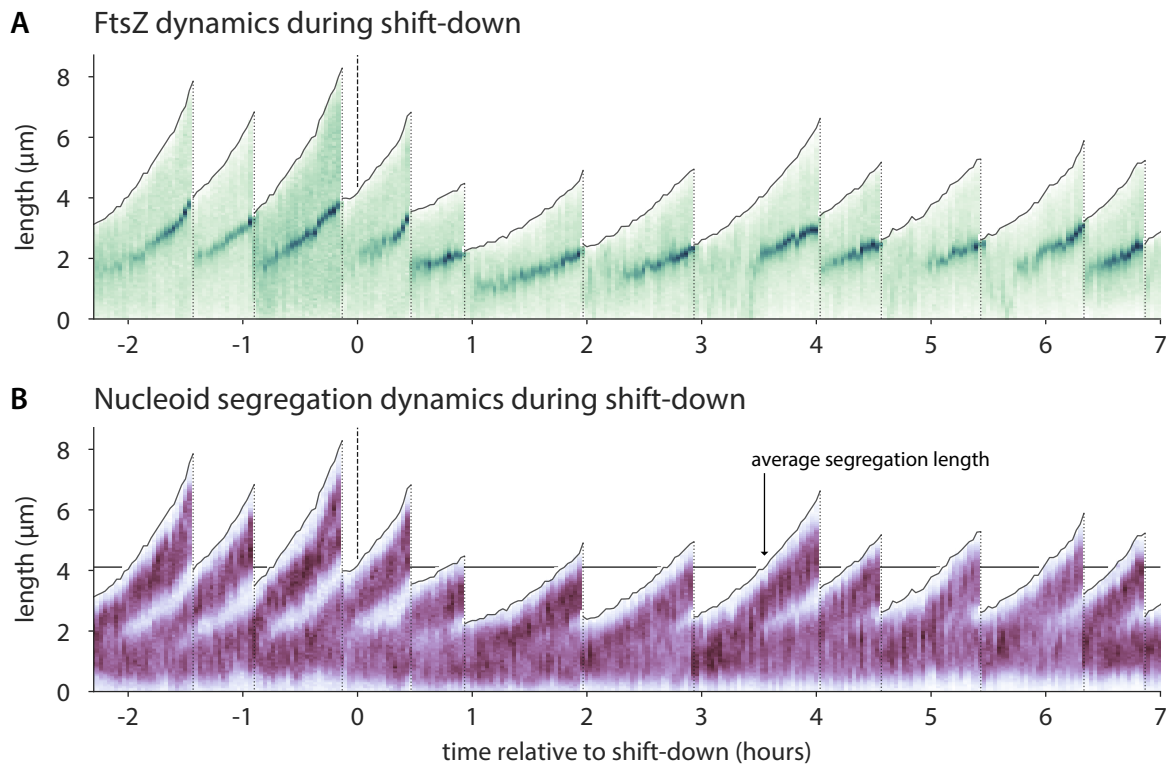


Figure 4.13: Ring formation and nucleoid segregation are independent. In a dual color imaging experiment during shift-down, there does not exist a clean relationship between Z-ring formation and nucleoid segregation. (A) Z-ring formation can occur before or after segregation, which is apparent in the slow growing cells after shift-down. Green signal is FtsZ-mVenus summed over the long axis of the cell. (B) Nucleoid segregation occurs at a fixed length before and after shift-down. Purple signal is HU-mCherry signal summed over the long axis of the cell.

Recent work has shown that nucleoid shape and position are greatly influenced by the cell boundary and molecular crowding via entropic forces²¹⁹.

Finally, nucleoid segregation does not correlate with the formation of the Z-ring (Figure 4.13). Contrary to several reports, my data shows that the Z-ring forms continuously at the midcell over the division cycle, regardless of the segregation state of the nucleoids. The Z-ring is normally positioned snugly between the nucleoids once they do segregate, but from my data it is not possible to distinguish a causal relationship between Z-ring formation and nucleoid segregation.

4.2.5 FtsZ accumulation and ClpX degradation control division at slow growth

ClpX is known to antagonize FtsZ and thus somehow regulate division. Here, we show that FtsZ degradation by ClpX regulates division timing when growth rate and the accumulation of FtsZ is slow.

As outlined in Subsection 2.4.5, ClpX is known to negatively affect FtsZ assembly in both *B. subtilis* and *E. coli*^{141,187-190}. In *E. coli*, ClpX degrades FtsZ with its partner protease ClpP^{141,188,191}. However, while the interaction is well recognized, it was unknown what the physiological role of this regulation was. Recently, we and collaborators determined that FtsZ regulation by ClpX is important during slow growth^{13,191}.

At slow growth, cells still grow in a balanced manner and thus FtsZ is produced at a rate proportional to growth rate. However, and unlike fast growth, the effects of active protein degradation cannot be ignored. Sekar and colleagues determined that it was this balance between production and degradation that determined the first division in cells waking from a non-growing state. In a collection of experimental set-ups, growing cells were starved by removing carbon. These cells cease growth, though do not necessarily enter stationary phase. The fraction of the cells in D period at the time of starvation contain two complete chromosomes and do not necessarily complete division.

Upon starvation, wild-type cells degrade FtsZ (see Sekar et al. Figure 8¹⁹¹ and Figure 4.14). Degradation happens on the order of a few hours, indicating it is active (the average half-life of an unregulated protein is 12 hours)²⁴. Cells lacking *clpX* do not degrade FtsZ during starvation and indeed have abnormal FtsZ localization, perhaps indicating that ClpX may also directly affect FtsZ assembly¹⁸⁷.

Cells without FtsZ do not divide. ClpX, which remains active during starvation, ensures that cells do not divide in the absence of protein production. When cells begin growing again, the

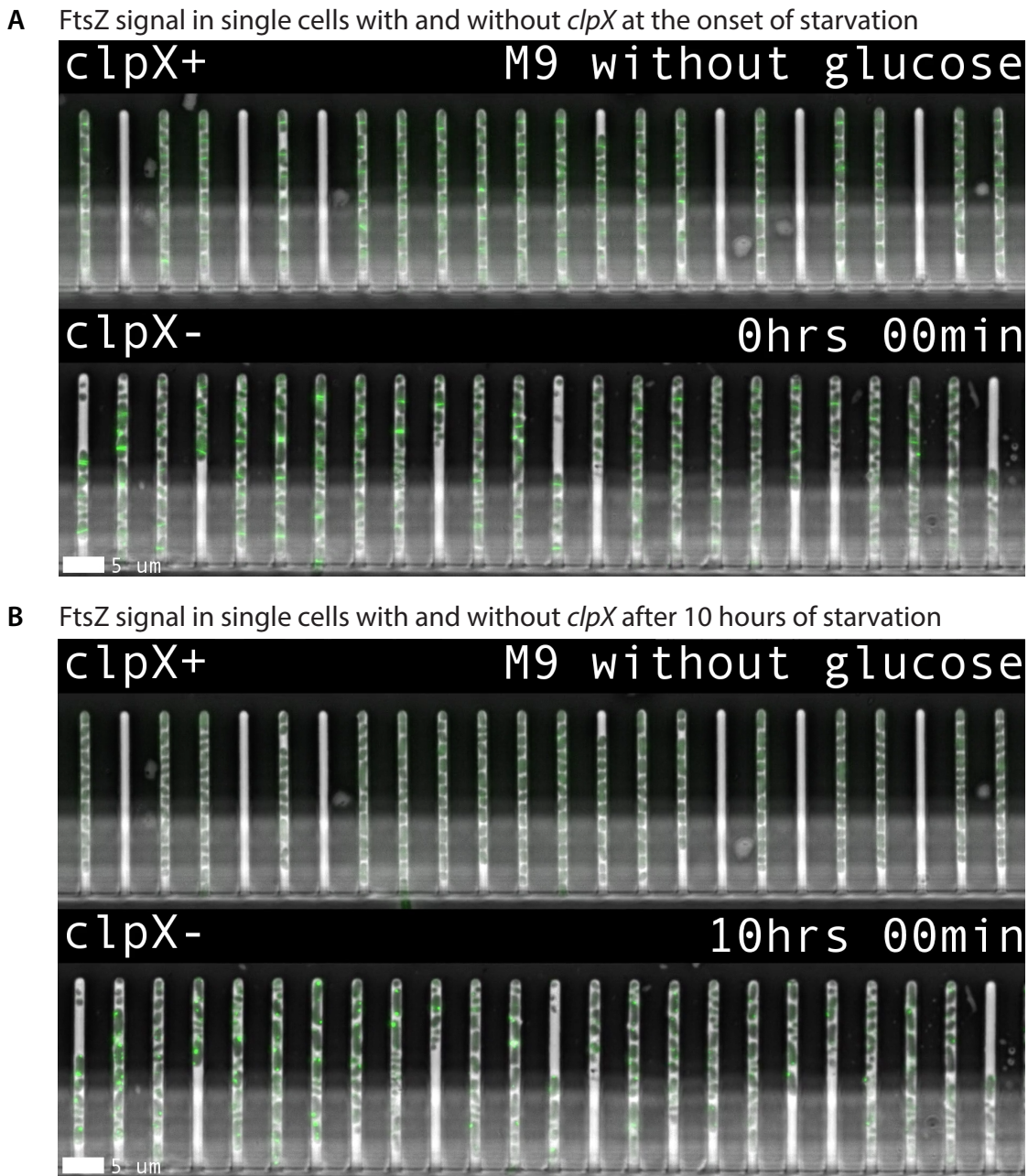


Figure 4.14: ClpX degrades FtsZ during starvation. Representative mother machine images of wild type cells with ClpX and mutant cells without ClpX before (A) and 10 hours after (B) carbon starvation.

production of FtsZ must overcome the degradation rate by ClpX such that cells can accumulate FtsZ to the requisite threshold amount. Sekar and colleagues showed this by pulse feeding small

amounts of glucose to the starved cells¹⁹¹. Upon addition of glucose to the culture medium, cells use the available carbon for biomass synthesis (no discernible amount of carbon sunk towards maintenance was observed). Some of this biomass synthesis includes FtsZ. If the time averaged pulse feeding rate was faster than the degradation rate, cells eventually divided after an accumulation time. However, if the feed rate was less than or equal to the degradation rate, cells never divided. Importantly, cells lacking *clpX* divide with minimal lag.

The pulse feeding experiments can be described with a simple model in which cells divide after they accumulate a threshold amount of FtsZ. The production of this FtsZ is a function of the feed rate (i.e., the growth rate) and the degradation rate. At slow growth, degradation is non-trivial, and has the effect of delaying division.

The pulse-feeding experiments demonstrate nicely how FtsZ is accumulated and degraded when transitioning into or out of growth. ClpX also affects division mechanics at slow growth in steady-state. It was reported that at slow growth, cells exhibit a sizer like behavior⁴¹. Si and colleagues showed that this behavior is due to non-trivial levels of FtsZ degradation in this condition. Effectively, FtsZ degradation leads to a lower autocorrelation in FtsZ amount between mother and daughter, which means the daughter will divide at a size more independent of the mother's division size.

Consider a cell without degradation that divides small. Its daughter is born small, and to accumulate enough FtsZ to divide it grows by the average birth size, equivalent to the constant added size (see Si et al. Figure 7¹³). When it divides, its size is halfway between its mother's size and the average size. This is the adder principle, and it means the cell fixes its size deviation and lack of FtsZ by one half every division, leading to an autocorrelation of one half after one generation. But if this cell also has active degradation, then it loses some FtsZ which is normally made in proportion to biomass growth. To divide, the cell must actually grow a little bit more than the average birth size, and the added size becomes a function (negatively correlated) with the birth size. The autocorrelation in size or FtsZ amount is thus less than one half after one

generation in these cells. By knocking down *clpX*, Si and colleagues showed that they could restore theadder phenotype even in slow growing cells.

4.3 Conclusion

Through advances in genetics, molecular biology, and imaging, we can now answer Arthur Koch's question with confidence³³. Replication initiation does not trigger division. Instead, both processes, and perhaps nucleoid segregation, are attached to cell growth and thus cell size at large. Even in dynamic environments, it is the production of initiating proteins that control the frequency of these events. A threshold mechanism is the fundamental control system. As such, it should be of interest to microbial engineers, especially those concerned with minimal cells.

The foundational position of the threshold model does not preclude or diminish the role of auxiliary systems which further increase the fidelity of chromosome replication and cell division. Indeed, such systems, while ultimately dispensable, are still responsible for the extremely high precession of whatever process they are concerned. Evolution clearly favors their existence. In addition, the diversity of these systems across prokaryotes is undoubtably high based on our meager knowledge of the model organisms. This alone warrants further study.

In terms of further exploration of the threshold mechanism and its implementation, I see two major avenues which require additional work. The first avenue, discussed in Subsection 4.2.3, is how the cell changes aspects of the threshold mechanism with growth rate in order to fit its form to different environments. Does it change its program at the the level of transcription, or is post-translational regulation at play? This avenue must address the idea that the cell likely has multiple programs which are employed at different time-scales.

The second is to focus on the molecular details of the threshold mechanism, that is, how can molecular interactions among molecules and other components of the cell trigger a structural event. In a circuit analogy, how can molecules behave as a transistor or capacitor? In synthetic

biology, significant effort has been put towards constructing genetic elements to behave as well characterized components, epitomized by the “transcriptor”²²⁰. Normally, the input to such a component is a transcription factor, and the output of such an element is the transcription of a target gene (perhaps another transcription factor). These genetic circuits and their components are normally defined by parameters such as the strength of promoters and ribosome binding sites.

The triggering of a structural cellular event, such as replication or division, can also be thought of as a component. The input is the number of molecules and the output is a physical event involving macromolecules or large protein complexes. However, the characterization of such a component is more difficult than for genetic elements. This is because it is based on complex molecular interactions that involve cooperatively and dynamics. While promoters and ribosome binding site strength can be predicted computationally, this is not the case for structural events. Without predictive ability, we do not truly understand how these systems work and cannot use them for other purposes.

Investigating the physiological orchestration of the cell is to ask what solution has evolution found for a difficult problem. By understanding this solution, we can better grasp the limitations felt by biological systems as well as the capabilities they have at hand. In the latter we will find inspiration for the problems that we have created and will have to solve ourselves.

Appendix A

Materials and methods

A.1 Strains

In Chapter 3, we used *B. subtilis* strains in the 3610 background with mutations to confer non-motility and reduce biofilm formation⁸. The background strain contained *comI*(Q12L) to confer competence²²¹. We used an inducible *lytF* construct to prevent chaining²⁰¹. For mother machine experiments in which replisomes were tracked, we used *dnaN-mGFPmut2*^{202,203}. Strain construction was performed using single crossover plasmid recombination or double crossover recombination from genomic DNA²²².

For *E. coli* in Chapters 3 and 4, we used a K-12 MG1655 strain containing a functional *dnaN-YPet* construct²¹⁶, *hupA-mCherry*, or *ftsZ-mVenus*¹³⁵. Strain construction was performed using P1 transduction and lambda Red recombination.

Strain genotypes for both species are provided in Table A.1.

A.2 Growth media and experimental conditions

For *B. subtilis*, we used S7₅₀ medium with different carbon sources and supplements. Importantly, we included additional iron(III) chloride and trisodium citrate. The latter acts as a siderophore for *B. subtilis*, and without it our strain cannot grow in the mother machine³⁰. To make rich conditions, we added 2 mg/mL casamino acids and 0.04 mg/mL tryptophan. For *E. coli*, we used MOPS glucose medium with or without an 11 amino acid supplement. Turbidostat and mother machine experiments used the same media with the following addition: bovine serum albumin was added at 0.5 mg/mL during mother machine experiments in order to reduce cell adherence to surfaces inside the device. Tables A.2 to A.4 provide detailed information on media composition.

For both turbidostat and mother machine experiments, chloramphenicol was added at concentrations between 1- and 4.2 μ M during translational inhibition experiments. All experiments were performed at 37°C in a climate controlled environmental room which housed the multiplex turbidostat and all optical components (Darwin Chambers Company, MO). Tables A.5 and A.6 enumerate experimental conditions and sample size for turbidostat and mother machine experiments, respectively.

A.3 Microscopy configuration

We performed phase contrast and fluorescent imaging on a Nikon Ti-E inverted microscope with Perfect Focus (PFS) and an LED transmission light source, controlled by Nikon Elements. For turbidostat experiments we used a PFS 2, CoolLED pE-100, 60X 1.4 NA Ph3 oil immersion objective (Nikon CFI Plan Apo DM Lambda 60X Oil), and Andor Technology Neo sCMOS camera. For fixed cell phase contrast imaging, we used exposure times between 50-100 ms and 100% transmission power.

For mother machine experiments, we used a PFS 3, Sutter Instruments TLED, 100X 1.45

NA Ph3 oil immersion objective (Nikon CFI Plan Apo DM Lambda 100X Oil), Photometrics Prime 95B sCMOS camera, and Coherent Obis laser 488LX for epifluorescent illumination. For laser epifluorescent illumination, we inserted a rotating diffuser in the optical train to reduce speckle. We also reduced the camera sensor region of interest to flatten the fluorescent illumination profile. We used a Chroma filter cube with dichroic mirror ZT488rdc and emission filter ET252/50m. For live cell phase contrast imaging, we used a 30 ms exposure time at 100% transmission power at an interval of 1.5 minutes. For fluorescent imaging, we used a 25 or 50 ms exposure time at 25% power at an interval of 3 minutes. This weak illumination minimized physiological effects due to phototoxicity on the cell and allowed for steady-state behavior over many hours.

A.4 Turbidostat cell preparation and sample collection

We grew all pre-cultures at 32°C or 37°C in a water bath shaker at 260 rpm. Seed cultures were inoculated into 1-3 mL LB medium from a single colony from an agar plate, streaked no more than 2 days before use. Cells were grown for several hours then diluted 1,000-fold into the target media without antibiotics and grown until OD_{600} 0.1. If multiple back dilution rounds were needed to control experimental timing, they were done such that cells did not enter stationary phase. The culture was then inoculated into each turbidostat vial with or without antibiotics to the target OD_{600} 0.05. Cultures grew for a minimum of 14 doublings to ensure steady-state conditions upon sample collection. For some conditions, cells adhered to the glass culture vial, evidence of residual biofilm activity we observed as changes in growth rate over the time course. In these cases, the sample was transferred to a clean glass vial at the end of the experiment for at least 1 additional doubling from which the growth rate was determined.

We collected samples for cell size and cell cycle measurements at OD_{600} 0.2. Approximately 20 mL of cell culture was immediately put on ice to arrest growth. The culture was

then split and pelleted, frozen, or fixed according to the subsequent measurement protocol. Our turbidostat design and function has been previously described³⁷.

A.5 Turbidostat growth rate measurement

The turbidostat maintained cells growing exponentially between OD₆₀₀ 0.05 and 0.2. In effect, it was run as a batch growth repeater, diluting the culture to OD₆₀₀ 0.05 when it reached OD₆₀₀ 0.2. An exponential line was fit to the growth periods between consecutive dilution events. From the exponential line $I = I_0 \cdot 2^{t/\tau}$, the growth rate was determined as $\lambda = \ln 2/\tau$, where τ is the doubling time. The turbidostat spectrometers were blanked with the appropriate medium before each experiment.

A.6 Turbidostat cell size measurement

We fixed cells with a glutaraldehyde and paraformaldehyde mixture and imaged within 24 hr as previously reported²²³, except for the following modifications: 2 μ l 25% glutaraldehyde was added to 1 ml 16% paraformaldehyde and cells were resuspended in 300 μ l GTE (50mM Glucose 25mM Tris 8.0 10mM EDTA 8.0) per sample after PBS washes.

Before imaging, we adjusted cells to an appropriate cell density as needed. Cells were pipetted onto a 2% agarose pad and briefly dried. The agarose pad was then flipped onto a Willco dish (WillCo Wells, Netherlands) and covered with a glass coverslip to reduce evaporation during imaging. Each experiment consisted of 80-200 images. Sample sizes are presented in Table A.6.

We performed fixed cell image analysis with a custom Python script using the OpenCV library. First, we detected contours using an active snakes edge detection algorithm. We then filtered for cell contours using a priori knowledge of cell size and shape, and manually checked for correctly segmented cells. Width and length were calculated from the long and short axis of

the cell segments using a simple threshold on the raw phase contrast images. All segmented cells where the width and length fell within 3 standard deviations of the mean for that measurement were kept for further analysis. To calculate cell volume, we assumed the cell was a cylinder with hemispherical ends.

A.7 Turbidostat C period measurement using qPCR

We estimated C period using qPCR and marker frequency analysis. Genomic DNA was prepared from each turbidostat sample using a standard phenol chloroform extraction. We amplified genomic DNA using PowerUp SYBR Green Master Mix (Thermo Fisher Scientific). We used primer pairs targeting chromosomal loci and calculated the C period using the ratio of relative loci copy numbers as discussed previously³⁷. Primers are listed in Table A.7.

A.8 Mother machine cell preparation and image acquisition

We prepared cultures for mother machine experiments the same as for turbidostat experiments except for the following difference: for translational inhibition experiments, the culture was diluted into the target media with appropriate antibiotics and allowed to grow for several generations before loading into the device.

We performed mother machine experiments as previously described^{8,13}. We used a custom centrifuge to load cells into the growth channels of the mother machine. The time required to remove cells from the water bath shaker, load them into the growth channels, and infuse fresh 37°C media was between 15 and 30 minutes. We then imaged cells for many hours under constant media infusion via a syringe pump (Harvard Apparatus, MA).

For nutrient shift experiments, two syringe pumps were used in conjunction with a manual Y-valve near the device inlet. Cells experienced the change in nutrients in a time interval shorter

than the imaging interval¹⁹¹.

A.9 Mother machine image processing

Mother machine images were processed with custom Python software. The pipeline takes raw images and produces objects which represent a cell and contains all measured parameters. It is described in detail in Appendix B, Briefly, the software aligns and crops images into single channels, segments cells, and links segments in time to construct cell lives and lineages. From the constructed cells we extracted physical parameters in space and time such as size and growth rate. The software has been previously described¹³ with the following modification: segmentation was accomplished with a convolutional neural network implemented with TensorFlow using manually annotated training data²²⁴.

After segmentation and lineage creation, the resulting cells were filtered for those with measured parameters (septum position, elongation rate, generation time, and birth, division and added length) within 4 standard deviations of their respective population means. We only considered cells in the time interval for which measured parameters and the fluorescent signal were in steady-state. This was normally 3-4 hours after imaging began until imaging ceased. For the growth condition glycerol rich with 3.5 μM chloramphenicol, we excluded cells which divided at the quarter positions, which were less than 5% of all cells. For all conditions, we further selected a subset of cells which could be followed for at least 4-6 consecutive generations. The later filtering step did not affect the parameter distributions, but ensured cell cycle determination was possible in light of the presence of overlapping cell cycles. We only considered mother cells during analysis, but note that other cells along the channel had identical elongation rates.

A.10 Single-cell cell cycle analysis

As described in Subsection 3.2.3 we used a functional fluorescent DnaN-mGFPmut2 fusion protein for *B. subtilis*. The construct was integrated at the chromosomal locus and expressed under the native promoter. The same genetic configuration was done for *E. coli* using DnaN-YPet. The gene product is the β -clamp subunit of DNA polymerase III, which is present at high stoichiometry in active replisomes²¹⁶.

Cell cycle analysis is as described previously¹³. Processed fluorescent images were used to determine the cell cycle parameters manually. We first identified replisome foci in the processed fluorescent images using a Laplacian of Gaussian blob detection method. We then constructed cell traces by plotting cell length versus time, with both the fluorescent signal and foci position projected against the long axis of the cell as demonstrated in Figure 3.6. Using an interactive program, we determined the start and end of replication visually based on the position and number of detected foci. For the fastest two growth conditions, glycerol rich with 0 and 1 μ M chloramphenicol, termination time and thus C and D period were not determined separately.

For nucleoid segregation time (Subsection 4.2.4), an analogous method with an interactive program was used to determine the segregation time.

A.11 Ensemble cell cycle analysis

In the ensemble method, we aligned cells by size and plotted the ensemble replication state. Based on ours and published measurements, we chose alignment by size as opposed to cell age⁴¹. To create the ensemble, we find the average number of foci as a function of cell size across all cells. For the slow growing case, the number of foci is 1 at small lengths until a transition period, at which it rises to and plateaus at 2. We take the initiation length to be the length at which the foci count rate of change is the highest, using a differentiation step of 0.2 μ m. By inferring

the average number of overlapping cell cycles n_{oc} from the traces, we can calculate C+D to be:

$$C + D = (n_{oc} + \log_2(S_d/S_i)) \cdot \tau$$

A.12 Tables

Table A.1: Strain information.

<i>B. subtilis</i> strains	Genotype	Notes
BS15	3610 comI(Q12L) hag::MLS(R)::MLS(S) amyE::[Phyperspank-lytF spcR] epsH::tet	Chapter 3
BS45	3610 comI(Q12L) motAB::Tn917 amyE::[Physpank-lytF kan] epsH::tet dnaN::[dnaN-gfp spec]	Chapter 3
<i>E. coli</i> strains		
SJ1535	K-12 MG1655 dnaN::[dnaN-yPet kan]	Chapter 4
SJ1724	K-12 MG1655 dnaN::[dnaN-yPet kan] hupA::[hupA-mRuby2 FRT-cat-FRT]	Chapters 3 and 4
SJ1725	K-12 MG1655 ftsZ::[ftsZ55-mVenus-56]	Chapter 4
SJ1728	K-12 MG1655 ftsZ::[ftsZ55-mVenus-56] hupA::[hupA-mRuby2 FRT-cat-FRT]	Chapter 4
SJ1741	K-12 MG1655 ftsZ::[ftsZ55-mVenus-56] clpX::[FRT-kan-FRT]	Chapter 4

Table A.2: Growth media.

Media name	Abbreviation	Carbon source	Nitrogen source	Buffer, salts and metals	Supplement
S7 ₅₀ succinate	suc	1% succinate	0.1% glutamate	S7 ₅₀ salts and metals	-
S7 ₅₀ mannose	man	1% mannose	0.1% glutamate	S7 ₅₀ salts and metals	-
S7 ₅₀ glycerol	gly	1% glycerol	0.1% glutamate	S7 ₅₀ salts and metals	-
S7 ₅₀ succinate rich	suc+	1% succinate	0.1% glutamate	S7 ₅₀ salts and metals	0.2 mg/ml casamino acids, 0.04 mg/ml tryptophan
S7 ₅₀ mannose rich	man+	1% mannose	0.1% glutamate	S7 ₅₀ salts and metals	0.2 mg/ml casamino acids, 0.04 mg/ml tryptophan
S7 ₅₀ glycerol rich	gly+	1% glycerol	0.1% glutamate	S7 ₅₀ salts and metals	0.2 mg/ml casamino acids, 0.04 mg/ml tryptophan
MOPS glucose	MOPS glc	0.2% glucose	9.5 mM ammonium chloride	MOPS modified buffer	-
LB	LB	0.5% glucose	-	-	1% tryptone, 0.5% yeast extract, 0.05% NaCl

Table A.3: Media components.

Component	Concentration
S7 ₅₀ salts and metals	
MOPS	50 mM
ammonium sulfate	1 mM
potassium phosphate monobasic	5 mM
magnesium chloride	2 mM
calcium chloride	0.7 mM
manganese(II) chloride	50 μ M
zinc chloride	1 μ M
iron(III) chloride	55 μ M
thiamine hydrochloride	1 mM
hydrogen chloride	20 μ M
trisodium citrate	50 μ M
MOPS modified buffer	
MOPS	40 mM
tricine	4 mM
iron(III) sulfate	0.1 mM
sodium sulfate	0.276 mM
calcium chloride	0.5 μ M
magnesium chloride	0.525 mM
sodium chloride	50 mM
ammonium molybdate	3 nM
boric acid	0.4 μ M
cobalt chloride	30 nM
cupric sulfate	10 nM
manganese(II) chloride	80 nM
zinc sulfate	10 nM
potassium phosphate monobasic	1.32 mM

Table A.4: Amino acid supplement.

Component	Concentration
L-methionine	500
L-histidine	500
L-arginine	500
L-proline	500
L-threonine	500
L-tryptophan	500
L-leucine	500
L-tyrosine	500
L-alanine	500
L-asparagine	500
L-aspartic acid	25

Table A.5: Turbidostat experimental conditions.

Strain	Growth medium	Perturbation	Replicates	Sample size
BS15	succinate	none	4	6592, 8769, 7418 7051
BS15	succinate	1.8 μM cam	4	16804, 11418, 15001, 8065
BS15	succinate	2.7 μM cam	4	7051, 7901, 13369, 7741
BS15	succinate	4.2 μM cam	2	4782, 3132
BS15	mannose	none	2	4782, 3132
BS15	mannose	1 μM cam	3	5368, 9213, 8086
BS15	mannose	2 μM cam	4	14080, 12865, 18524, 15191
BS15	mannose	3.5 μM cam	3	6623, 7218, 9140
BS15	succinate rich	none	2	7861, 18963
BS15	mannose rich	none	2	3346, 3387
BS15	glycerol rich	none	3	4807, 3152, 4819
BS15	glycerol rich	1 μM cam	3	3551, 4894, 2199
BS15	glycerol rich	2 μM cam	4	7821, 3332, 9554, 7973
BS15	glycerol rich	3.5 μM cam	4	5786, 5143, 7059, 4910

Table A.6: Mother machine experimental conditions.

Strain	Growth medium	Perturbation	Sample size	With initiation size
BS45	succinate	none	2530	506
BS45	succinate	2 μ M cam	2586	534
BS45	mannose	none	5478	504
BS45	mannose	2 μ M cam	3375	561
BS45	mannose	3.5 μ M cam	2151	553
BS45	glycerol rich	none	2355	514
BS45	glycerol rich	2 μ M cam	4743	476
BS45	glycerol rich	3.5 μ M cam	1416	198
BS43	succinate, succinate rich	nutrient shift	7671	1695
SJ1724	MOPS glucose	none	4681	437

Table A.7: qPCR primers.

Primer name	Sequence	Location g on genome; <i>ori</i> = 0 <i>ter</i> = 1
SJO1152	CGTTGATAGGAACTAGTAGGGA	<i>ori</i> forward (right arm)
SJO1153	AGCATTTCGCTCAAGGATG	<i>ori</i> reverse (right arm)
SJO1232	GGAATTTCTTTCTCAGGAGAACATTTG	0.2 forward (right arm)
SJO1233	TCTTTATAACGCAGGCATACGG	0.2 reverse (right arm)
SJO1167	CAGTTCGAGCGAAACGATAGA	0.4 forward (right arm)
SJO1168	CGCCACTTTCTCCCTCATAC	0.4 reverse (right arm)
SJO1136	AGAGATGGGTACGATTGTTTG	0.73 forward (right arm)
SJO1137	TTGTCCGCAGCAAGTTC	0.73 reverse (right arm)
SJO1138	TTAACTCGGACATCTTCATCAG	<i>ter</i> forward
SJO1139	CAAGGATCAGGAGCAGTTTAT	<i>ter</i> reverse
SJO1140	CAGTTCTGCGTTTAGCTGTA	-0.74 forward (left arm)
SJO1141	TTCGGTCATTCTTGTGATAGTT	-0.74 reverse (left arm)
SJO1175	TCAAACACATACTTACTCGGATACA	-0.41 forward (left arm)
SJO1176	CTTGCAGGATTTGAAAGGGAAA	-0.41 reverse (left arm)
SJO1177	CATAACCGGGTACTGAGGAAA	-0.22 forward (left arm)
SJO1178	TCGGATTACGGAAGTTGAAGAG	-0.22 reverse (left arm)
SJO1179	CACTGCCAGCATATTGTTTATCG	<i>ori</i> forward (left arm)
SJO1180	GAATGGTTGATCGGTATGGCTA	<i>ori</i> reverse (left arm)

Appendix B

Mother machine image processing with mm3

B.1 Introduction

A hallmark of modern measurement methods is that they simply produce a lot of information. This is especially true in imaging, whether for scientific purposes or otherwise. When the CIA launched its first spy satellites, behemoth spacecraft at the technological forefront, they would take a single picture to film and launch a canister to Earth. Agents would collect and develop the negatives, and teams would pour over the image for tens or even hundreds of hours²²⁵. In 2019, companies like Planet Labs take thousands of pictures of Earth a day with an orbiting array of satellites, each the size of a loaf of bread.

In the realm of microbiology, microscopy predated photography by over 200 years. To capture information from microscopes meant describing what the viewer saw or to sketch it. This approach has its advantages, but it was certainly cumbersome. Moreover, an argument can be made that quantitative imaging cannot be done without photographs as the eye is a fallible cypher. In either case, a dearth of data is no longer a problem: a typical mother machine experiment

produces 50,000 images.

This is an awesome technological achievement, yet if we step back an obvious problem arises. If you cannot examine these images, they are worthless. And unless you are taking pictures of cats and putting them on the internet (or have a Red Scare inflated CIA budget), it is not feasible to muster enough eyes to look at each image. Here, necessity is the mother of invention; the impracticality of manual analysis motivates the creation of automated methods. Zooming out, the advent of the so-called “big data” era is actually a story of two companions. The first are the tools we have created to take many measurements, the second is the methods we have developed to get a hold on what we have measured.

In this chapter I will describe the development of an image analysis platform, named mm3, that I helped design to address the problem introduced here. In a nutshell, the software takes raw images and outputs a dataset containing a collection of cells and their observable features, such as their birth size, generation time, and elongation rate. The two major algorithmic tasks involved are segmentation (the detection of cells in the image), and lineage creation (the linking of these cells through time to define birth, division, and genealogy)²²⁶. The output are cell objects which encapsulate information concerning one cell from birth to division and the basis for all single-cell data presented in this thesis.

Before we continue I will first define some terms to allay confusion.

1. I refer to the act of taking raw image data and producing curated data as both image processing and image analysis. However, “data analysis” describes the further investigation or plotting of this curated data.
2. There is an unfortunate nomenclature conflict that in microscopy, images taken of the same field of view, focal height, and nominal time, but with different illumination or other methods, are called channels. As we also refer to the dead end cell traps of the mother machine as channels, I will refer to microscopy channels as color planes or simply planes.

Finally, I would like to note that there are a number of other software packages designed for mother machine image processing, as well as general segmentation and tracking works of note^{226–235}.

B.2 mm3 image processing workflow

In this section I review the general workflow of mm3.

In order to address the problems outlined above, I, with the help of other lab members, developed a highly automated image processing pipeline. mm3 attempts to find a balance between two contradicting forces which often pull at home-grown software: to be specific enough that it can be readily applied to new datasets, but be general and flexible enough that it can be modified for specific experimental setups. As such the workflow is modular, such that certain tasks can be substituted or ignored.

The code is written in Python and is run as a command line tool with the occasional graphical user interface (GUI). The pipeline takes as an input raw TIFF images and related metadata. The output is an associative array, that is, a dictionary of cell objects. These cell objects can be used for further analysis and plotting. Parameters are passed to the individual scripts via a text file in YAML format and as command line options.

mm3 expects phase contrast (bright field) images, which it uses to identify channels and segment the cells. Additional color planes are accepted, specifically fluorescent images. These are not used for the main goals of cell segmentation and tracking. However, they are kept with the phase contrast images as this greatly streamlines downstream, experiment specific processing. mm3 contains a number of functions for fluorescent analysis.

The general pipeline proceeds as follows (Figure B.1). Raw images are processed for metadata and the location of channels. Channels are cropped out and compiled in a way that reflects the multiplicity and dimensionality of the data. Each field of view (FOV) can have some

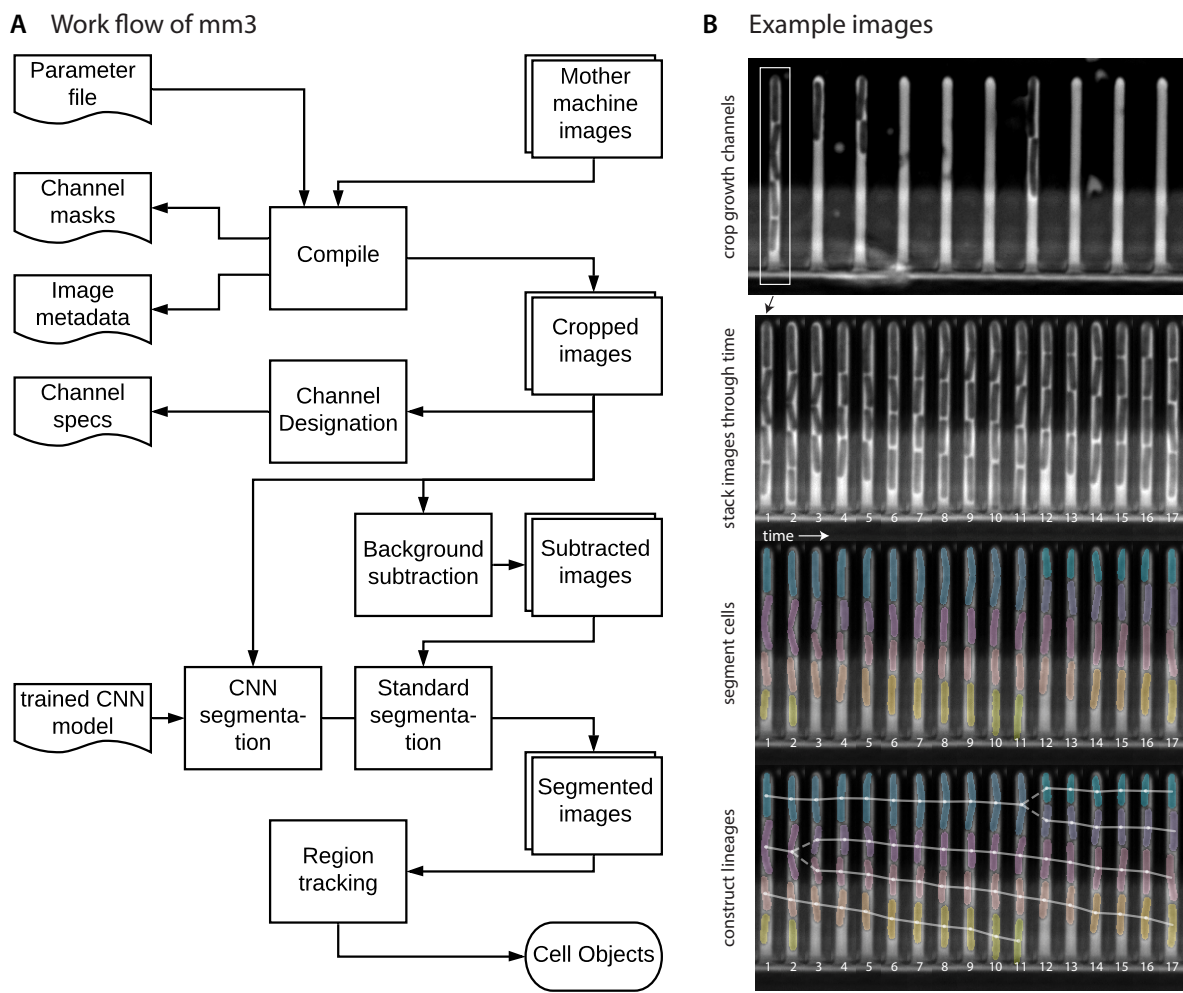


Figure B.1: mm3 workflow. (A) Workflow of mm3 with major processes. Processes in the pipeline are shown in the middle column as plain squares. Inputs and outputs are shown on the left (parameter and metadata files) and right (raw and processed image data, including cell objects). Note that all of the processes draw from parameter and metadata files, but not all lines are shown for clarity. (B) Example images from various steps during processing.

number of channels, and each channel is functionally its own unit that does not interact with other channels. Each channel has an expansion and time and perhaps additional color planes. Cropped channels are either saved as stacked TIFF files, or in a compendium HDF5 format for downstream analysis. This step is known as compiling (Appendix B.2.1).

Channels are then assessed on whether they should be used for analysis. That is, that they both contain cells and are free of other defects or other reasons for exclusion. Empty channels are

designated for the purposes of background subtraction (Appendix B.2.2). If using the standard image analysis methods for segmentation, subtraction is performed (Appendix B.2.3).

Segmentation is then done on an image by image basis in one of two ways. The first method relies on more traditional image analysis procedures (Appendix B.2.4). The second relies on training data and a convolutional neural network (CNN), i.e., a deep learning method (Appendix B.2.5). The output of both methods, the segmented image, is an 8 bit array where each cell is represented by pixels of the same value starting from 1, with background pixels being zero.

Finally, segments are connected through time to create the cell lineages. This algorithm utilizes a simple decision tree to determine cell growth and division (Appendix B.2.6).

The output are cell objects which constitute the life of a single cell from birth to division. Each cell has a unique identifier, which can be used to locate the segments that make up that cell in the cropped channel images. This facilitates post processing, such as retrieving and adding fluorescent data associated with the cell. Cell objects also contain attributes which indicate their parent and children. It is then trivial to reconstruct the lineage tree of all cells in a channel using graph traversal algorithms.

Below, the individual sections of the image analysis pipeline are described in greater detail.

B.2.1 Crop and compile images

The first step in the pipeline is mostly associated with bookkeeping and organizing metadata. The goal of this process is to output cropped channel images and pool relevant metadata.

The mother machine input data is a series of TIFF files. TIFF files are separated by time point and FOV. Each image file contains this information in its name as a suffix. If there is more than one image taken at each time point and FOV, such as a fluorescent exposure in addition to a phase contrast image, these color planes are stacked within one TIFF. Each TIFF may also

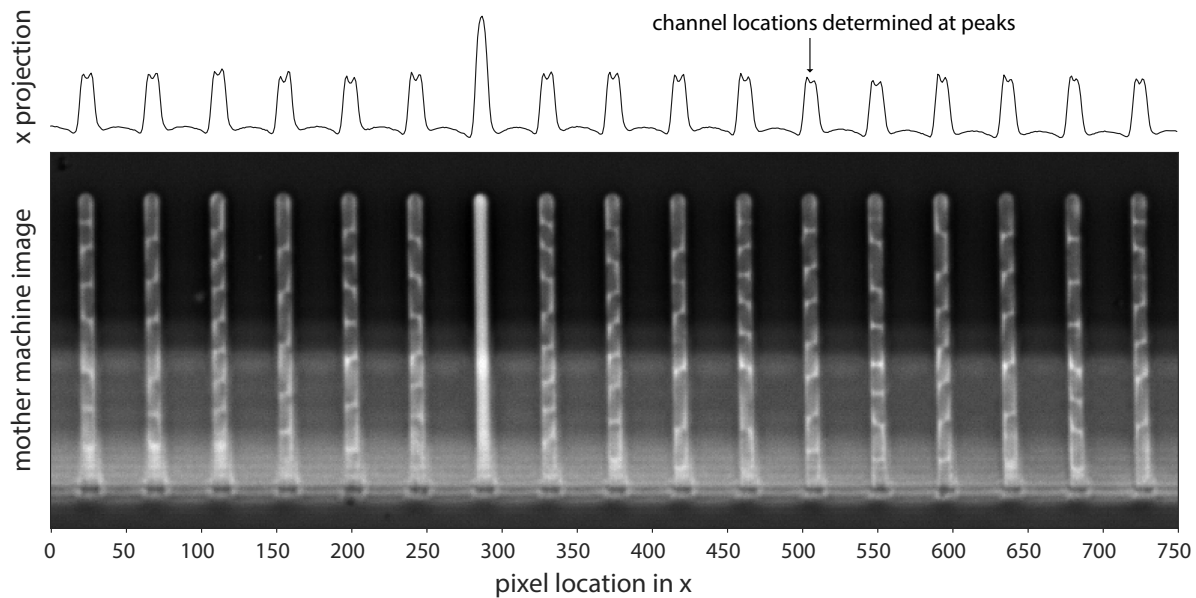


Figure B.2: Channel detection. Summing along the short axis of the mother machine images produces an X projection. Because the channels have higher pixel values than the background, even when they contain cells, distinct peaks appear. The location of the channels is found via a wavelet transform on this X projection. The open and closed end of the channels are found via the Y projection, which has a higher value than the very top and bottom of the image.

contains metadata stored in the header of the file in JSON format. Depending on the source of the image, this includes the above information such as the absolute (wall) time that the image was taken, the microscope stage position of the image, and the optical configuration of the image planes.

Images are first analyzed individually to collect this metadata in a dictionary. This dictionary, as well as a table that relates the nominal time index to the absolute time an image was taken are saved for future reference. Importantly, each phase contrast image is analyzed for the location of the mother machine channels. The location information is used to crop out individual channel images. This reduces the amount of data that must be processed (because the sum area of the resulting images are smaller). Moreover, since each channel contains an independent lineage, cropping them separately is a convenient and logical way to process and organize the data.

Locating channels relies on a wavelet transform, taking advantage of the regular spacing

of the channels in a mother machine image (Figure B.2). In a normal mother machine image, the channels appear lighter than the background PDMS or main flow cell. Image preprocessing requires that the channels be aligned vertically. Thus if the image is summed over the X axis, the 1D projection of the image is a series of peaks. To find the location of these peaks, a Mexican hat wavelet is convolved across the 1D projection. Where the wavelet aligns well to the peaks of the projection, a local maxima arises. This is true even when the channel contains cells. The peaks are chosen where the maxima to noise ratio is above a specified threshold. These peaks are the location of the channels and are the basis for cropping in the X dimension.

To find the ends of the channel we again take advantage of the fact that the channel pixels are lighter than the foreground. We then sum over the Y axis, and the 1D projection has a higher value in the location of the channel. In preprocessing the channels are arranged such that the open end faces down. Additionally, images are cropped such that we can make the assumption that the closed and open end of the channel are within the top and bottom third of the image, respectively. We then take the numerical derivative of the Y projection. In the first third of the derivative of the projection, the maxima correspond to the closed end of the channel. This is where, where the projection has a quick transition from dark to light. Similarly, the open end of the channel is the location of the minima in the last third of the projection derivative, where it goes from light to dark.

The X and Y projections give both the center pixel of each channel (the peak value from the wavelet transform) and the averaged location of the closed and open end of the channels across the image. The same Y projection method to determine the closed and open end of the channels is then repeated for each individual channel to account for subtle differences between channels or deformations in the device. If the result of this individual accounting is significantly different than the average, then the average is taken as a default. These three pixel values (peak, open, and closed end), effectively define the location of every channel in every image.

For the purposes of cropping out the individual channels, the width of the channel is taken

as a parameter that is to be measured and entered by the user. Two additional parameters for the desired width and length padding finally dictate the crop areas in each raw image. Explicitly, each channel peak location is expanded in X by the channel width and channel width pad, and the open and closed end pixels are expanded by the length pad. This gives four numbers for each channel that together form a mask.

The masks are created for each time point for a particular FOV, and are then combined into a consensus mask which is then applied to all time points. This process accounts for aberrations in particular time points, such as transient illumination artifacts that may cause errors in channel location. However, it requires that there is not significant XY translation of the FOV during imaging.

The consensus mask is created by stacking all masks from a particular FOV to create an occupancy map. Each pixel in the map takes a value between 0 and 1 corresponding to the fraction of time that pixel is part of a mask across all time points. Pixels with a minimum occupancy are taken to be part of the consensus mask. Finally, this process often leads to individual channel masks with jagged edges. These edges are squared by taking the smallest rectangle that can contain the mask. Additionally, each channel mask can be expanded so that they are the same size across the experiment. This is mostly an aesthetic decision, but has some benefits when doing image post-processing. The consensus channel mask is saved and can be directly edited if desired.

The channels are then cropped individually and saved as 3D image stacks through time. Individual color planes are saved separately. Stacks are named with a unique suffix identifying their FOV, channel (peak) number, and color plane.

The wavelet transform and derivative method of finding the location of the channels has the advantage of being computationally fast. However, it requires an assumption about the appearance of the images which may not be true in all cases. Alternatively, the channels can be found directly using a deep learning approach analogous to the one used for segmentation described later. This

method is much slower but much more amenable arbitrary channel appearances. Because deep learning segmentation is discussed in Appendix B.2.5 in more detail, we will not delve into this method here.

Going forward, all processes are applied to the cropped channel stacks individually.

B.2.2 Channel designation

In the previous step, all channels are located and cropped regardless of if they contain cells or not. However, it is valuable to partition channels into groups based on if they should be analyzed (i.e., contain growing cells), or do not. This is mainly to minimize the computational load of downstream steps by simply reducing the number of images that must be analyzed. In addition, some channels which contain cells may not be prime for analysis because of artifacts in the device which distorts how the cells grow (i.e., as microcolonies rather than in lines). Or the channel simply loses its cells early in the experiment, and thus will not contribute much data overall. Finally, channels which do not contain cells but are otherwise pristine can be used for background subtraction. Discussed in Appendix B.2.3, background subtraction is necessary for one of the two segmentation methods and is usually done as a precursor to fluorescent image analysis.

For the above reasons, mm3 contains a dedicated step in which channels are designated into one of three categories: analyze, empty (use for background subtraction), or ignore. This is done in a semi-automated way: the cells can algorithmically be categorized into either analyze or ignore, but the user is highly encouraged to check over this categorization and must designate empty channel manually. Practically, it is not necessary to create an algorithm that can correctly designate channels for every experiment. The development or training of such a method would take far longer than manually designating the channels for each experiment. Moreover, it is simply good practice to force the user to look at their processed data before the more critical steps of segmentation and lineage tracking are performed. While a typical mother machine experiment

may consist of 1000 individual channels, these can be sufficiently inspected in 30 minutes.

Yet automated pre-sorting does ease manual annotation. The automated designation of channels as either containing cell (analyze) or not (ignore) can be done in one of two ways. The first uses the 2D cross correlation of images of the channel across time. The latter uses a deep learning approach, which is accurate but slow. We will discuss the cross correlation method here.

The 2D cross correlation method takes advantage of the fact that a channel that contains no cells does not change in appearance over time. On the other hand, the appearance of a channel which contains cells is very dependent on time as the cells grow, divide, and change their position throughout the experiment. In fact, the cross correlation can be used to create a single value similarity index. The cross correlation from second time point onward is calculated against the first time point and these numbers are averaged. A value of 1 indicates that the image is completely time invariant, while a value of -1 indicates the images are inverse of one another. A threshold is used to separate channels with high similarity and those with lower similarity, which likely contain growing cells.

In practice all channel images with or without cells are highly similar through time, so their similarity index is often above 0.90. Also, it is unnecessary to calculate the cross correlation at all time points. A subset of 10% of the images is used to calculate the similarity index in order to reduce computation time.

While this method can distinguish between active and inactive channels, it cannot designate a channel as truly empty. For example, if a channel contains a dead cell from the beginning of the experiment, it will have a very high similarity index, but is not appropriate to use for background subtraction. More commonly, small imperfections which are difficult to assess algorithmically preclude the ability of many channels to be representative empty channels. For these reasons, empty channel designation is done manually via a GUI. The GUI is also used to review and correct improperly designated channels from the automated step.

Figure B.3 shows the GUI. The top column shows the first image from all the channels in

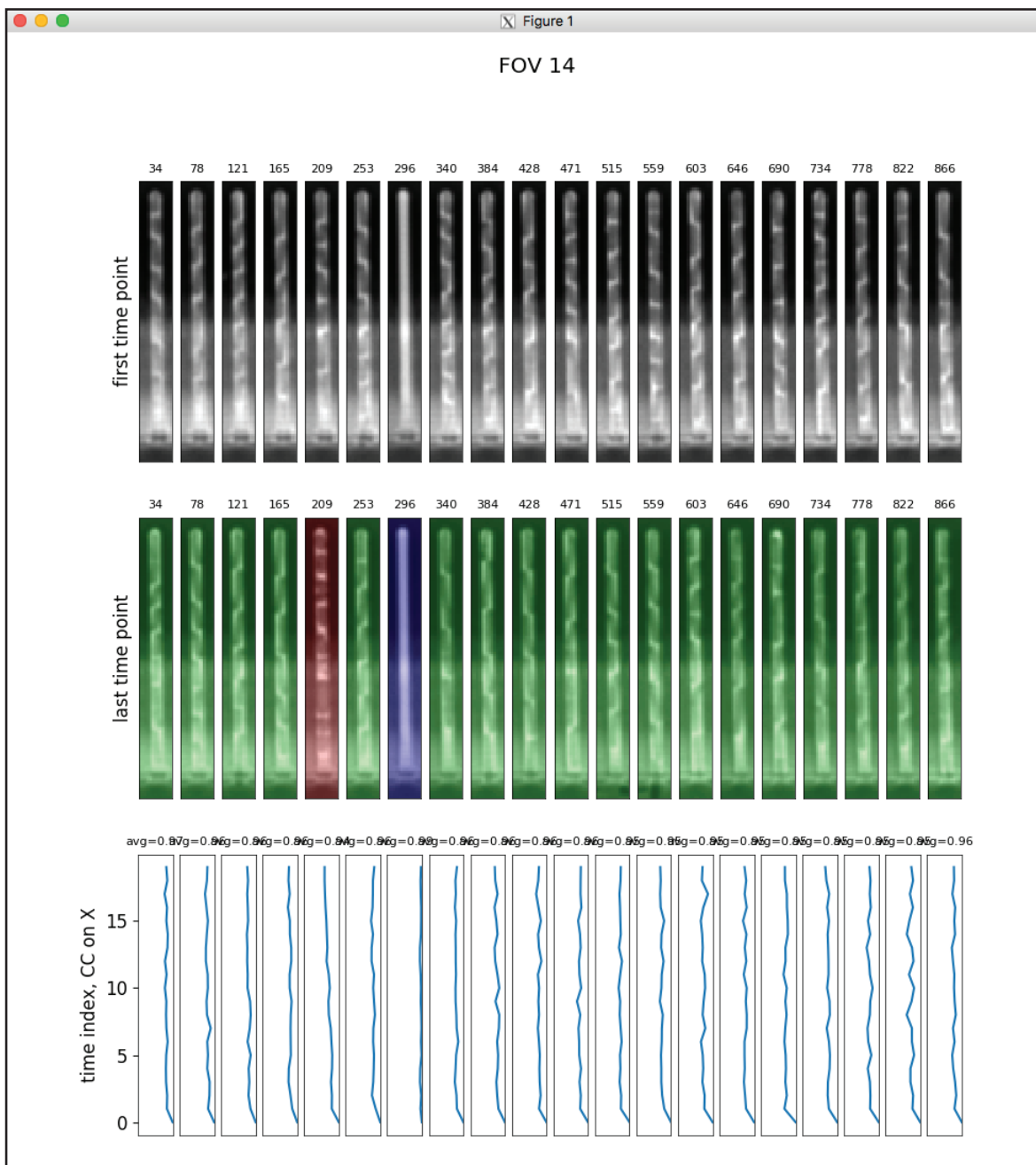


Figure B.3: Channel designation GUI. See text for information.

the FOV. The channel number (its X location in the original image) is shown above the frame. The middle row shows the last image from the channel. They are colored by whether they should be analyzed (green), ignored (red), or used for background subtraction (blue). Clicking on the

images cycles among the designations. The bottom column shows the similarity index of the channel across time. Values farther to the right are more similar, such as for the empty channel.

The output of this step is a YAML file which contains the designations of all channels, organized by FOV, for the experiment. This file is known as the specifications file and can be directly edited. Channels with designation analyze have value 1, those with designation ignore have value -1, and those with designation empty have value 0. It is used in all downstream image processing.

B.2.3 Background subtraction

Broadly speaking, the purpose of background subtraction in image analysis is to remove uninformative signal from the data. Ideally, this leaves only pixels which contain useful data and greatly simplifies analysis. Mother machine images are well suited for background subtraction because of their regular appearance. Background subtraction is a precursor to one of the segmentation routines and is done before most fluorescent image analysis.

Background subtraction is achieved in three parts: determining an appropriate background, aligning this background to the image being processed (known somewhat confusingly as the foreground image), and finding the difference in intensity on a pixel by pixel basis.

As alluded to above, we use empty channels as the background for subtraction. One empty channel is used for each FOV. The empty channel is itself a channel stack through time, such that at each time point has a corresponding background image. This is because long-term changes in lighting or focus precludes the ability to use one image for all time points.

During channel designation, if only one channel in the FOV is designated as an empty channel, then it is used directly. If more than one channel are deemed empty in a FOV, then they are averaged together to create a representative empty. At each time point, the empty channel images are aligned to one another using a tiling cross correlation described in more detail below. The aligned images are then averaged on a pixel-by-pixel basis. It is beneficial to use an averaged

empty channel for background subtraction to remove all minor artifacts which may propagate through subtraction. If no empty channels are designated for a particular FOV, an empty channel is borrowed from the closest available FOV.

The background image must be aligned to the foreground image before subtraction such that the features of the channels overlap precisely. Even a small misalignment will create confounding artifacts in the subtracted result. We employ a 2D cross correlation to find the best alignment. This is a commonly used method in image analysis for template matching. The background image is first padded with additional pixels on all sides to ensure it is larger than the foreground image. The value of these padded pixels are drawn by mirroring at the edge of the image. The foreground image is then slid across the background image across all positions for which it completely overlaps with the background. At each position we calculate the cross correlation. This is equivalent to a 2D convolution of the foreground image against the background. The maximum value of the convolution corresponds to the position at which the foreground is most similar to the background. Even though the foreground image may contain cells in the channel, the shared features, specifically the PDMS-liquid interface at the open end of the channel and the channel itself, drive images to be well aligned. With alignment position in hand, we then shift and trim the background image so that it is the same size as the foreground image.

With aligned images, subtraction itself is decidedly simple. We subtract the foreground image from the background image element wise. We find the difference in this order so the cells, which are dark in the phase contrast images, are light in the subtracted images. Note that no normalization is performed. Values below zero are set to zero as they are effectively undefined.

B.2.4 Segmentation routine 1: Otsu threshold and random walker

The first segmentation routine uses fairly standard image analysis algorithms, and I refer to it as the standard method. The standard method takes the subtracted images as input. The

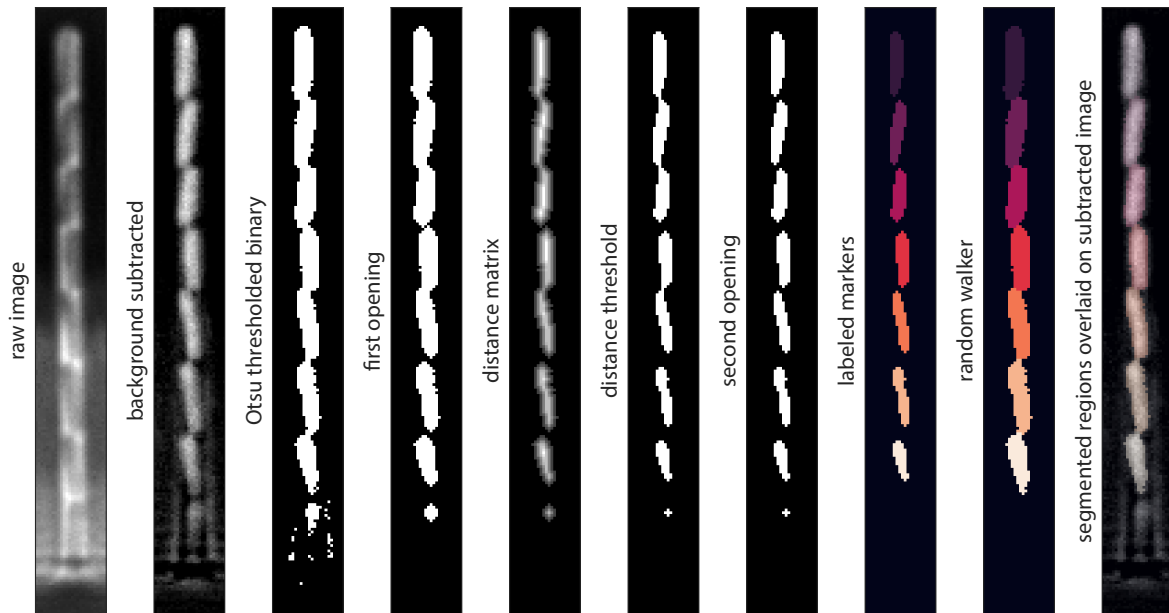


Figure B.4: Standard segmentation algorithm. Segmentation via the standard algorithm progresses from the raw image (far left) to segmented regions for each cell (far right). After background subtraction, the image is binarized via Otsu’s method, markers for each cell are determined, and each marker is expanded to encompass the entire cell. See text for descriptions of each process.

subtracted images are unsigned 16 bit gray scale images where the background is dark and the foreground (i.e., cells), are light. There are three general sections of the routine: binarization, marker creation, and enlarging markers to the cells’ boundaries (Figure B.4).

The first step is binarization, also known as thresholding, and is done via Otsu’s method. Otsu’s method considers a histogram of pixel intensities of an image. It finds the threshold intensity that maximizes the variance between the two classes of pixel intensities that are created on either side of the threshold intensity. This is equivalent to minimizing the variance of each class individually. The grayscale image is then converted to a binary image by setting all pixels above the Otsu threshold to 1, and all other pixels to 0. Otsu’s method works well when the distribution of pixel intensities is approximately bimodal. And although it exhaustively tests all pixel values to be the candidate threshold, it is a fast calculation that does not scale with the size

of the image.

The second general step, marker creation, has the key goal of spatially separating each unique cell. Binarization does a good job of distinguishing foreground objects from the background. But because of the physical proximity of the cells in the mother machine channels, binarization often results in one mass of white pixels. To efficiently label individual cells, we instead require islands of white pixels surrounded by black pixels.

Marker creation is thus achieved by “contracting” the binarized foreground. This is accomplished with both morphological operations and an edge distance threshold. These methods work because we take advantage of the fact that in the mother machine, cells mostly touch each other at the cell poles. Moreover, these connections in the binary image are usually smaller than the width of the cell. Thus, we can specifically target the removal of these thin connections.

Morphological image operations are manipulations that target the boundary between black and white pixels in a binary image. They utilize a kernel (a small binary image), such as a square three pixels to a side. There are two fundamental morphological operations: erosion and dilation. In erosion, the kernel is superimposed on each white pixel of the image. Whenever the kernel does not completely overlap with white pixels, it turns the white pixel on which it is centered to black. In dilation, the kernel is again superimposed on each white pixel in the image. If the kernel overlaps with black pixels, it turns those pixels white. For either operation, the transformation of each pixel is calculated at each index individually, so the order of superposition is not important. Morphological operations of binary images are not computationally expensive.

Functionally, erosion and dilation result in erasing or adding white pixels at binary boundaries, respectively. Take a round island (represented by white pixels) sitting in a sea (of black pixels). A dredging crane (the kernel) removes land by traversing the boundary of the island, resulting in a smaller island via erosion. Conversely, the crane can circle the island and add land, resulting in a larger island via dilation (known as accretion in topography).

We employ erosion followed by dilation, a process known as opening, in order to remove

image features we wish to discard while retaining the underlying size of the foreground object. Imagine a peninsula with a narrow isthmus to the mainland. When the crane erodes the land along the shore, the isthmus is destroyed and the peninsula becomes an island. The island is smaller than the original peninsula. Yet when the crane returns to the shoreline restore the size of the land via dilation, there is no isthmus to use as a guide. Thus the island grows to the size of the original peninsula, but it is still an island. We use opening to remove the isthmuses (that is, thin connections) between cells in our images.

The second technique is a simple edge distance threshold. Each white pixel is given a value equivalent to its Euclidian distance from a black pixel. A simple threshold is then used, where white pixels less than a certain value, or distance from an edge, are turned black. This has the effect of shrinking all foreground objects.

In total, marker creation is achieved by a morphological opening, a distance threshold, and then a second opening. The second opening is not strictly required, but helps to break additional connections and generally smooths the final output. This output is ideally a collection of foreground markers which are separated and have one-to-one correspondence with each and every cell in the original image. Markers which touch the image edge or are beneath a minimum size are considered errors and removed. Normally, the marker is in the shape of a small ellipse which overlaps with the middle of the cell. The markers are then labeled. Labeling is a process by which all contiguous pixel groups are given a unique pixel value. Unique numbers are given based on the location of the object.

The separated, labeled markers represent unique cells in the channel, but they do not accurately reflect the shape and size of the actual cells. In order to do so, we want to “fill out” the markers. We use the subtracted images, masked by the binary image created by the Otsu threshold, to determine the cell boundaries. We expand the markers up to these boundaries as well as each other (without overlapping). The result is the segmented image

For this task we use the “random walker” algorithm to determine which pixels should

be grouped with which markers²³⁶. Practically, random walker is similar to the more common watershedding algorithm. However, wathershedding can have undesired behavior at intersections between segments.

Random walker is a diffusion inspired, probabilistic method. It poses the question: if I am a particle starting at a given pixel in the image, what is the probability that I will land first at a particular marker via Brownian motion? Importantly, the intensity of image is used to weight the most likely direction the particle will take in a given time step. Specifically, the diffusion coefficient is greater between neighboring pixels when they have similar values. In this way, pixels close to and not separated by high gradients from a particular marker will be likely to land at that marker. We only consider pixels which are in the foreground (as dictated by the Otsu threshold) as candidates to be associated with a particular marker and thus become part of a cell.

Random walker it is solved as an optimization problem. In a brute force approach, for every pixel which is part of the foreground and not part of a marker, the probability that it will reach a marker is calculated for each marker. The pixel then receives the label of the marker on which it is most likely to land. Computationally, this is formed as a set of linear equations and solved such that the final combination of pixel assignments has the maximum likelihood of all possible combinations. In practice, the brute force approach is slow and the linear programming problem is solved with an approximate method.

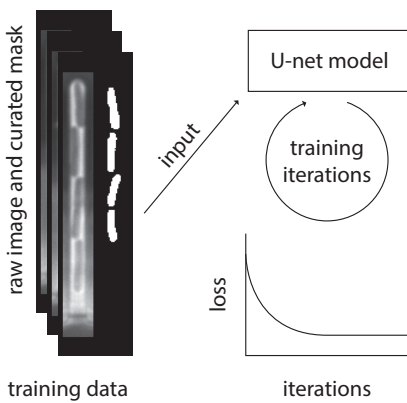
B.2.5 Segmentation routine 2: U-net convolutional network

mm3 also has a second, deep learning segmentation method based on a convolution network of the U-net architecture.

The traditional segmentation method has the advantage that it is relatively simple and fast. However, it relies on a number of parameters which must be specified by the user. Moreover, it is specifically designed for phase contrast images of rod shaped bacteria. Fission yeast, which are also amenable to growth in mother machine devices, is not well segmented by the method.

U-net segmentation workflow

A Model training



B Segmentation

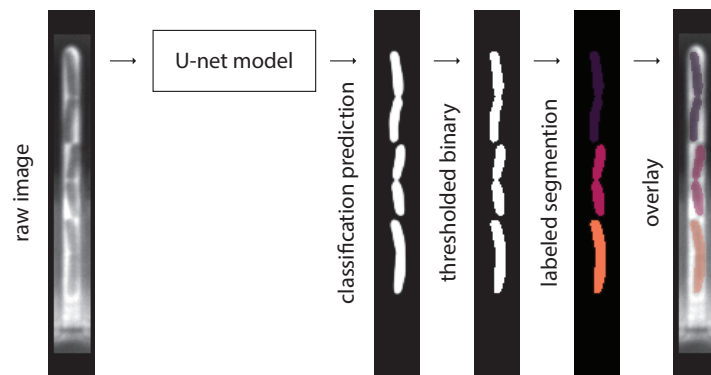


Figure B.5: U-net segmentation workflow. (A) U-net segmentation requires the training of a model using pre-labeled training data. Over many iterations, the model is able to create predictions from the raw image which accurately reflect the pre-labeled mask. This accuracy is reflected in the loss. (B) With a trained model, segmentation is applied directly to raw images. The output is a classification prediction array. Values from 0 to 1 correspond to the confidence that a given pixel is part of a cell. This image is binarized via a threshold and labeled to make the segmented image.

Convolutional networks are a class of generalized image classification algorithms that do not rely on significant manual parameterization or preprocessing of images. Segmentation is such a classification problem, that is, classifying which pixels belong to cells. Convolution networks as applied to images determine the probability that a pixel is of a class (in our case, part of a cell or part of the background). It does this using a model which recognizes local patterns in the image which indicate its class. The architecture of that model is pre-defined, and it contains many parameters.

The parameters of the model are effectively hidden from the user. To determine the parameters that most accurately classify pixels, convolution networks use supervised machine learning. In supervised machine learning, the classification algorithm is given training data which has been manually annotated and contains “true” data. In our case the training data is a binary mask of cells along with the raw image from which they were determined. The algorithm then iteratively runs classification and adjusts its internal parameters. Its goal during iteration is to

determine the set of parameters (weights) that produces a classification that is most similar to the given training data. Similarity is determined by minimizing a loss function. This function quantifies the distance between the model output and the training data input. In our case the cross entropy is used for the loss, which quantifies the unnecessary information contained in the output image when compared to the input image.

The model architecture we use is called U-net^{224,237}. This architecture uses both local and distant information in the image for pixel classification. When the image is contracted into a feature vector, it passes through alternating steps of convolutions and downsampling. The convolution sets always use 3x3 kernels, of which only the real part is taken (thus the edge pixels are lost). Each set of convolutions increases the number of feature channels, while the downsampling decreases the 2D resolution. Later convolution steps are effectively drawing information from a larger swath of the original image.

The resulting 1D feature vector is then successively expanded via 2x2 up-convolutions which use the training weights. Each up-convolution doubles the size of the array in X and Y and halves the number of features. In addition, the corresponding feature map from contraction is cropped and concatenated with the result of the up-convolution, adding contextual information. This feature array is then convolved similarly as during contraction. By using the same number of expansion steps as contraction steps, the resulting output image is of the same resolution as the input (however, it is smaller due to pixels being lost at the border during every convolution). This symmetry is also what gives the architecture its ‘U’ shape.

Regardless of the details of the U-net segmentation algorithm, it effectively works as follows (Figure B.5). The user makes training data. These are binary segmentation masks paired with the raw source images. These can be made via another algorithm such as the standard method described above, curated by hand, or a combination of both. Usually, the size of the training dataset is augmented by applying numerous affine transformation to the set to create “new” data. The user then trains a U-net model using this labeled data. This trained U-net model is applied to

unsegmented images. The output are probabilistic predictions of cell containing pixels. These prediction arrays are binarized with a threshold and distinct cells are labeled. The final result is an 8 bit image array is the same format as the result from the traditional segmentation algorithm.

The advantage of the U-net segmentation, and deep learning in general, is that it can be applied to diverse datasets and requires little configurations. It is also far more accurate than the traditional method in many cases. The disadvantages are several. Convolutions are computationally expensive, so this method is slower than traditional methods. Curating training data is a time intensive process, and different experimental conditions (such as different lighting or devices) may require the training of new models. Additionally, unexpected behavior can be hard to debug because the internal workings of the model are obscured. However, in my experience the benefits outweigh the costs. Once a sufficient model is trained it can be used indefinitely to produce consistent results. Segmentation for typical experiment is on the order of hours, but will most likely be done overnight on a personal computer for either method. Most importantly, the decrease in segmentation errors greatly improves the fidelity of the tracking algorithm. This results in much larger datasets of analyzable cells (or equivalently requires less raw data to produce the same amount).

B.2.6 Region tracking and cell lineage creation

Creating cell lineages entails linking segmented regions through time. In computer vision, this problem is known as region tracking. This could be tracking the location of a car as it moves in a video. For us, it means tracking a cell as it grows and moves in a mother machine channel. If we know which set of regions across time belong to one cell, we have the requisite information to measure physiological parameters such as birth size, elongation rate, and generation time.

Our goal goes slightly beyond region tracking, because we also want to define the cell ancestry or lineage. That is, we want to identify the parent and children of each cell. When a cell's life is over, it likely becomes two cells. It can also die or escape the channel, though these

are treated as corner cases for our purposes. When all is said and done, cell objects are defined as a collection of regions through time which are born from another cell and have two daughter cells. The process of creating cell objects from regions and identifying their parents and children is lineage creation.

Lineage creation is naively accomplished with a decision tree algorithm based on *a priori* knowledge of how cells grow as well as the normal arrangement of cells in mother machine channels. The algorithm traverses a single channel through time. It assesses how the regions at the current time point relate to regions in the previous time point, thereby initializing and building cell objects. In this way, a graph is built which links regions from the current time point to the cells present in the previous time point. The cells in the previous time point are the leaves in the graph. The graph is effectively stored in the cell objects, which are fundamentally a collection of linked regions.

The algorithm starts at the first time point, and all regions at that time point are initialized as cell objects. Each cell object has an experiment-wide unique ID and contains information about the regions of which it is composed (which at the start is just one region). These cells are stored as current leaves (leaf cells) and the algorithm progresses to the next time point. All current regions are then assigned to a leaf cell. This assignment is based on the Y locations of the regions and the most recent Y locations of the leaf cells. Importantly, cells in the mother machine are arranged vertically and cannot pass each other. Thus, a current region with a small Y displacement from a particular leaf cell is most likely part of that cell, or is perhaps its daughter.

The result is a map where each current region is linked to one and only one leaf cell. However, each leaf cell may be linked to zero, one, two, or more current regions. The next step is to inspect each leaf cell and its potential links to decide what the fate of the linked regions should be. This step relies on assumptions about normal cell growth while acknowledging that some regions may be meaningless as they are the result of segmentation errors.

The most important piece of information is how many regions are linked to a leaf cell.

This determines what kind of checks are made.

1. If a leaf cell is linked to no regions, then that leaf is skipped over. This could mean that the cell died, escaped the channel, moved a great deal vertically, or segmentation errors corrupted the region to leaf cell map. They are left in the list of current leaf cells and can still be linked to regions in future time points. However, after several time points, leaf cells to which no regions link are removed from the list of current leaf cells. That cell is then the tail of a dead end lineage.
2. If a leaf cell is linked to one region, it is possible that the cell has grown. The region is checked that it is no smaller or larger than the last region of the leaf cell to which it is linked by a defined factor. These parameters are chosen based on the growth rate of the cells and picture taking frequency. If it passes this test, the region is added to the current leaf cell and becomes part of that cell object. The cell object remains in the list of current leaf cells. If the region does not pass this test, it is discarded.
3. If a leaf cell is linked to two regions then there are the following possibilities: the two regions are the daughters of the divided cell, one of the two regions is the cell growing and the other is an error, or both regions are errors. First, the size of each region is checked against the size of the last region in the leaf cell. If either region satisfies the requirements for a growing cell as above, then the cell is grown by that region and the other region is initialized as a new leaf cell.

In the case that the cell has divided, each region would be too small to satisfy the growth requirements. Instead, the size of the two regions are combined and compared to the size of the leaf cell. If the difference in size between the combined regions and the leaf cell is within set bounds it is possible that the cell has divided. An additional check is made in that one of the region's centroid must fall within the top half of the bounding box that contains the leaf cell, and the other must fall within the bottom half. If these requirements

are met, two new cells are initialized and added to the list of current leaf cells. A cell that is born in this way is initialized with a pointer to the ID of its parent. The previous leaf cell is divided (with pointers to its two daughters stored) and removed from the list of leaf cells.

If the regions cannot be assigned as growing or daughter cells, then they are discarded.

4. Finally, if a leaf cell is linked to three or more regions, only the two closest regions are considered for the above possibility. The other regions are initialized at new leaf cells.

There is some nuance as to when unassignable regions should be discarded and when they should be initialized as new cells and added to the list of leaf cells. The former can miss potential cells, while the latter can complicate the graph with spurious leaf cells. If for some reason during tracking all leaf cells become dead ends and a later time point has regions, all those regions are initialized as new leaf cells. This can happen due to errors in segmentation, or a rare event such as a channel becoming empty and then a cell entering the channel from the open end. This process is continued for every time point. The result is a dictionary of cell objects using the cell IDs as keys. Normally, this dictionary is further refined to just “complete” cells. A complete cell is one that has both a mother and two daughters. Thus, cells that are initialized in a manner other than being daughters, such as the cells in the first time point, are ignored for the purposes of data analysis because their true history is unknown. Cells which do not divide are also ignored as they are likely the result of segmentation or tracking errors, cell death, or escaping the channel. However, in cases where cell death is a key aspect of the research question, it is necessary to return to the dictionary of all cell objects and apply tailored filtering methods.

Bibliography

- [1] J. W. Schopf, “Fossil evidence of Archaean life,” *Philosophical Transactions of the Royal Society B: Biological Sciences*, 361, 869–885, 2006.
- [2] Gilbert Walter, “Origin of life: The RNA world,” *Nature*, p. 86, 1986.
- [3] A. Pohorille & D. Deamer, “Self-assembly and function of primitive cell membranes,” *Research in Microbiology*, 160, 449–456, 2009.
- [4] J. Lombard, P. López-García, & D. Moreira, “The early evolution of lipid membranes and the three domains of life,” *Nature Reviews Microbiology*, 10, 507–515, 2012.
- [5] C. R. Woese, “The universal ancestor,” *Proceedings of the National Academy of Sciences*, 95, 6854–6859, jun 1998.
- [6] C. R. Woese, “On the evolution of cells,” *Proceedings of the National Academy of Sciences*, 99, 8742–8747, jun 2002.
- [7] A. L. Koch, “Primeval cells: Possible energy-generating and cell-division mechanisms,” *Journal of Molecular Evolution*, 21, 270–277, 1985.
- [8] S. Taheri-Araghi, S. Bradde, J. T. Sauls, N. S. Hill, P. A. Levin, J. Paulsson, M. Vergassola, & S. Jun, “Cell-size control and homeostasis in bacteria.” *Current biology*, 25, 385–91, feb 2015.
- [9] P. Wang, L. Robert, J. Pelletier, W. L. Dang, F. Taddei, A. Wright, & S. Jun, “Robust growth of *Escherichia coli*.” *Current biology*, 20, 1099–103, jun 2010.
- [10] M. Schaechter, “From growth physiology to systems biology.” *International Microbiology*, 9, 157–61, sep 2006.
- [11] J. T. Sauls, S. E. Cox, V. Castillo, Z. Ghulam-Jelani, & S. Jun, “Gram-positive and Gram-negative Bacteria Share Common Principles to Coordinate Growth and the Cell Cycle at the Single-cell Level,” *bioRxiv*, 2019.
- [12] C. E. Helmstetter, S. Cooper, O. Pierucci, & E. Revelas, “On Bacterial Life Sequence,” *Cold Spring Harbor Symposia on Quantitative Biology*, 33, 809–&, 1968.

- [13] F. Si, G. Le Treut, J. T. Sauls, S. Vadia, P. A. Levin, & S. Jun, “Mechanistic Origin of Cell-Size Control and Homeostasis in Bacteria,” *Current Biology*, 29, 1760–1770, jun 2019.
- [14] S. Jun, F. Si, R. Pugatch, & M. Scott, “Fundamental Principles in Bacterial Physiology - History, Recent progress, and the Future with Focus on Cell Size Control: A Review,” *Reports on Progress in Physics*, 2017.
- [15] W. D. Donachie, “Relationship between Cell Size and Time of Initiation of DNA Replication,” *Nature*, 219, 1077–1079, sep 1968.
- [16] M. Schaechter, O. Maaløe, & N. O. Kjeldgaard, “Dependency on medium and temperature of cell size and chemical composition during balanced grown of *Salmonella typhimurium*.” *Journal of General Microbiology*, 19, 592–606, dec 1958.
- [17] S. Cooper, “The origins and meaning of the Schaechter-Maalae-Kjeldgaard experiments,” *Journal of General Microbiology*, 1117–1124, 1993.
- [18] M. Schaechter, “A brief history of bacterial growth physiology,” *Frontiers in Microbiology*, 6, 1–5, 2015.
- [19] M. Basan, M. Zhu, X. Dai, M. Warren, D. Sévin, Y.-p. Wang, & T. Hwa, “Inflating bacterial cells by increased protein synthesis.” *Molecular Systems Biology*, 11, p. 836, 2015.
- [20] F. C. Neidhardt, “Bacterial growth: constant obsession with dN/dt ,” *Journal of Bacteriology*, 181, 7405–8, dec 1999.
- [21] R. E. Buchanan, “Life Phases in a Bacterial Culture,” *Journal of Infectious Diseases*, 23, 109–125, aug 1918.
- [22] F. C. Neidhardt & B. Magasanik, “Studies on the role of ribonucleic acid in the growth of bacteria,” *Biochimica et Biophysica Acta*, 42, 99–116, jan 1960.
- [23] a. D. Hershey, “Factors Limiting Bacterial Growth,” *Journal of Bacteriology*, 38, 563–578, 1939.
- [24] K. Nath & A. L. Koch, “Protein degradation in *Escherichia coli*. I. Measurement of rapidly and slowly decaying components.” *Journal of Biological Chemistry*, 245, 2889–900, jun 1970.
- [25] O. Maaløe, “Regulation of the Protein-Synthesizing Machinery Ribosomes, tRNA, Factors, and So On,” in *Biological Regulation and Development*, 487–542, Boston, MA: Springer US, 1979.
- [26] P. P. Dennis & H. Bremer, “Modulation of Chemical Composition and Other Parameters of the Cell at Different Exponential Growth Rates,” *EcoSal Plus*, 3, 2008.

- [27] D. W. Erickson, S. J. Schink, V. Patsalo, J. R. Williamson, U. Gerland, & T. Hwa, “A global resource allocation strategy governs growth transition kinetics of *E. coli*,” *Nature Publishing Group*, 2017.
- [28] A. Campbell, “Synchronization of cell division,” *Bacteriological reviews*, 21, 263–72, dec 1957.
- [29] T. Akerlund, K. Nordstrom, & R. Bernander, “Analysis of cell size and DNA content in exponentially growing and stationary-phase batch cultures of *Escherichia coli*,” *Journal of Bacteriology*, 177, 6791–6797, 1995.
- [30] S. Taheri-Araghi, S. D. Brown, J. T. Sauls, D. B. McIntosh, & S. Jun, “Single-Cell Physiology,” *Annual Review of Biophysics*, 44, 123–42, 2015.
- [31] A. Zaritsky, “On dimensional determination of rod-shaped bacteria,” *Journal of Theoretical Biology*, 54, 243–248, 1975.
- [32] S. Cooper & C. E. Helmstetter, “Chromosome replication and the division cycle of *Escherichia coli* B/r,” *Journal of Molecular Biology*, 31, 519–40, feb 1968.
- [33] A. L. Koch, “Does the Initiation of Chromosome Replication Regulate Cell Division?,” *Advances in Microbial Physiology*, 16, 49–98, 1977.
- [34] J. B. S. Haldane, “On Being the Right Size,” 1928.
- [35] A. L. Koch, “What Size Should a Bacterium Be? A Question of Scale,” *Annual Review of Microbiology*, 50, 317–348, oct 1996.
- [36] Pritchard R H, P. T. Barth, & J. F. Collins, “Control of DNA synthesis in Bacteria,” *Symp. Soc. Gen. Microbiol*, 19, 263–297, 1968.
- [37] F. Si, D. Li, S. E. Cox, J. T. Sauls, O. Azizi, C. Sou, A. B. Schwartz, M. J. Erickstad, Y. Jun, X. Li, & S. Jun, “Invariance of Initiation Mass and Predictability of Cell Size in *Escherichia coli*,” *Current Biology*, 27, 1278–1287, may 2017.
- [38] L. Sompayrac & O. Maaløe, “Autorepressor Model for Control of DNA Replication,” *Nature New Biology*, 241, 133–135, jan 1973.
- [39] A. Løbner-Olesen, K. Skarstad, F. G. Hansen, K. von Meyenburg, & E. Boye, “The DnaA protein determines the initiation mass of *Escherichia coli* K-12,” *Cell*, 57, 881–889, 1989.
- [40] S. Wold, K. Skarstad, H. B. Steen, T. Stokke, & E. Boye, “The initiation mass for DNA replication in *Escherichia coli* K-12 is dependent on growth rate,” *The EMBO journal*, 13, 2097–2102, 1994.
- [41] M. Wallden, D. Fange, E. Gregorsson Lundius, Ö. Baltekin, & J. Elf, “The synchronization of replication and division cycles in individual *E. coli* cells (in press),” *Cell*, 729–739, 2016.

- [42] J. T. Sauls, D. Li, & S. Jun, “Adder and a coarse-grained approach to cell size homeostasis in bacteria,” *Current Opinion in Cell Biology*, 38, 38–44, feb 2016.
- [43] I. Santi, N. Dhar, D. Bousbaine, Y. Wakamoto, & J. D. McKinney, “Single-cell dynamics of the chromosome replication and cell division cycles in mycobacteria,” *Nature Communications*, 4, p. 2470, jan 2013.
- [44] L. Robert, M. Hoffmann, N. Krell, S. Aymerich, J. Robert, & M. Doumic, “Division in *Escherichia coli* is triggered by a size-sensing rather than a timing mechanism.” *BMC biology*, 12, p. 17, 2014.
- [45] M. Osella, E. Nugent, & M. Cosentino Lagomarsino, “Concerted control of *Escherichia coli* cell division.” *Proceedings of the National Academy of Sciences*, 111, 3431–5, mar 2014.
- [46] J.-B. Nobs & S. J. Maerkl, “Long-term single cell analysis of *S. pombe* on a microfluidic microchemostat array.” *PLoS ONE*, 9, p. e93466, 2014.
- [47] S. Iyer-Biswas, C. S. Wright, J. T. Henry, K. Lo, S. Burov, Y. Lin, G. E. Crooks, S. Crosson, A. R. Dinner, & N. F. Scherer, “Scaling laws governing stochastic growth and division of single bacterial cells.” *Proceedings of the National Academy of Sciences*, 111, 15912–7, nov 2014.
- [48] M. Campos, I. V. Surovtsev, S. Kato, A. Paintdakhi, B. Beltran, S. E. Ebmeier, & C. Jacobs-Wagner, “A constant size extension drives bacterial cell size homeostasis.” *Cell*, 159, 1433–46, dec 2014.
- [49] S. Jun & S. Taheri-Araghi, “Cell-size maintenance: universal strategy revealed.” *Trends in Microbiology*, 23, 4–6, jan 2015.
- [50] M. Deforet, D. van Ditmarsch, & J. B. Xavier, “Cell-Size Homeostasis and the Incremental Rule in a Bacterial Pathogen.” *Biophysical Journal*, 109, 521–8, aug 2015.
- [51] A. L. Koch & M. Schaechter, “A model for statistics of the cell division process.” *Journal of General Microbiology*, 29, 435–54, nov 1962.
- [52] D. J. Clark & O. Maaløe, “DNA replication and the division cycle in *Escherichia coli*,” *Journal of Molecular Biology*, 23, 99–112, 1967.
- [53] W. D. Donachie, D. T. M. Martin, & K. J. Begg, “Independence of cell division and DNA replication in *Bacillus subtilis*,” *Nature New Biology*, 231, 274–276, 1971.
- [54] D. E. Dix & C. E. Helmstetter, “Coupling between chromosome completion and cell division in *Escherichia coli*,” *Journal of Bacteriology*, 115, 786–795, 1973.
- [55] R. Bernander & K. Nordström, “Chromosome replication does not trigger cell division in *E. coli*,” *Cell*, 60, 365–374, 1990.

- [56] W. D. Donachie, “Co-ordinate regulation of the Escherichia coli cell cycle or The cloud of unknowing,” *Molecular Microbiology*, 40, 779–785, 2001.
- [57] P. C. L. John, *The Cell Cycle*. London: Cambridge University Press, 1981.
- [58] H. X. Chao, R. I. Fakhreddin, H. K. Shimerov, R. J. Kumar, G. P. Gupta, & J. Purvis, “Evidence that the cell cycle is a series of uncoupled, memoryless phases,” *bioRxiv*, 2018.
- [59] A. C. Chien, N. S. Hill, & P. A. Levin, “Cell size control in bacteria,” *Current Biology*, 22, R340–R349, 2012.
- [60] N. E. Kleckner, K. Chatzi, M. A. White, J. K. Fisher, & M. Stouf, “Coordination of Growth, Chromosome Replication/Segregation, and Cell Division in E. coli,” *Frontiers in Microbiology*, 9, 1–12, 2018.
- [61] G. Witz, E. V. Nimwegen, & T. Julou, “Initiation of chromosome replication controls both division and replication cycles in E. coli through a double-adder mechanism,” *bioRxiv*, 2019.
- [62] O. Maaløe, “The control of normal DNA replication in bacteria.,” *Cold Spring Harbor Symposia on Quantitative Biology*, 26, 45–52, 1961.
- [63] N. S. Hill, R. Kadoya, D. K. Chatteraj, & P. A. Levin, “Cell size and the initiation of DNA replication in bacteria,” *PLoS Genetics*, 8, p. e1002549, jan 2012.
- [64] T. G. Bernhardt & P. A. J. De Boer, “SlmA, a nucleoid-associated, FtsZ binding protein required for blocking septal ring assembly over chromosomes in E. coli,” *Molecular Cell*, 18, 555–564, 2005.
- [65] J. Lutkenhaus, “Assembly dynamics of the bacterial MinCDE system and spatial regulation of the Z ring.,” *Annual Review of Biochemistry*, 76, 539–62, 2007.
- [66] J. Männik & M. W. Bailey, “Spatial coordination between chromosomes and cell division proteins in Escherichia coli,” *Frontiers in Microbiology*, 6, 1–8, 2015.
- [67] A. Zaritsky & C. L. Woldringh, “Chromosome replication, cell growth, division and shape: a personal perspective.,” *Frontiers in microbiology*, 6, p. 756, 2015.
- [68] E. J. Harry, “Coordinating DNA replication with cell division: Lessons from outgrowing spores,” *Biochimie*, 83, 75–81, 2001.
- [69] D. Bates & N. Kleckner, “Chromosome and replisome dynamics in E. coli: loss of sister cohesion triggers global chromosome movement and mediates chromosome segregation.,” *Cell*, 121, 899–911, jun 2005.
- [70] O. Espeli, R. Borne, P. Dupaigne, A. Thiel, E. Gigant, R. Mercier, & F. Bocard, “A MatP-divisome interaction coordinates chromosome segregation with cell division in E. coli,” *The EMBO journal*, 31, 3198–3211, 2012.

- [71] T. den Blaauwen, “Prokaryotic cell division: Flexible and diverse,” *Current Opinion in Microbiology*, 16, 738–744, 2013.
- [72] K. Jonas, “To divide or not to divide: control of the bacterial cell cycle by environmental cues,” *Current opinion in microbiology*, 18, 54–60, apr 2014.
- [73] D. Magnan, M. C. Joshi, A. K. Barker, B. J. Visser, & D. Bates, “DNA Replication Initiation Is Blocked by a Distant Chromosome Membrane Attachment,” *Current Biology*, 25, 2143–2149, aug 2015.
- [74] I. V. Hajduk, C. D. Rodrigues, & E. J. Harry, “Connecting the dots of the bacterial cell cycle: Coordinating chromosome replication and segregation with cell division,” *Seminars in Cell and Developmental Biology*, 53, 2–9, 2016.
- [75] A. H. Stouthamer, “A theoretical study on the amount of ATP required for synthesis of microbial cell material,” *Antonie van Leeuwenhoek*, 39, 545–565, dec 1973.
- [76] F. Forro & S. A. Wertheimer, “The organization and replication of deoxyribonucleic acid in thymine-deficient strains of *Escherichia coli*,” *Biochimica et Biophysica Acta*, 40, 9–21, jan 1960.
- [77] C. E. Helmstetter & D. J. Cummings, “Bacterial Synchronization By Selection of Cells At Division,” *Proceedings of the National Academy of Sciences*, 50, 767–74, oct 1963.
- [78] N. C. Chai & K. G. Lark, “Cytological studies of deoxyribonucleic acid replication in *Escherichia coli* 15T-: replication at slow growth rates and after a shift-up into rich medium,” *Journal of Bacteriology*, 104, 401–409, 1970.
- [79] J. D. Watson & F. H. C. Crick, “Molecular Structure of Nucleic Acids: A Structure for Deoxyribose Nucleic Acid,” *Nature*, 171, 737–738, apr 1953.
- [80] M. Meselson & F. W. Stahl, “The replication of DNA in *Escherichia coli*,” *Proceedings of the National Academy of Sciences*, 44, 671–682, jul 1958.
- [81] J. Cairns, “The Chromosome of *Escherichia coli*,” *Cold Spring Harbor Symposia on Quantitative Biology*, 28, 43–46, jan 1963.
- [82] F. Jacob, S. Brenner, & F. Cuzin, “On the Regulation of DNA Replication in Bacteria,” *Cold Spring Harbor Symposia on Quantitative Biology*, 28, 329–348, jan 1963.
- [83] H. Yoshikawa & N. Sueoka, “Sequential replication of *Bacillus subtilis* chromosome. I. Comparison of marker frequencies in exponential and stationary growth phases,” *Proceedings of the National Academy of Sciences*, 49, 559–66, apr 1963.
- [84] B. Müller-Hill, “The lac Operon,” 1996.
- [85] M. Ptashne, *A Genetic Switch*. New York: Cold Spring Harbor Laboratory Press, third edit ed., 1986.

- [86] E. M. Witkin, "Ultraviolet mutagenesis and inducible DNA repair in *Escherichia coli*." *Bacteriological reviews*, 40, 869–907, dec 1976.
- [87] W. D. Donachie, K. J. Begg, N. F. Sullivan, R. Losick, & L. Shapiro, "Morphogenes of *Escherichia coli*," in *Microbial Development*, 27–62, 1984.
- [88] T. Katayama, S. Ozaki, K. Keyamura, & K. Fujimitsu, "Regulation of the replication cycle: conserved and diverse regulatory systems for DnaA and oriC.," *Nature Reviews Microbiology*, 8, 163–70, mar 2010.
- [89] K. Skarstad & T. Katayama, "Regulating DNA replication in bacteria.," *Cold Spring Harbor perspectives in biology*, 5, p. a012922, apr 2013.
- [90] D. Li, *DNA replication and cell size control in Escherichia coli*. PhD thesis, Univeristy of California San Diego, 2018.
- [91] B. H. Rosenberg, L. F. Cavalieri, & G. Ungers, "The Negative Control Mechanism for *E. coli* DNA Replication," *Proceedings of the National Academy of Sciences*, 63, 1410–1417, aug 1969.
- [92] H. Margalit & N. B. Grover, "Initiation of chromosome replication in bacteria: analysis of an inhibitor control model.," *Journal of Bacteriology*, 169, 5231–40, nov 1987.
- [93] F. G. Hansen, B. B. Christensen, & T. Atlung, "The initiator titration model: computer simulation of chromosome and minichromosome control," *Research in Microbiology*, 142, 161–167, 1991.
- [94] Y. Hirota, J. Mordoh, & F. Jacob, "On the process of cellular division in *Escherichia coli*. III. Thermosensitive Mutants of *Escherichia coli* Altered in the Process of DNA Initiation," *Journal of Molecular Biology*, 53, 369–387, 1970.
- [95] F. G. Hansen & T. Atlung, "The DnaA tale," *Frontiers in Microbiology*, 9, 1–19, 2018.
- [96] R. S. Fuller, J. M. Kaguni, & A. Kornberg, "Enzymatic replication of the origin of the *Escherichia coli* chromosome (oriC plasmids/dnaA gene/DNA replication)," *Biochemistry*, 78, 7370–7374, 1981.
- [97] R. S. Fuller, B. E. Funnell, & A. Kornberg, "The dnaA protein complex with the *E. coli* chromosomal replication origin (oriC) and other DNA sites," *Cell*, 38, 889–900, 1984.
- [98] F. G. Hansen, S. Koefoed, L. Sørensen, & T. Atlung, "Titration of DnaA protein by oriC DnaA-boxes increases dnaA gene expression in *Escherichia coli*." *The EMBO journal*, 6, 255–8, jan 1987.
- [99] R. M. Teather, J. F. Collins, & W. D. Donachie, "Quantal behavior of a diffusible factor which initiates septum formation at potential division sites in *Escherichia coli*," *Journal of Bacteriology*, 118, 407–413, 1974.

- [100] H. I. Adler, W. D. Fisher, A. Cohen, & A. A. Hardigree, "Miniature Escherichia coli Cells Deficient in DNA," *Proceedings of the National Academy of Sciences*, 57, 321–6, 1967.
- [101] M. A. de Pedro, J. E. Llamas, & J. L. Canovas, "A timing control of cell division in Escherichia coli," *Journal of General Microbiology*, 91, 307–314, 1975.
- [102] J. F. Lutkenhaus & W. D. Donachie, "Identification of the ftsA gene product," *Journal of Bacteriology*, 137, 1088–1094, 1979.
- [103] J. F. Lutkenhaus, H. Wolf-Watz, & W. D. Donachie, "Organization of genes in the ftsA-envA region of the Escherichia coli genetic map and identification of a new fts locus (ftsZ)," *Journal of Bacteriology*, 142, 615–620, 1980.
- [104] J. F. Lutkenhaus, "Coupling of DNA replication and cell division: sulB is an allele of ftsZ," *Journal of Bacteriology*, 154, 1339–46, jun 1983.
- [105] J. E. Ward & J. Lutkenhaus, "Overproduction of FtsZ induces minicell formation in E. coli," *Cell*, 42, 941–949, 1985.
- [106] E. Bi & J. Lutkenhaus, "FtsZ regulates frequency of cell division in Escherichia coli," *Journal of Bacteriology*, 172, 2765–2768, 1990.
- [107] W. D. Donachie & K. J. Begg, "'Division potential' in Escherichia coli," *Journal of Bacteriology*, 178, 5971–5976, 1996.
- [108] K. J. Begg, Y. Nikolaichik, N. Crossland, & W. D. Donachie, "Roles of FtsA and FtsZ in activation of division sites," *Journal of Bacteriology*, 180, 881–884, 1998.
- [109] T. Garrido, M. Sánchez, P. Palacios, M. Aldea, & M. Vicente, "Transcription of ftsZ oscillates during the cell cycle of Escherichia coli.," *The EMBO journal*, 12, 3957–3965, 1993.
- [110] L. K. Harris & J. A. Theriot, "Relative Rates of Surface and Volume Synthesis Set Bacterial Cell Size," *Cell*, 165, 1479–1492, 2016.
- [111] P. Van De Putte, J. Van Dillewijn, & A. Rörsch, "The selection of mutants of escherichia coli with impaired cell division at elevated temperature," *Mutation Research*, 1, 121–128, 1964.
- [112] K. Nordstrom, R. Bernander, & S. Dasgupta, "The Escherichia coli cell cycle: one cycle or multiple independent processes that are coordinated?," *Molecular Microbiology*, 5, 769–774, 1991.
- [113] E. Boye & K. Nordström, "Coupling the cell cycle to cell growth. A look at the parameters that regulate cell-cycle events," *EMBO Reports*, 4, 757–760, 2003.
- [114] L. Robert, "Size sensors in bacteria, cell cycle control, and size control.," *Frontiers in microbiology*, 6, p. 515, 2015.

- [115] L. Dewachter, N. Verstraeten, M. Fauvart, & J. Michiels, “An integrative view of cell cycle control in *Escherichia coli*,” *FEMS Microbiology Reviews*, 42, 116–136, 2018.
- [116] B. Di Ventura, B. Knecht, H. Andreas, W. J. Godinez, M. Fritsche, K. Rohr, W. Nickel, D. W. Heermann, & V. Sourjik, “Chromosome segregation by the *Escherichia coli* Min system,” *Molecular Systems Biology*, 9, 1–12, 2013.
- [117] K. H. Jameson & A. J. Wilkinson, “Control of initiation of DNA replication in *Bacillus subtilis* and *Escherichia coli*,” *Genes*, 8, 2017.
- [118] F. G. Hansen & K. von Meyenburg, “Characterization of the *dnaA*, *gyrB* and other genes in the *dnaA* region of the *Escherichia coli* chromosome on specialized transducing phages λ tna,” *Molecular and General Genetics*, 175, 135–144, sep 1979.
- [119] E. B. Hansen, T. Atlung, F. G. Hansen, O. Skovgaard, & K. von Meyenburg, “Fine structure genetic map and complementation analysis of mutations in the *dnaA* gene of *Escherichia coli*,” *Molecular and General Genetics*, 196, 387–396, 1984.
- [120] R. E. Bird, J. Louarn, J. Martuscelli, & L. Caro, “Origin and sequence of chromosome replication in *Escherichia coli*,” *Journal of Molecular Biology*, 70, 549–566, oct 1972.
- [121] S. Hiraga, “Novel F prime factors able to replicate in *Escherichia coli* Hfr strains.,” *Proceedings of the National Academy of Sciences*, 73, 198–202, jan 1976.
- [122] T. Katayama, K. Kasho, & H. Kawakami, “The DnaA Cycle in *Escherichia coli*: Activation, Function and Inactivation of the Initiator Protein,” *Frontiers in Microbiology*, 8, 1–15, 2017.
- [123] J. Kato & T. Katayama, “Hda, a novel DnaA-related protein, regulates the replication cycle in *Escherichia coli*.,” *The EMBO journal*, 20, 4253–62, aug 2001.
- [124] R. E. Braun, K. O’Day, & A. Wright, “Autoregulation of the *dnaA* gene in *E. coli*,” *Cell*, 40, 459–469, 1985.
- [125] Y. Ogura, Y. Imai, N. Ogasawara, & S. Moriya, “Autoregulation of the *dnaA*-*dnaN* operon and effects of DnaA protein levels on replication initiation in *Bacillus subtilis*,” *Journal of Bacteriology*, 183, 3833–3841, 2001.
- [126] T. Atlung & F. G. Hansen, “Three distinct chromosome replication states are induced by increasing concentrations of DnaA protein in *Escherichia coli*,” *Journal of Bacteriology*, 175, 6537–6545, 1993.
- [127] P. A. J. de Boer, “Classic spotlight: Discovery of *ftsZ*,” *Journal of Bacteriology*, 198, p. 1184, 2016.
- [128] T. den Blaauwen, L. W. Hamoen, & P. A. Levin, “The divisome at 25: the road ahead,” *Current Opinion in Microbiology*, 36, 85–94, 2017.

- [129] B. F. Johnson & J. Greenberg, “Mapping of sul, the suppressor of lon in Escherichia coli,” *Journal of Bacteriology*, 122, 570–574, 1975.
- [130] B. F. Johnson, “Fine structure mapping and properties of mutations suppressing the lon mutation in Escherichia coli K-12 and B strains,” *Genet. Res.*, 273–286, 1977.
- [131] S. Gottesman, E. Halpern, & P. Trisler, “Role of sulA and sulB in filamentation by lon mutants of Escherichia coli K-12 . Role of sulA and sulB in Filamentation by Lon Mutants of Escherichia coli K-12,” *Journal of Bacteriology*, 148, 265–273, 1981.
- [132] E. Bi & J. Lutkenhaus, “FtsZ ring structure associated with division in Escherichia coli,” *Nature*, 354, 161–164, nov 1991.
- [133] Q. Sun & W. Margolin, “FtsZ dynamics during the division cycle of live Escherichia coli cells,” *Journal of Bacteriology*, 180, 2050–2056, 1998.
- [134] T. den Blaauwen, N. Buddelmeijer, M. E. Aarsman, C. M. Hameete, & N. Nanninga, “Timing of FtsZ assembly in Escherichia coli,” *Journal of Bacteriology*, 181, 5167–5175, 1999.
- [135] D. A. Moore, Z. N. Whatley, C. P. Joshi, M. Osawa, & H. P. Erickson, “Probing for Binding Regions of the FtsZ Protein Surface through Site-Directed Insertions: Discovery of Fully Functional FtsZ-Fluorescent Proteins,” *Journal of Bacteriology*, 199, e00553–16, jan 2017.
- [136] L. A. Amos & J. Lowe, “Crystal structure of the bacterial cell-division protein FtsZ,” *Nature*, 391, 203–206, 1998.
- [137] L. Romberg & P. A. Levin, “Assembly Dynamics of the Bacterial Cell Division Protein FtsZ: Poised at the Edge of Stability,” *Annual Review of Microbiology*, 57, 125–154, 2003.
- [138] H. P. Erickson, D. W. Taylor, K. A. Taylor, & D. Bramhill, “Bacterial cell division protein FtsZ assembles into protofilament sheets and minirings, structural homologs of tubulin polymers.,” *Proceedings of the National Academy of Sciences*, 93, 519–523, 1996.
- [139] D. Shiomi & W. Margolin, “Dimerization or oligomerization of the actin-like FtsA protein enhances the integrity of the cytokinetic Z ring,” *Molecular Microbiology*, 66, 1396–1415, 2007.
- [140] G. Lan, B. R. Daniels, T. M. Dobrowsky, D. Wirtz, & S. X. Sun, “Condensation of FtsZ filaments can drive bacterial cell division.,” *Proceedings of the National Academy of Sciences*, 106, 121–126, 2009.
- [141] S. Sugimoto, K. Yamanaka, S. Nishikori, A. Miyagi, T. Ando, & T. Ogura, “AAA+chaperone ClpX regulates dynamics of prokaryotic cytoskeletal protein FtsZ,” *Journal of Biological Chemistry*, 285, 6648–6657, 2010.
- [142] K. H. Huang, J. Durand-Heredia, & A. Janakiraman, “FtsZ ring stability: Of bundles, tubules, crosslinks, and curves,” *Journal of Bacteriology*, 195, 1859–1868, 2013.

- [143] F. Si, K. K. Busiek, W. Margolin, & S. X. Sun, “Organization of FtsZ filaments in the bacterial division ring measured from polarized fluorescence microscopy,” *Biophysical Journal*, 105, 1976–1986, 2013.
- [144] M. Loose & T. J. Mitchison, “The bacterial cell division proteins ftsA and ftsZ self-organize into dynamic cytoskeletal patterns,” *Nature Cell Biology*, 16, 38–46, 2014.
- [145] P. Szwedziak, Q. Wang, T. A. M. Bharat, M. Tsim, & J. Löwe, “Architecture of the ring formed by the tubulin homologue FtsZ in bacterial cell division,” *eLife*, 3, p. e04601, 2014.
- [146] C. Coltharp & J. Xiao, “Beyond force generation: Why is a dynamic ring of FtsZ polymers essential for bacterial cytokinesis?,” *BioEssays*, 39, 1–11, 2017.
- [147] A. W. Bisson-Filho, Y.-P. Hsu, G. R. Squyres, E. Kuru, F. Wu, C. Jukes, Y. Sun, C. Dekker, S. Holden, M. S. VanNieuwenhze, Y. V. Brun, & E. C. Garner, “Treadmilling by FtsZ filaments drives peptidoglycan synthesis and bacterial cell division.,” *Science*, 355, 739–743, feb 2017.
- [148] X. Yang, Z. Lyu, A. Miguel, R. McQuillen, K. C. Huang, & J. Xiao, “GTPase activity-coupled treadmilling of the bacterial tubulin FtsZ organizes septal cell wall synthesis.,” *Science*, 355, 744–747, feb 2017.
- [149] J. M. Monteiro, A. R. Pereira, N. T. Reichmann, B. M. Saraiva, P. B. Fernandes, H. Veiga, A. C. Tavares, M. Santos, M. T. Ferreira, V. Macário, M. S. VanNieuwenhze, S. R. Filipe, & M. G. Pinho, “Peptidoglycan synthesis drives an FtsZ-treadmilling-independent step of cytokinesis,” *Nature*, 2018.
- [150] N. Nanninga, “Cell division and peptidoglycan assembly in *Escherichia coli*,” *Molecular Microbiology*, 5, 791–795, apr 1991.
- [151] M. E. Aarsman, A. Piette, C. Fraipont, T. M. Vinkenvleugel, M. Nguyen-Distèche, & T. Den Blaauwen, “Maturation of the *Escherichia coli* divisome occurs in two steps,” *Molecular Microbiology*, 55, 1631–1645, 2005.
- [152] R. Van der Ploeg, J. Verheul, N. O. Vischer, S. Alexeeva, E. Hoogendoorn, M. Postma, M. Banzhaf, W. Vollmer, & T. Den Blaauwen, “Colocalization and interaction between elongasome and divisome during a preparative cell division phase in *Escherichia coli*,” *Molecular Microbiology*, 87, 1074–1087, 2013.
- [153] M. J. Tsang & T. G. Bernhardt, “Guiding divisome assembly and controlling its activity,” *Current Opinion in Microbiology*, 24, 60–65, 2015.
- [154] B. Söderström, K. Mirzadeh, S. Toddo, G. von Heijne, U. Skoglund, & D. O. Daley, “Coordinated disassembly of the divisome complex in *Escherichia coli*,” *Molecular Microbiology*, 101, 425–438, 2016.

- [155] S. Du & J. Lutkenhaus, “Assembly and activation of the Escherichia coli divisome,” *Molecular Microbiology*, 105, 177–187, jul 2017.
- [156] E. Mulder & C. L. Woldringh, “Actively replicating nucleoids influence positioning of division sites in Escherichia coli filaments forming cells lacking DNA.,” *Journal of Bacteriology*, 171, 4303–4314, 1989.
- [157] Q. Sun & W. Margolin, “Effects of perturbing nucleoid structure on nucleoid occlusion-mediated toporegulation of FtsZ ring assembly,” *Journal of Bacteriology*, 186, 3951–3959, 2004.
- [158] H. Cho, H. R. McManus, S. L. Dove, & T. G. Bernhardt, “Nucleoid occlusion factor SlmA is a DNA-activated FtsZ polymerization antagonist,” *Proceedings of the National Academy of Sciences*, 108, 3773–3778, 2011.
- [159] M. Schaechter, J. P. Williamson, J. R. Hood, & A. L. Koch, “Growth, cell and nuclear divisions in some bacteria.,” *Journal of General Microbiology*, 29, 421–34, nov 1962.
- [160] S. Hiraga, “Partitioning of nucleoids,” *Research in Microbiology*, 141, 50–56, jan 1990.
- [161] N. Nanninga, “Morphogenesis of Escherichia coli,” *Microbiology and Molecular Biology Reviews*, 62, 110–125, 1998.
- [162] C. L. Woldringh, J. A. Valkenburg, E. Pas, P. E. Taschner, P. Huls, & F. B. Wientjes, “Physiological and geometrical conditions for cell division in Escherichia coli,” *Annales de l’Institut Pasteur Microbiology*, 136, 131–138, 1985.
- [163] W. R. Cook, P. A. J. de Boer, & L. I. Rothfield, “Differentiation of the Bacterial Cell Division Site,” *International Review of Cytology*, 118, 1–31, 1989.
- [164] C. L. Woldringh, E. Mulder, J. A. C. Valkenburg, F. B. Wientjes, A. Zaritsky, & N. Nanninga, “Role of the nucleoid in the toporegulation of division,” *Research in Microbiology*, 141, 39–49, 1990.
- [165] D. W. Adams, L. J. Wu, & J. Errington, “Cell cycle regulation by the bacterial nucleoid,” *Current Opinion in Microbiology*, 22, 94–101, 2014.
- [166] B. Youngren, H. J. Nielsen, S. Jun, & S. Austin, “The multifork Escherichia coli chromosome is a self-duplicating and self-segregating thermodynamic ring polymer,” *Genes & Development*, 28, 71–84, 2014.
- [167] J. Männik, F. Wu, F. J. H. Hol, P. Bisicchia, D. J. Sherratt, J. E. Keymer, & C. Dekker, “Robustness and accuracy of cell division in Escherichia coli in diverse cell shapes,” *Proceedings of the National Academy of Sciences*, 109, 6957–6962, 2012.

- [168] J. Cambridge, A. Blinkova, D. Magnan, D. Bates, & J. R. Walker, “A Replication-inhibited unsegregated nucleoid at mid-cell blocks Z-ring formation and cell division independently of SOS and the SlmA nucleoid occlusion protein in *Escherichia coli*,” *Journal of Bacteriology*, 196, 36–49, 2014.
- [169] M. W. Bailey, P. Bisicchia, B. T. Warren, D. J. Sherratt, & J. Männik, “Evidence for Divisome Localization Mechanisms Independent of the Min System and SlmA in *Escherichia coli*,” *PLoS Genetics*, 10, 2014.
- [170] M. Pazos, M. Casanova, P. Palacios, W. Margolin, P. Natale, & M. Vicente, “FtsZ placement in nucleoid-free bacteria,” *PLoS ONE*, 9, 2014.
- [171] J. A. Buss, C. Coltharp, G. Shtengel, X. Yang, H. Hess, & J. Xiao, “A Multi-layered Protein Network Stabilizes the *Escherichia coli* FtsZ-ring and Modulates Constriction Dynamics,” *PLoS Genetics*, 11, 1–24, 2015.
- [172] J. Männik, D. E. Castillo, D. Yang, G. Siopsis, & J. Männik, “The role of MatP, ZapA and ZapB in chromosomal organization and dynamics in *Escherichia coli*,” *Nucleic Acids Research*, p. gkv1484, 2016.
- [173] B. Monterroso, S. Zorrilla, M. Sobrinos-Sanguino, M. Á. Robles-Ramos, C. Alfonso, B. Söderström, N. Y. Meiresonne, J. Verheul, T. den Blaauwen, & G. Rivas, “The Bacterial DNA Binding Protein MatP Involved in Linking the Nucleoid Terminal Domain to the Divisome at Midcell Interacts with Lipid Membranes,” *mBio*, 10, 1–14, may 2019.
- [174] H. Niki, Y. Yamaichi, & S. Hiraga, “Dynamic organization of chromosomal DNA in *Escherichia coli*,” *Genes & Development*, 14, 212–23, jan 2000.
- [175] R. Reyes-Lamothe, X. Wang, & D. Sherratt, “*Escherichia coli* and its chromosome,” *Trends in Microbiology*, 16, 238–245, 2008.
- [176] E. Galli & K. Gerdes, “Spatial resolution of two bacterial cell division proteins: ZapA recruits ZapB to the inner face of the Z-ring,” *Molecular Microbiology*, 76, 1514–1526, 2010.
- [177] M. Stouf, J.-C. Meile, & F. Cornet, “FtsK actively segregates sister chromosomes in *Escherichia coli*,” *Proceedings of the National Academy of Sciences*, 110, 11157–11162, 2013.
- [178] C. Coltharp, J. A. Buss, T. M. Plumer, & J. Xiao, “Defining the rate-limiting processes of bacterial cytokinesis,” *Proceedings of the National Academy of Sciences*, 113, E1044–1053, 2016.
- [179] E. Galli, C. Midonet, E. Paly, & F.-X. Barre, “Fast growth conditions uncouple the final stages of chromosome segregation and cell division in *Escherichia coli*,” *PLoS Genetics*, 13, p. e1006702, 2017.

- [180] X. Ma & W. Margolin, “Genetic and functional analyses of the conserved C-terminal core domain of Escherichia coli FtsZ,” *Journal of Bacteriology*, 181, 7531–7544, 1999.
- [181] E. Bi & J. Lutkenhaus, “Cell division inhibitors SulA and MinCD prevent formation of the FtsZ ring,” *Journal of Bacteriology*, 175, 1118–25, feb 1993.
- [182] N. S. Hill, P. J. Buske, Y. Shi, & P. A. Levin, “A moonlighting enzyme links Escherichia coli cell size with central metabolism,” *PLoS Genetics*, 9, p. e1003663, jan 2013.
- [183] R. B. Weart, A. H. Lee, A. C. Chien, D. P. Haeusser, N. S. Hill, & P. A. Levin, “A Metabolic Sensor Governing Cell Size in Bacteria,” *Cell*, 130, 335–347, 2007.
- [184] R. B. Weart & P. A. Levin, “Growth rate dependent regulation of medial FtsZ ring formation in Bacillus subtilis,” *Journal of Bacteriology*, 185, p. 2826, 2003.
- [185] K. C. Keiler, P. R. H. Waller, & R. T. Sauer, “Role of a Peptide Tagging System in Degradation of Proteins Synthesized from Damaged Messenger RNA Author (s): Kenneth C . Keiler , Patrick R . H . Waller and Robert T . Sauer Published by : American Association for the Advancement of Science Stable URL,” *Science*, 271, 990–993, 1996.
- [186] S. Gottesman, E. Roche, Y. N. Zhou, & R. T. Sauer, “The ClpXP and ClpAP proteases degrade proteins with carboxy-terminal peptide tails added by the SsrA-tagging system,” *Genes & Development*, 12, 1338–1347, 1998.
- [187] R. B. Weart, S. Nakano, B. E. Lane, P. Zuber, & P. A. Levin, “The ClpX chaperone modulates assembly of the tubulin-like protein FtsZ,” *Molecular Microbiology*, 57, 238–249, 2005.
- [188] J. L. Camberg, J. R. Hoskins, & S. Wickner, “ClpXP protease degrades the cytoskeletal protein, FtsZ, and modulates FtsZ polymer dynamics,” *Proceedings of the National Academy of Sciences*, 106, 10614–10619, 2009.
- [189] D. P. Haeusser, A. H. Lee, R. B. Weart, & P. A. Levin, “ClpX Inhibits FtsZ Assembly in a manner that does not require its ATP hydrolysis-dependent chaperone activity,” *Journal of Bacteriology*, 191, 1986–1991, 2009.
- [190] J. L. Camberg, J. R. Hoskins, & S. Wickner, “The Interplay of ClpXP with the cell division machinery in Escherichia coli,” *Journal of Bacteriology*, 193, 1911–1918, 2011.
- [191] K. Sekar, R. Rusconi, J. T. Sauls, T. Fuhrer, E. Noor, J. Nguyen, V. I. Fernandez, M. F. Buffing, M. Berney, S. Jun, R. Stocker, & U. Sauer, “Synthesis and degradation of FtsZ quantitatively predict the first cell division in starved bacteria,” *Molecular Systems Biology*, 14, nov 2018.
- [192] J. Männik, B. E. Walker, & J. Männik, “Cell cycle-dependent regulation of FtsZ in Escherichia coli in slow growth conditions,” *Molecular Microbiology*, 1, 0–2, sep 2018.

- [193] H. F. Judson, *The Eight Day of Creation*. Simon and Schuster, 1979.
- [194] M. Scott, C. W. Gunderson, E. M. Mateescu, Z. Zhang, & T. Hwa, “Interdependence of cell growth and gene expression: origins and consequences.,” *Science*, 330, 1099–1102, nov 2010.
- [195] I. Lozada-Chávez, S. C. Janga, & J. Collado-Vides, “Bacterial regulatory networks are extremely flexible in evolution,” *Nucleic Acids Research*, 34, 3434–3445, 2006.
- [196] M. E. Sharpe, P. M. Hauser, R. G. Sharpe, & J. Errington, “Bacillus subtilis cell cycle as studied by fluorescence microscopy: Constancy of cell length at initiation of DNA replication and evidence for active nucleoid partitioning,” *Journal of Bacteriology*, 180, 547–555, 1998.
- [197] R. J. Paulton, “Nuclear and cell division in filamentous bacteria.,” *Nature New Biology*, 231, 271–274, jun 1971.
- [198] T. M. Norman, N. D. Lord, J. Paulsson, & R. Losick, “Stochastic Switching of Cell Fate in Microbes,” *Annual Review of Microbiology*, 69, p. 150902154308007, 2015.
- [199] R. J. Paulton, “Analysis of the multiseptate potential of Bacillus subtilis.,” *Journal of Bacteriology*, 104, 762–767, 1970.
- [200] N. Nanninga, L. J. Koppes, & F. C. de Vries-Tijssen, “The cell cycle of Bacillus subtilis as studied by electron microscopy,” *Archives of Microbiology*, 123, 173–181, 1979.
- [201] R. Chen, S. B. Guttenplan, K. M. Blair, & D. B. Kearns, “Role of the σ^D -dependent autolysins in Bacillus subtilis population heterogeneity,” *Journal of Bacteriology*, 191, 5775–5784, 2009.
- [202] L. A. Simmons, B. W. Davies, A. D. Grossman, & G. C. Walker, “Beta clamp directs localization of mismatch repair in Bacillus subtilis.,” *Molecular Cell*, 29, 291–301, feb 2008.
- [203] S. M. Mangiameli, B. T. Veit, H. Merrikh, & P. A. Wiggins, “The Replisomes Remain Spatially Proximal throughout the Cell Cycle in Bacteria,” *PLoS Genetics*, 13, 1–17, 2017.
- [204] X. Wang, P. Montero Llopis, & D. Z. Rudner, “Bacillus subtilis chromosome organization oscillates between two distinct patterns.,” *Proceedings of the National Academy of Sciences*, 111, jul 2014.
- [205] A. I. Goranov, A. M. Breier, H. Merrikh, & A. D. Grossman, “Yba of bacillus subtilis controls DnaA-mediated replication initiation but not the transcriptional response to replication stress,” *Molecular Microbiology*, 74, 454–466, 2009.
- [206] H. Merrikh & A. D. Grossman, “Control of the replication initiator DnaA by an anti-cooperativity factor,” *Molecular Microbiology*, 82, 434–446, oct 2011.

- [207] E. Cho, N. Ogasawara, & S. Ishikawa, “The functional analysis of YabA, which interacts with DnaA and regulates initiation of chromosome replication in *Bacillus subtilis*,” *Genes & Genetic Systems*, 83, 111–125, 2008.
- [208] T. R. Beattie, N. Kapadia, E. Nicolas, S. Uphoff, A. J. Wollman, M. C. Leake, & R. Reyes-Lamothe, “Frequent exchange of the DNA polymerase during bacterial chromosome replication,” *eLife*, 6, 1–20, 2017.
- [209] S. M. Mangiameli, C. N. Merrikh, P. A. Wiggins, & H. Merrikh, “Transcription leads to pervasive replisome instability in bacteria,” *eLife*, 6, 1–27, 2017.
- [210] M. Holmes, M. Rickert, & O. Pierucci, “Cell division of cycle of *Bacillus subtilis*: evidence of variability in period D.,” *Journal of Bacteriology*, 142, 254–61, apr 1980.
- [211] N. O. Kjeldgaard, O. Maaløe, & M. Schaechter, “The transition between different physiological states during balanced growth of *Salmonella typhimurium*,” *Journal of General Microbiology*, 19, 607–16, dec 1958.
- [212] S. Cooper, “Cell division and DNA replication following a shift to a richer medium,” *Journal of Molecular Biology*, 43, 1–11, jul 1969.
- [213] M. F. Dion, M. Kapoor, Y. Sun, S. Wilson, J. Ryan, A. Vigouroux, S. van Teeffelen, R. Oldenbourg, & E. C. Garner, “*Bacillus subtilis* cell diameter is determined by the opposing actions of two distinct cell wall synthetic systems,” *Nature Microbiology*, 2019.
- [214] J. Löwe & L. A. Amos, “Evolution of cytomotive filaments: The cytoskeleton from prokaryotes to eukaryotes,” *International Journal of Biochemistry and Cell Biology*, 41, 323–329, 2009.
- [215] J. Errington & L. J. Wu, “Cell Cycle Machinery in *Bacillus subtilis*,” in *Prokaryotic Cytoskeletons*, vol. 84, 67–101, 2017.
- [216] R. Reyes-Lamothe, D. J. Sherratt, & M. C. Leake, “Stoichiometry and architecture of active DNA replication machinery in *Escherichia coli*,” *Science*, 328, 498–501, apr 2010.
- [217] N. B. Grover, C. L. Woldringh, A. Zaritsky, & R. F. Rosenberger, “Elongation of rod-shaped bacteria,” *Journal of Theoretical Biology*, 67, 181–193, 1977.
- [218] W. D. Donachie, K. J. Begg, & M. Vicente, “Cell length, cell growth and cell division,” *Nature*, 264, 328–333, 1976.
- [219] F. Wu, A. Japaridze, X. Zheng, J. W. J. Kerssemakers, & C. Dekker, “Direct imaging of the circular chromosome in a live bacterium *Fabai*,” *bioRxiv*, 1–15, 2018.
- [220] J. Bonnet, P. Yin, M. E. Ortiz, P. Subsoontorn, & D. Endy, “Amplifying Genetic Logic Gates,” *Science*, 340, 599–603, may 2013.

- [221] M. A. Konkol, K. M. Blair, & D. B. Kearns, “Plasmid-encoded comI inhibits competence in the ancestral 3610 strain of *Bacillus subtilis*,” *Journal of Bacteriology*, 195, 4085–4093, 2013.
- [222] P. R. Bennallack, S. R. Burt, M. J. Heder, R. A. Robison, & J. S. Griffiths, “Characterization of a novel plasmid-borne thiopeptide gene cluster in *Staphylococcus epidermidis* strain 115,” *Journal of Bacteriology*, 196, 4344–4350, 2014.
- [223] P. A. Levin, “6 Light microscopy techniques for bacterial cell biology,” in *Methods in Microbiology*, 115–132, 2002.
- [224] O. Ronneberger, P. Fischer, & T. Brox, “U-Net: Convolutional Networks for Biomedical Image Segmentation,” in *Medical Image Computing and Computer-Assisted Intervention-MICCAI 2015*, vol. 9351, 234–241, 2015.
- [225] E. Kulas, R. Smith, & S. V. Smith, “Planet Money Goes To Space,” 2017.
- [226] V. Ulman, M. Maška, K. E. G. Magnusson, O. Ronneberger, C. Haubold, N. Harder, P. Matula, P. Matula, D. Svoboda, M. Radojevic, I. Smal, K. Rohr, J. Jaldén, H. M. Blau, O. Dzyubachyk, B. Lelieveldt, P. Xiao, Y. Li, S. Y. Cho, A. C. Dufour, J. C. Olivo-Marin, C. C. Reyes-Aldasoro, J. A. Solis-Lemus, R. Bensch, T. Brox, J. Stegmaier, R. Mikut, S. Wolf, F. A. Hamprecht, T. Esteves, P. Quelhas, Ö. Demirel, L. Malmström, F. Jug, P. Tomancak, E. Meijering, A. Muñoz-Barrutia, M. Kozubek, & C. Ortiz-De-Solorzano, “An objective comparison of cell-tracking algorithms,” *Nature Methods*, 14, 1141–1152, 2017.
- [227] M. Arnoldini, I. A. Vizcarra, R. Peña-Miller, N. Stocker, M. Diard, V. Vogel, R. E. Beardmore, W.-D. Hardt, & M. Ackermann, “Bistable Expression of Virulence Genes in *Salmonella* Leads to the Formation of an Antibiotic-Tolerant Subpopulation,” *PLoS Biology*, 12, p. e1001928, aug 2014.
- [228] K. E. G. Magnusson, J. Jaldén, P. M. Gilbert, & H. M. Blau, “Global linking of cell tracks using the viterbi algorithm,” *IEEE Transactions on Medical Imaging*, 34, 911–929, 2015.
- [229] C. C. Sachs, A. Grunberger, S. Helfrich, C. Probst, W. Wiechert, D. Kohlheyer, & K. Nöh, “Image-based single cell profiling: High-throughput processing of mother machine experiments,” *PLoS ONE*, 11, 1–15, 2016.
- [230] D. A. Van Valen, T. Kudo, K. M. Lane, D. N. Macklin, N. T. Quach, M. M. DeFelice, I. Maayan, Y. Tanouchi, E. A. Ashley, & M. W. Covert, “Deep Learning Automates the Quantitative Analysis of Individual Cells in Live-Cell Imaging Experiments,” *PLOS Computational Biology*, 12, p. e1005177, nov 2016.
- [231] Y. Yang, X. Song, & A. B. Lindner, *Time-lapse microscopy and image analysis of Escherichia coli cells in mother machines*, vol. 43. Elsevier Ltd., 1 ed., 2016.

- [232] D. Bannon, E. Moen, E. Borba, A. Ho, I. Camplisson, B. Chang, E. Osterman, W. Graf, & D. V. Valen, “DeepCell 2.0: Automated cloud deployment of deep learning models for large-scale cellular image analysis,” *bioRxiv*, p. 505032, 2018.
- [233] M. Kaiser, F. Jug, T. Julou, S. Deshpande, T. Pfohl, O. K. Silander, G. Myers, & E. van Nimwegen, “Monitoring single-cell gene regulation under dynamically controllable conditions with integrated microfluidics and software,” *Nature Communications*, 9, p. 212, 2018.
- [234] J.-B. Lugagne, H. Lin, & M. J. Dunlop, “DeLTA: Automated cell segmentation, tracking, and lineage reconstruction using deep learning,” *bioRxiv*, 1–17, 2019.
- [235] A. Smith, J. Metz, & S. Pagliara, “MMHelper: An automated framework for the analysis of microscopy images acquired with the mother machine,” *Scientific Reports*, 9, p. 10123, dec 2019.
- [236] L. Grady, “Random walks for image segmentation,” *IEEE Transactions on Pattern Analysis and Machine Intelligence*, 28, 1768–1783, 2006.
- [237] T. Falk, D. Mai, R. Bensch, Ö. Çiçek, A. Abdulkadir, Y. Marrakchi, A. Böhm, J. Deubner, Z. Jäckel, K. Seiwald, A. Dovzhenko, O. Tietz, C. Dal Bosco, S. Walsh, D. Saltukoglu, T. L. Tay, M. Prinz, K. Palme, M. Simons, I. Diester, T. Brox, & O. Ronneberger, “U-Net: deep learning for cell counting, detection, and morphometry,” *Nature Methods*, 16, 67–70, 2019.